Russian Original Vol. 35, No. 6, December, 1973

June, 1974

SATEAZ 35(6) 1063-1202 (1973)

SOVIET ATOMIC ENERGY

АТОМНАЯ ЭНЕРГИЯ
(ATOMNAYA ÉNERGIYA)

TRANSLATED FROM RUSSIAN

CONSULTANTS BUREAU, NEW YORK

SOVIET ATOMIC ENERGY

Soviet Atomic Energy is a cover-to-cover translation of *Atomnaya Énergiya*, a publication of the Academy of Sciences of the USSR.

An arrangement with Mezhdunarodnaya Kniga, the Soviet book export agency, makes available both advance copies of the Russian journal and original glossy photographs and artwork. This serves to decrease the necessary time lag between publication of the original and publication of the translation and helps to improve the quality of the latter. The translation began with the first issue of the Russian journal.

Consultants Bureau journals appear about six months after the publication of the original Russian issue. For bibliographic accuracy, the English issue published by Consultants Bureau carries the same number and date as the original Russian from which it was translated. For example, a Russian issue published in December will appear in a Consultants Bureau English translation about the following June, but the translation issue will carry the December date. When ordering any volume or particular issue of a Consultants Bureau journal, please specify the date and, where applicable, the volume and issue numbers of the original Russian. The material you will receive will be a translation of that Russian volume or issue.

Subscription
$80 per volume (6 Issues)
2 volumes per year
(Add $5 for orders outside the United States and Canada.)

Single Issue: $30
Single Article: $15

CONSULTANTS BUREAU, NEW YORK AND LONDON

227 West 17th Street
New York, New York 10011

Davis House
8 Scrubs Lane
Harlesden, NW10 6SE
England

Published monthly. Second-class postage paid at Jamaica, New York 11431.

Soviet Atomic Energy is abstracted or indexed in *Applied Mechanics Reviews, Chemical Abstracts, Engineering Index, INSPEC—Physics Abstracts and Electrical and Electronics Abstracts, Current Contents,* and *Nuclear Science Abstracts.*

SOVIET ATOMIC ENERGY

A translation of *Atomnaya Énergiya*

June, 1974

Volume 35, Number 6 December, 1973

CONTENTS

CONTENTS

(continued)

CONTENTS

(continued)

The Russian press date (podpisano k pechati) of this issue was 11/28/1973. Publication therefore did not occur prior to this date, but must be assumed to have taken place reasonably soon thereafter.

IN MEMORIAM: SAVELII MOISEEVICH FEINBERG

(DECEMBER 24, 1910-OCTOBER 20, 1973)

A. M. Petros'yan, P. S. Neporozhnii,
A. P. Aleksandrov, N. A. Dollezhal',
A. N. Grigor'yants, A. G. Meshkov,
I. K. Kikoin, B. B. Kadomtsev,
V. V. Goncharov, N. S. Khlopkin,
A. I. Vasin, E. P. Velikhov,
and V. M. Balebanov

On October 20, 1973, following a relatively short illness, Savelii Moiseevich Feinberg, head of the nuclear reactor theory sector of the I. V. Kurchatov Institute of Atomic Energy, Doctor of Physical and Mathematical Sciences, Professor of the Moscow Engineering Physics Institute, and recipient of the Lenin Prize and various State Prizes, died in his 63rd year of life.

S. M. Feinberg was one of the late I. V. Kurchatov's closest collaborators, a renowned scientist, and specialist in the field of peaceful uses of atomic energy.

In 1946, within three years after sustaining severe front-line wounds in the war, he left his research on applied mathematics, in elasticity and plasticity theory, to take an active part in the program of developing the then fledgling atomic science.

Up to the end of his life, S. M. Feinberg worked at the Institute of Atomic Energy, where he performed major investigations on the physics, engineering, design, and costs of reactors of various types and functions.

Translated from Atomnaya Énergiya, Vol. 35, No. 6, p. 370, December, 1973.

S. M. Feinberg made a great contribution to the development of Soviet atomic science and atomic engineering, from the first experimental reactor to the power reactors of the Novaya Voronezh', Leningrad, Kola power stations and other power stations now under construction, from series-manufactured research reactors to unique custom-engineered heavy-duty high-load equipment. He is credited with some of the ideas embodied by industry in living reality, and successfully developed at the present time. He trained numerous scientific students who are now working in industry, in scientific-research institutes, and in design and planning institutes. S. M. Feinberg was acknowledged as the leader of the Soviet school of specialists in reactor theory.

The merits demonstrated by S. M. Feinberg were recognized by the Homeland in the form of Orders of Lenin, the Order of the Labor Red Banner, and various medals.

Everyone who was closely acquainted with Savelii Moiseevich held his spiritual qualities, his profound many-sided intellect, and his extensive erudition in high esteem.

The brilliant memory of Savelii Moiseevich will always be held dear in our hearts.

ARTICLES

CREEP OF URANIUM DIOXIDE

Yu. V. Miloserdin, K. V. Naboichenko,
I. S. Golovnin, Yu. K. Bibilashvili,
T. S. Men'shikova, P. A. Mandryka,
K. G. Bobkov, N. I. Arlamenkov,
A. N. Bogatov, E. M. Minaev,
and L. S. Podval'nyi

UDC 621.039.543.4

One of the main characteristics required in order to estimate the deformation of a fuel-element can is the creep velocity of the core material. A number of authors have made tests in fields of reactor radiation [1-6] and observed an increase in the creep rate of nuclear fuel. As part of a program of creep-testing on ceramic fuel it has been proposed to carry out the first series of experiments in an IRT-2000 thermal reactor with a thermal neutron flux of 10^{12} neutrons/$cm^2 \cdot sec$ at the target, and then in a BR-10 reactor with fast-neutron fluxes of $(2-3) \cdot 10^{13}$ neutrons/$cm^2 \cdot sec$, so as to be able to compare the experimental results obtained with different neutron spectra and different fission densities.

Apparatus for Studying Creep

The experimental apparatus intended for studying the creep of ceramic fuel in the field of neutron radiation arising from the IRT-2000 reactor is placed in the position usually occupied by one of the 180-mm diameter channels.

The lower part of the assembly forms a high-temperature chamber (Fig. 1). The cylindrical casing of the chamber, 170 mm in diameter, is closed hermetically with upper and lower flanges. Inside the casing, thermal screens are fixed on supports forming the guides of the measuring rods. Mounted on the lower flange is the loading unit, constituting a hermetic cylinder with a stainless steel bellows sealed into it; this works in compression under the pressure of gas supplied through a pipeline. The sample, situated in the molybdenum cylinder of the loading device, is subjected to stress through a stainless steel rod, the molybdenum holder, and a tungsten plunger. The creep deformation of the sample is recorded by way of a balance beam, aided by rods and sensors.

Mounted on the upper flange is the heating system of the chamber, consisting of molybdenum current loads, one of which (Fig. 1, position 14) is directly connected to the body, while the second (position 4) is insulated. The heater is of Ω-shape, made of sheet tungsten; it is fixed to the current leads with molybdenum bolts. The loading system constitutes a demountable rod, which is inserted into the chamber along a bearing tubular conduit, and is fixed to the upper flange of the chamber by means of a bayonet closure.

The deformation taking place during creep was measured with inductive sensors of two types. Relatively large deformations were measured with a multirange sensor of the solenoid type, forming a cylindrical coil with an Armco steel core inside it. The tip was pressed against the source of deformation with a spring. The ranges of the sensor were 0-0.5, 0-1.0, 0-2.5, and 0-10 mm. The limiting maximum error at room temperature was 0.48%. Tests carried out with this sensor at 40 and 80°C showed that its characteristic and sensitivity were independent of the steady temperature level.

In order to determine small deformations we used a BV-662 multichannel sensor. The ranges were here 0-0.04, 0-0.08, 0-0.2, and 0-0.4 mm. The limiting relative error was 0.5%. In recording the creep deformation the body of the sensor was adjusted by means of a selsyn drive situated in the top cover of the reactor.

Translated from Atomnaya Énergiya, Vol. 35, No. 6, pp. 371-375, December, 1973. Original article submitted July 30, 1973.

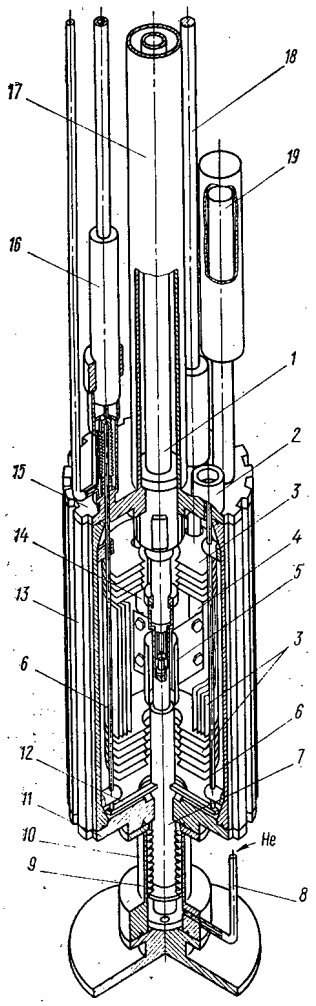

Fig. 1. Arrangement of the apparatus for studying creep: 1) loading system; 2, 16) sensors; 3) heat screens; 4, 14) current leads; 5) heater; 6) measuring rods; 7) lower plunger; 8) pipeline; 9) bellows; 10) hermetic cylinder; 11, 15) lower and upper flanges; 12) balance beam; 13) casing of chamber; 17) bearing pipeline; 18, 19) services of measuring lines.

For studying the radiation-induced creep of the fuel in the channel of the BR-10 reactor (diameter 50 mm), a special high-temperature apparatus is provided. Like the one used for the thermal reactor, this apparatus consists of a penumatic loading system situated in the lower flange and a molybdenum supporting framework. In view of the specific working conditions of the 50 mm-diameter channel, the apparatus is given the following characteristics: 1) the heater is placed in the outer surface of the chamber covered with aluminum oxide; 2) the deformation of the sample is measured with an acoustic sensor of small radial dimensions; 3) the temperature operating range of the apparatus is 1200-1600°K for a load of up to 120 kg on the sample.

Results of Laboratory Tests

The UO_2 test samples were prepared by cold pressing and then sintering at ~1920°K; they constituted cylinders 4.18 mm in diameter and 4-7 mm in height with grain dimensions of 12-15 μ and an oxygen coefficient of 2.00-2.01. The geometrical dimensions of the samples were measured in an IZB-2 vertical comparator to an accuracy of ± 1 μ. The average length and diameter of the samples were determined from the results of three readings.

In these tests the deformation of the samples was in general no greater than 3.5%; this should not lead to any serious error such as might be associated, for example, with a change in sample cross section during the tests. The deformation ε of the sample is typified as a function of time τ in Fig. 2 for various values of the structure factor.

During the deformation of the sample in the creep tests, a difference appears between the radial dimensions of the samples obtained by measuring after the tests and the dimensions calculated from the condition that the volume should remain constant during the deformation:

$$\frac{d_\varepsilon}{d_0} = \frac{1}{\sqrt{1-\varepsilon}}, \quad (1)$$

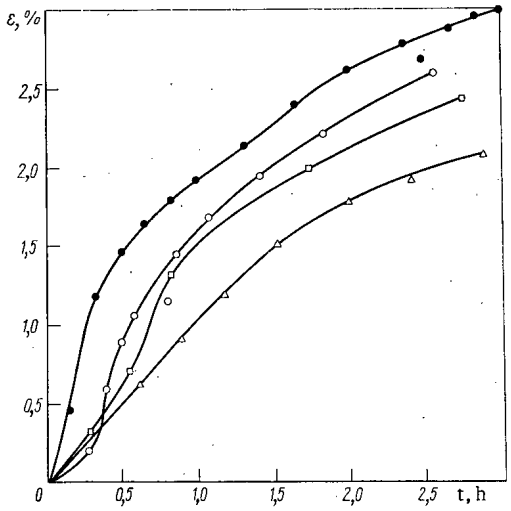

Fig. 2

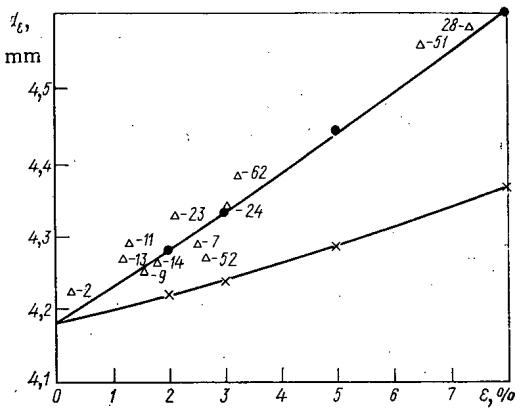

Fig. 3

Fig. 2. Dependence of ε on τ for $\sigma = 3$ kg/mm^2 and T = 1593°K: ○) sample No. 7; △) No. 23; ●) No. 50; □) No. 52.

Fig. 3. Dependence of the external diameter of the sample on ε: △) experimental value of d_ε (here and subsequently the numbers on the points indicate the numbers of the samples); ×) calculation based on Eq. (1); ●) calculation based on Eq. (2).

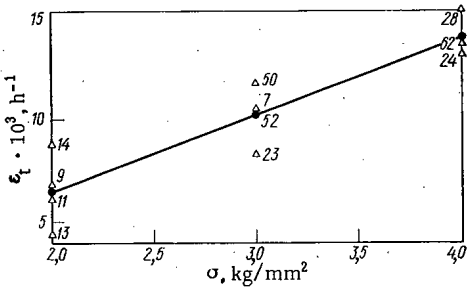

Fig. 4

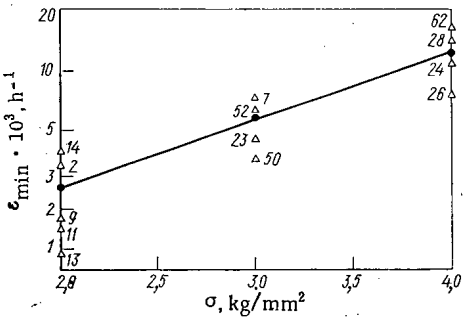

Fig. 5

Fig. 4. Dependence of the mean creep velocity on σ (T = 1593°K): △) experimental values; ●) average experimental values.

Fig. 5. Dependence of $\dot{\varepsilon}_{min}$ on σ (T = 1593°K, Q = 106 kcal/mole, B = 2.36 kcal · mm^2/mole · kg, A = 2.4 · 10^{11} h^{-1}): △) experimental values; ●) average experimental values.

where d_ε is the diameter of the sample after deformation; d_0 is the diameter of the sample before the beginning of the tests.

Figure 3 shows the calculated relationship (1) and the experimental values for the samples tested. For ε = 4% the difference between the calculated and experimental results is 3%, while for a deformation of 8% it is around 6%. This evidently indicates disruption of the continuous structure of the sample during the tests.

The experimental dependence of sample diameter on deformation may conveniently be approximated by the relation

$$\frac{d_\varepsilon}{d_0} = \frac{1}{\sqrt{1-k\varepsilon}}, \qquad (2)$$

where k is an empirical coefficient equal to 2.2.

These experiments should be classified as short-term tests. Despite the fact that the experimental data exhibit a considerable scatter, such as is typical in creep tests on polycrystalline materials, two methods of estimating the creep velocity may be proposed.

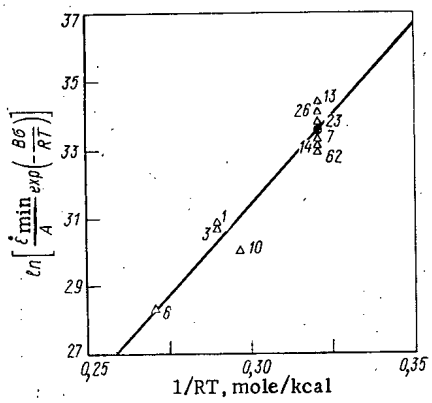

Fig. 6

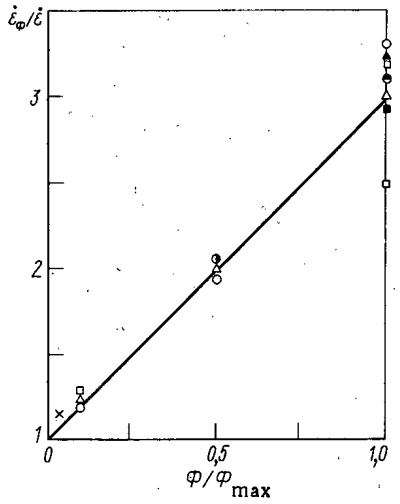

Fig. 7

Fig. 6. Comparison between the experimental results and those calculated from Eq. (4) for Q = 106 kcal/mole: Δ) experimental values; •) average experimental values.

Fig. 7. Dependence of the relative creep velocity on the relative fission density. For σ = 3 kg/mm^2 and T values of: □) 1373°K; ■) 1473°K; ▲) 1573°K; ×) 1593°K. For σ = 4 kg/mm^2 and T values of: ○) 1373°K; ◑) 1473°K; ◓) 1573°K; Δ) average values.

The majority of samples exhibit a tendency for the creep velocity ($\dot{\varepsilon}_\tau = \varepsilon/\tau$) to fall asymptotically to a certain specific value. In the case under consideration the value of ε_τ for the conditions specified was determined over a period of τ = 2.3 h, as the arithmetic mean for the individual samples.

Figure 4 shows the dependence of the creep velocities on stress in the sample, which is described by the linear expression

$$\dot{\varepsilon}_\tau = 3.7 \cdot 10^{-3} \sigma h^{-1}. \quad (3)$$

Figure 4 illustrates the average value of the creep velocities from which the approximating relation was constructed, and the values of ε_τ obtained for each of the samples. A linear dependence on σ had already been observed for polycrystalline UO_2 [7] in long-term tests at a lower temperature. Under these conditions the actual creep velocity should differ very little from the "steady" creep velocity, since in the long-term tests the transient region of creep makes a relatively slight contribution to the deformation. Thus, in the first method of estimation, due allowance is made for the transient region of creep.

The second method lies in estimating the minimum creep velocity. The arithmetic mean values of these velocities for various test conditions may be satisfactorily described by the relation

$$\dot{\varepsilon}_{min} = A \exp\left\{-\frac{Q - B\sigma}{RT}\right\} h^{-1}, \quad (4)$$

where $A = 2.4 \cdot 10^{11}$ h^{-1} is the structure factor, which on passing from one sample to another varies over the range $(1.1\text{-}3.2) \cdot 10^{11}$ h^{-1}; Q = 106 kcal/mole is the activation energy; B = 2.4 kcal · mm^2/mole · kg is the stress constant.

The difference between the experimental and calculated data may be seen from Figs. 5 and 6, which give the average values and the results of each experiment. The activation energy of the creep process was determined over the temperature range 1600-1900°K.

An analogous method of analyzing the experimental data for UO_2 samples was employed in [8]. On comparing the experimental results of the present investigation with those of [8], we find excellent agreement between the activation energies, but a slight difference in the values of B (2.4 and 2.8 kcal · mm^2/mole · kg, respectively), and a considerable difference in the values of A ($2.4 \cdot 10^{11}$ and $1.2 \cdot 10^9$ h^{-1}).

Results of Tests inside the Channel

For the experiments inside the channel we used bushing-shaped UO_2 samples obtained by the method already indicated; they had a diameter of 5.9 mm and an inner aperture of 1.8 mm, while the enrichment factor was 2%. Two samples were placed one over the other and were centered in the sleeves of two tungsten–rhenium thermocouples 0.8 mm in diameter. The beads of the thermocouples lay in the middle of the lower samples. One of the thermocouples was used to measure the temperature of the working part, using a PP-63 potentiometer of class 0.05. The second thermocouple was connected to a VRT-3 temperature regulator which was used to keep the temperature in the working region at a level of 1400°K to an accuracy of 0.1%. The preparation of the experiment and the calibration of the various systems in the apparatus were described in full detail in [9].

The main problem in the experiments inside the channel lay in determining the quantitative relationship between the creep velocity and the fission density. The experiment was therefore carried out in one working section while varying the fission density from 0 to $0.625 \cdot 10^{12}$ fissions/$cm^3 \cdot sec$ at a temperature of 1373°K and stresses of 3 and 4 kg/mm^2. During the tests the temperature and load on the sample were kept constant. The fission density in the sample was varied by varying the power of the reactor. In the second working section the fission density was held at its maximum, and the creep velocity was studied at stresses of 3 and 4 kg/mm^2 and temperatures of 1373, 1473, and 1523°K. Creep was also studied in the absence of neutron radiation in the same working sections under all the foregoing conditions.

The dependence of the creep velocity on the fission density is of a linear character (Fig. 7); in this case it may be described by the relation

$$\frac{\dot{\varepsilon}_{\Phi\,\min}}{\dot{\varepsilon}_{\min}} = 1 + c\Phi, \tag{5}$$

where $\dot{\varepsilon}_{\Phi\,\min}$ is the minimum creep velocity for a specific fission density in the sample; $\dot{\varepsilon}_{\min}$ is the minimum creep velocity in the absence of fission; $C = 3.2 \cdot 10^{-12}$ $cm^3 \cdot sec$/fission is an empirical coefficient.

CONCLUSIONS

1. We have presented some experimental results relating to the creep of polycrystalline sintered UO_2 over the temperature range 1600–1900°K for stresses of 0.4–4 kg/mm^2.

2. The deformation of the UO_2 samples during the tests leads to the formation of inhomogeneities and the development of cracks.

3. The average creep velocity depends linearly on stress at 1593°K. The minimum creep velocity may be satisfactorily described as a function of temperature and stress by Eq. (4).

4. When a neutron flux acts on the sample, the creep velocity increases and varies linearly with the fission density. For maximum fission densities of $0.625 \cdot 10^{12}$ fissions/$cm^3 \cdot sec$ in the temperature range 1373–1523°K, and for stresses of 3 and 4 kg/mm^2 in the sample, the creep velocity increases by a factor of three by comparison with laboratory tests.

LITERATURE CITED

1. S. G. Konobeevskii et al., in: Research in the Field of Geology, Chemistry, and Metallurgy, First Geneva Conference (1955) [in Russian], Izd. AN SSSR, Moscow (1956), p. 263.
2. A. S. Zaimovskii et al., At. Énerg., 5, 412 (1958).
3. A. Cottrell, Brit. J. Appl. Phys., 5, No. 43 (1956).
4. A. Cottrell and A. Roberts, Phil. Mag., 1, No. 8 (1956).
5. D. Brulacher and W. Dienst, J. Nucl. Materials, 36, No. 2, 244 (1970).
6. J. Perrin, J. Nucl. Materials, 42, 101 (1972).
7. D. Brulacher and W. Dienst, J. Nucl. Materials, 42, 285-296 (1972).
8. K. Kummerer and D. Vollas, At. Tekh. za Rubezh., No. 1, 25 (1972).
9. Yu. V. Miloserdin et al., Contribution to the Franco-Soviet Colloquium on Fuel Elements [in Russian], Obninsk (1972).

METHODS OF PREPARING CORES FROM URANIUM MONOCARBIDE, MONONITRIDE, AND CARBONITRIDE FOR THE FUEL ELEMENTS OF FAST REACTORS

F. G. Reshetnikov, R. B. Kotel'nikov,
B. D. Rogozkin, S. N. Bashlykov,
I. A. Samokhvalov, G. V. Titov,
M. G. Shishkov, V. S. Belevantsev,
Yu. E. Fedorov, and V. P. Simonov

UDC 621.039.542.3

Refractory, oxygen-free compounds of uranium and plutonium, such as carbides and nitrides, satisfy the requirements normally imposed upon nuclear fuel as regards the majority of their properties, while in certain respects carbonitrides are much better than oxides. The importance of these compounds is becoming particularly recognized in connection with the fast-reactor development program. The economics of the fuel cycle improve substantially on using carbide fuel, owing to the shortening of the "doubling time."

The advantages of carbide–nitride fuel can only be properly realized if the cores are of a high quality and if the processes involved in producing the compounds, making cores from these, and constructing the corresponding fuel elements are competitive. Various methods of producing uranium and plutonium monocarbides, mononitrides, and carbonitrides, using the metal or oxides as initial materials, are now being developed [1-7]. Each method has its advantages and disadvantages. In order to choose the best method a careful analysis is required; both the results of radiation tests and the technical-economic indices have to be estimated. Deserving of considerable attention are questions associated with the achievement of a continuous process, and also the development of operating modes producing compounds with compositions capable of being regulated at will. Some of these questions will be considered in this paper.

EXPERIMENTAL METHOD

Possibility of Obtaining Oxygen-Free Uranium Compounds by Continuous Methods

When studying the synthesis of refractory compounds, special attention must be paid to the conditions of formation of the compounds, so as to obtain materials of high purity, and also to the development of continuous processes, as well as to the development of the corresponding equipment.

Continuous Process for Obtaining Uranium Nitride. Methods of obtaining powders of uranium mononitride and monocarbide with a specified composition from metallic uranium at relatively low temperatures were described in [1-5]. However, in every case so described the process was a periodic one. We accordingly attempted to establish a continuous process for producing uranium nitride. The investigations were carried out in an apparatus (Fig. 1) consisting of a loading chamber 1, a device for hydrogenating the uranium with hydrogen 2, 3, a bunker, a nitriding system 5, an electric furnace 6, an unloading chamber 7, and a receiver 8. The metallic uranium, in the form of small ingots passes from the loading chamber to the hydrogenation device. The resultant finely-divided uranium hydride (particle size less than 0.5 μ) passes into the loading bunker and then into the nitriding system through the feeder 4, which ensures the correct rate of flow. The product is agitated in the reaction system 5 by means of a screw conveyer set in motion by en electric motor through the gear 9. The feeder and conveyer are placed on a single shaft.

Translated from Atomnaya Énergiya, Vol. 35, No. 6, pp. 377-386, December, 1973. Original article submitted July 30, 1973.

TABLE 1. Impurity Content and Characteristics or Uranium Monocarbide, Mononitride, and Sesquinitride Powders

Compound	N, %	C, %	O, %	Lattice constant	Surface, m^3/g	Bulk weight, g/cm^3	Mean particle size, μ
Uranium monocarbide	0,05	4,7	0,05	4,961	5—6	1,7—1,9	2—4
Uranium mononitride	5,4	0,05	0,08	4,889	2—3	2,1—2,2	5—10
Uranium sesquinitride	7,8	0,05	0,08	5,322	2—3	2,0—2,2	3—8

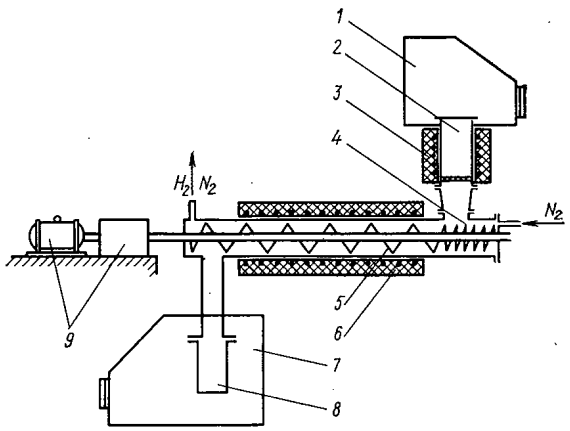

Fig. 1. Apparatus for the continuous production of uranium nitride.

Nitrogen is passed into the nitriding system close to the feeder; it is taken out at the unloading aperture and passes through a filter into the blower system.

In all these experiments the excess nitrogen pressure was kept below 20-30 mm water, while its flow amounted to 100-150% more than was needed for the formation of the stoichiometric sesquinitride. After passing the nitrogen (the oxygen content of the latter being no greater than 0.003 vol. %), the apparatus was heated to the specified temperature. Then the uranium hydride (500-700 g) was passed from the hydrogenation system into the bunker, being gradually admitted via the feeder to the reaction zone. At the exit from the apparatus the nitrided product was poured into a receiving container. The bunker was loaded with the hydride within 20-30 min. The optimum rate chosen for rotating the screw conveyer was 2 rpm. The time spent by the powder in the reaction zone was then no more than 20 min.

We studied the effect of nitriding temperature on the composition of the resultant products between 400 and 800°C. The results showed that on increasing the nitriding temperature from 400 to 800°C the nitrogen content in the nitriding products increased from 6.96 to 8.4%, respectively. According to x-ray diffraction analysis, under these conditions the nitride obtained has a pseudoface-centered crystal structure with a lattice constant of 5.320-5.323 Å. These parameters correspond to uranium nitride of composition $UN_{1.545}-UN_{1.57}$. No other phases appear on the x-ray diffraction patterns. The amount of oxygen in the uranium nitride was no greater than 0.1%. At a temperature of less than 400°C under these conditions a nitride of variable composition containing free uranium is formed, i.e., the interaction with nitrogen is unable to pass to completion. On increasing the temperature to 800°C the rate of nitriding increases, but so does the particle size of the resultant nitride powder. Above 600°C weak conglomerates of particles are formed, breaking up under a light pressure. The agitation of the product, the conditions of gas flow, and the corresponding temperature conditions create a favorable state of affairs for retaining the finely-divided form of the powder. The particle size of the uranium nitride powders obtained at 400-550°C averages 3-8 μ. The uranium nitride is suitable for making cores without subjection to further crushing. The apparatus tested gives 1.5-2 kg of uranium sesquinitride per hour.

If it is required to produce uranium mononitride, the sesquinitride is subjected to vacuum treatment at 900-950°C. The powder size of the mononitride averages 5-12 μ. Table 1 shows the amounts of impurities in the uranium monocarbide, mononitride, and sesquinitride, and also the characteristics of the powders obtained from metallic uranium.

Production of Oxygen-Free Uranium Compounds in a Fluidized Bed from Uranium Dioxide. Among the various known methods of producing uranium monocarbide, mononitride, and carbonitride from the dioxide, the fluidized-bed method possesses a certain advantage, namely, the possibility of initiating a continuous and reasonably vigorous process.

We studied the carbiding process in an apparatus consisting of a conical–cylindrical graphite reactor (internal diameter 24 mm) with a graphite heater, together with special systems for purifying the working gases from oxygen and water vapor, monitoring the parameters of the process, and dust-trapping, and also a gas analyzer (Fig. 2). Preliminary investigations with a model of the reactor showed that the "fluidizing"

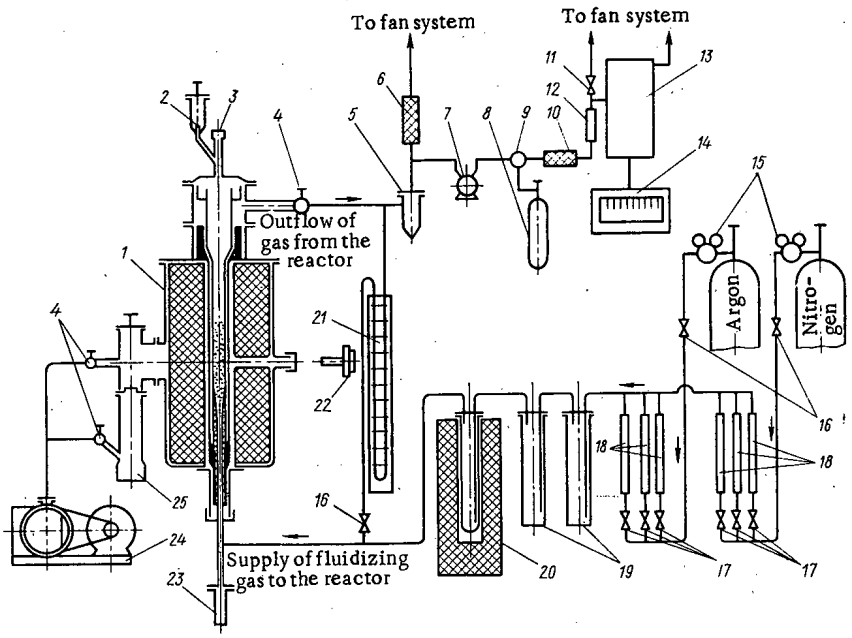

Fig. 2. Arrangement of the apparatus for studying the carbiding of UO_2 in a fluidized bed: 1) reactor; 2) bunker containing the charge; 3) opening for the direct observation of the process; 4, 9, 11, 16, 17) regulating valves; 5, 6, 10) dust purification system; 7) flow exciter; 8) control gas cylinder; 12, 18) flowmeters; 13, 14) opticoacoustic gas analyzer; 15) reducers; 19, 20) gas purification system; 21) manometer; 22) pyrometer; 23) receiver for the finished product; 24, 25) vacuum pumps.

process might be regarded as reasonably dependable if the size of the fluidized particles were no smaller than 20 μ (specific gravity of the particles ~14 g/cm^3). The gas velocity for particles 300-400 and 200-300 μ in size should be no lower than $37.1G^{0.44}$ and $12.8\,G^{0.5}$ liters/h respectively (here G is the weight of the charge in g).

Using the full-scale working apparatus, the conditions for "fluidization" and the production of a product of the desired composition at maximum yield were then duly determined. To this end we studied the effect of the geometry of the apparatus, the particle size in the original charge, the rate of inflow of the fluidizing gas, the nature of the carbon-containing material and the binder, the magnitude of the charge, the working temperature, and the rate of production on the composition and yield of the product, and also on the state of "fluidization."

A charge of UO_2 + C in the form of granules of 200-400 μ in size was loaded into the reactor from the top, to meet a flow of working gas fed in from the bottom. The resultant compounds were passed out through the lower opening after the supply of working gas had ceased. We studied the process at temperatures of 1500-2000°C; the duration of the process was determined by reference to the time required to evolve CO, using a gas analyzer with continuous recording.

As carbon-containing materials we used coal tar, lamp black, flaky graphite, and ordinary graphite crushed; as binder we used paraffin, raw rubber, and coal tar (Table 2). The process works successfully if the binder ensures the wholeness of the granules. Paraffin and raw rubber do not satisfy this requirement, since the charge separates partly or completely into its components, which are carried away from the reaction zone or become sintered on to the walls of the reactor (positions 1-6, Table 2). The best results are obtained on using coal tar, which plays the part of both carburizer and binder (positions 7 and 8, Table 2). The replacement of even part of the coal tar with soot (lamp black) has a deleterious effect on the carbiding process (positions 4-6, Table 2). On the basis of these investigations we found the optimum carbiding condition: temperature 1600°C, velocity of working gas in the cylindrical part of the apparatus (24 mm in diameter) between 0.9 and 1.4 m/sec. Under these conditions a yield of 97-99% is obtained, the monocarbide being of almost stoichiometric composition (U = 94.7-94.9; C = 4.7-5.0; O = 0.1%). The total carbiding time, determined by reference to the end of CO evolution (Fig. 3) was 40-50 min, the greatest rate of reduction being achieved in the first 10 min of the process.

TABLE 2. Results of Experiments on Producing Uranium Carbide in a Fluidized Bed

No. of positions	Type of carbon and binder	Conditions of the process			Behavior of the material	Balance of the product, wt.%			Chemical composition of the product, wt. %			
		T, °C	W,* m/sec	t, min		useful	remained on the wall	carried away with the gases	U	C_{tot}	C_{Fr}	O
1	Lamp black	1600	0,7—1,4	60	P. F. †	26—46	12—20	42—54	(93,2—93,5) ‡	(4,9—5,0)	(0,2—0,4)	(1,5—1,8)
2	Paraffin	1700—2000	0,7—2,0	10—30	S	0	65—98	2—35	(93,8—94,0)	(5,3—6,0)	(0,1—0,2)	(0,1—0,5)
3	Lamp black; paraffin + rubber	1600—1700	0,7—1,4	60	S P. F	0—20	53—89	11—27	93,7—94,0	4,9—5,5	0,1	0,3—1,2
4	Lamp black + coal tar (4:1)	1500	0,7—1,4	60	F	57	0	43	89,6	6,7	1,4	3,1
5		1600—1700	0,7—1,4	60	P. F	52—57	19—49	3—11	93,5—94,7	4,6—4,8	0,1—0,2	0,2—1,0
6	Lamp black + coal tar (1 : 1)	1600—1700	0,7—1,4	60	P. F	66—78	15—31	3—7	93,9—94,5	4,6—4,8	0,1—0,2	0,2—1,0
7	Coal tar	1600	0,9—1,4	60	S	99,1—99,6	0—0,2	0,2—0,4	94,7—94,9	4,7—4,9	0,1	0,1—0,2
8		1700	0,9—1,4	60	S	99,2—99,3	0,4—0,5	0,2—0,3	94,4—94,8	4,8—5,0	0,1	0,1

*Gas velocity referred to the cylindrical part of the system (D = 24 mm).
† S. = sintered-on; P. F. = fluidization with partial sintering-on; F. = normal fluidization.
‡The figures in brackets refer to the material sintered on to the walls of the reactor tube.

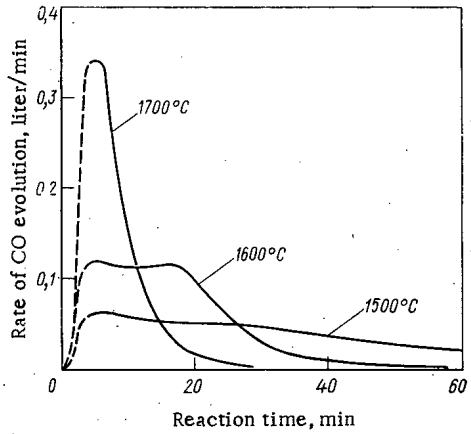

Fig. 3. Temperature dependence of the change in the carbon monoxide content of the effluent gases during the reaction of uranium dioxide with carbon.

Of considerable theoretical and practical value in determining the optimum mode is a knowledge of the mechanism of mass transfer in the UO_2-C system [6, 7]. According to the results obtained, mass transfer in the UO_2-C system is mainly based on two processes: the diffusion of the components through the layer of reaction products so created, and the evaporation of the oxide with its subsequent deposition on the carbon particles (sublimation–condensation). Whether the first or the second mechanism prevails depends on the temperature. At 1600-1800°C the main part is played by the diffusion of the components through the layer of reaction products. The microstructures of the intermediate products formed in the interaction between UO_2 and carbon show quite clearly that the formation of the carbide starts at the points of contact of the dioxide with the carbon (Fig. 4a); the presence of a carbide phase on the graphite lying close to the dioxide grain is not detected metallographically (Fig. 4b). With increasing temperature the role of carbiding by the evaporation and condensation of the UO_2 becomes more important.

TABLE 3. Results of Experiments on Producing Uranium Nitride in a Fluidized Bed (t = 1600°C, τ = 30 min)

Specified composition	Conditions of the reaction	Chemical analysis of the products, wt.%					Lattice constant, A ± 0,001	Actual composition
		U	C_{tot}	C_{Fr}	N	O		
$UC_{0,75}N_{0,25}$	P_{N_2} = 760 mm Hg (pure nitrogen)	92,00	3,38	2,65	4,45	<0,1	4,902	$UC_{0,19-0,21}N_{0,79-0,81}+C_{Fr}$
U 95,01 wt.% N 1,39 wt.% C 3,60 wt.%	P_{N_2} = 380 mm Hg (mixture Ar+N = 1:1)	92,90	3,68	1,90	4,00	0,1	4,915	$UC_{0,30-0,34}N_{0,66-0,70}+C_{Fr}$
U 95,01 wt.% N 1,39 wt.% C 3,60 wt.%	P_{N_2} = 80 mm Hg (mixture Ar+N = 10:1)	93,20	3,58	1,60	3,32	0,1	4,921	$UC_{0,41-0,42}N_{0,58-0,59}+C_{Fr}$

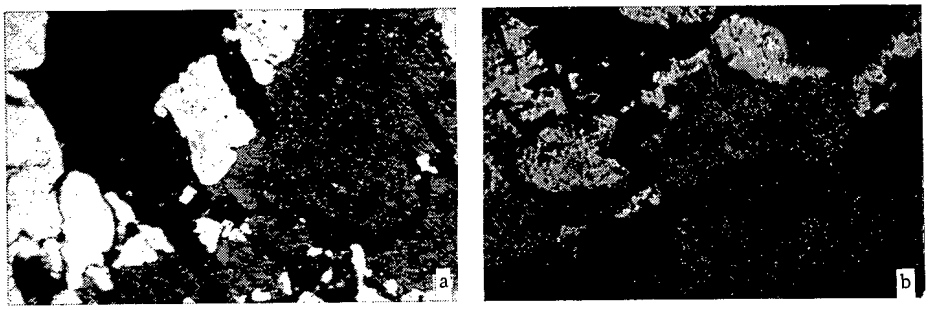

Fig. 4. Microstructure of the reaction products after the interaction of uranium dioxide with soot (a) for 10 min and with graphite (b) for 60 min at 1600°C (×1000).

When studying the production of uranium mononitride and carbonitride, the nitriding agent was nitrogen itself. The size of the original dioxide and coal-tar granules was as before (200-400 μ). We studied the reactions

$$UO_2 + C + N \rightarrow UN + CO; \quad (1)$$

$$UO_2 + C + xN \rightarrow UC_{1-x}N_x + CO. \quad (2)$$

We found that the velocity of reactions (1) and (2) was roughly twice that found when obtaining the carbide (Fig. 5). The final products contained no more than 0.1% oxygen, i.e., less than the monocarbide. A typical composition of the uranium mononitride (wt. %) was: U = 93.8-94; N = 5.5-5.7; C = 0.1-0.2; O < 0.1; lattice constant a = 4.889 ± 0.001 Å. The composition of the resultant carbonitride depended on the partial nitrogen pressure (Table 3). According to [6, 7] the carbonitride is in equilibrium either with the dicarbide (at a temperature of the order of 2000°C) or with carbon (at lower temperatures). We found that a carbonitride without any free carbon, containing no more than 40 mole % UC, could be obtained for a nitrogen pressure no greater than 80 mm Hg at 1600°C.

On increasing the nitrogen partial pressure from 80 to 380 and 760 mm Hg and processing a mixture intended to produce a carbonitride of composition $UC_{0.75}N_{0.25}$, alloys containing free carbon with compositions of $UC_{0.41-0.42}N_{0.58-0.59} + C_{Fr}$; $UC_{0.3-0.34}N_{0.66-0.70} + C_{Fr}$, and $UC_{0.2}N_{0.8} + C_{Fr}$, respectively, were obtained (Table 3). These results agree with thermodynamic calculations. The velocity of reaction (2) at a nitrogen pressure of 80 mm Hg is approximately the same as at 760 mm Hg, but diminishes on reducing the pressure further. The carbonitride containing free carbon is easily converted into a single-phase solid solution on subsequent vacuum heat treatment.

We verified the semicontinuous production of uranium monocarbide, mononitride, and carbonitride in our apparatus. Loading and unloading of the reactor were carried out in batches without cooling the furnace. The results are presented in Table 4, and some of the properties of the resultant powders in Table 5. These results thus indicate the fundamental possibility of producing refractory uranium compounds semicontinuously from the dioxide in a fluidized bed.

TABLE 4. Results of Experiments on Producing Uranium Carbide and Nitride in a Fluidized Bed at t = 1600°C

Specified composition	Chemical analysis of the product, wt. %					Phase and crystal lattice constant, Å ± 0.001
	U	C_{tot}	C_{Fr}	O	N	
UC (C=3,5%)	95,0—95,6	3,2—3,8	0,02—0,1	1,2—1,5	<0,01	UC; 4,950—4,953 UO_2; 5,468—5,469
UC (C=4,8%)	94,0—94,6	4,8—5,0	0,02—0,1	0,1—0,2	—	UC; 4,958—4,960
UC+UC_2 (C=7,0%)	93,0—93,2	6,8—7,0	0,1	0,1—0,2	—	—
UC_2 (C=9,5%)	89,5—89,8	9,0—9,4	1,1—1,4	0,3—0,5	—	—
UN	93,6—94,2	0,05—0,2	—	0,1	5,5—5,7	UN; 4,889

Note. The useful yield was in all cases 97.0-99.5 wt. %; the amount carried away by the gases averaged not more that 0.2 wt. %.

TABLE 5. Some Properties of the Powders Obtained in the Fluidized Bed

Property	Material		
	UC (C = 4.8-5.0)	UC_2(C = 9.0-9.4)	UN
Pyknometric density, g/cm³	12.1–12.6	10.1–10.7	12.4–13.6
Bulk weight without shaking down, g/cm³	5.2–5.6	3.2–3.4	4.6–4.9
Bulk weight after shaking down, g/cm³	5.4–6.0	3.4–3.6	5.1–5.3
Granular composition, %			
−630 + 400 μ	–	0.2	0.4
−400 + 315 μ	2.3	2.1	6.0
−315 + 200 μ	52.8	53.2	51.8
−200 + 100 μ	44.2	43.7	40.8
−100 + 150 μ	0.7	0.8	1.0

METHODS OF MAKING THE CORES

In developing methods of making the cores we allowed for the specific properties of the powders formed from the original compounds.

Manufacture of Cores Using Refractory-Compound Powders Obtained from the Metal

Pressing. The high degree of dispersion of the original powders enabled us to use only small quantities of binder and to eliminate the operation of drying the powder containing the binder.

Pressing was carried out in demountable molds when studying the effect of the pressing pressure on the characteristics of the cores and making small batches of cores for prereactor and reactor tests. Multiple-socket stamp and automatic presses were used in order to determine the best conditions of pressing the billets in large quantities, and also when producing large batches of cores for reactor tests.

As binder we used oleic acid, paraffin, and stearic acid dissolved in benzine or trichloroethylene. Preliminary experiments showed that the total quantity of solution mixed with the powder could be reduced to 1.5-3% for 1.5-2% of binder in solution. This is approximately 50-100 times less than the amount of binder usually employed when pressing samples from various powders. The stablest results were obtained on using paraffin. For pressing in the stamp and automatic presses we used previously-granulated powders. For this purpose the powder was molded at a pressure of 2-5 tons/cm² and then triturated through

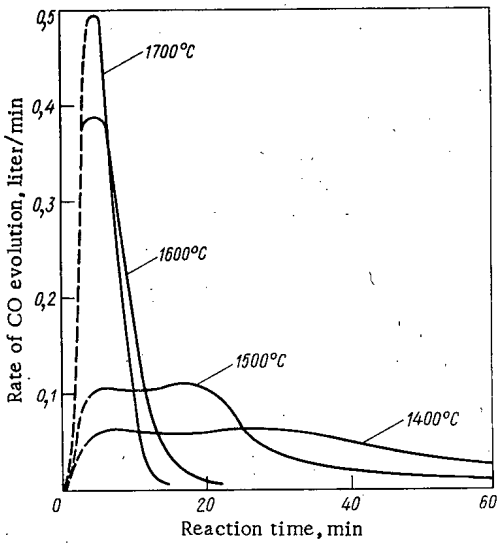

Fig. 5

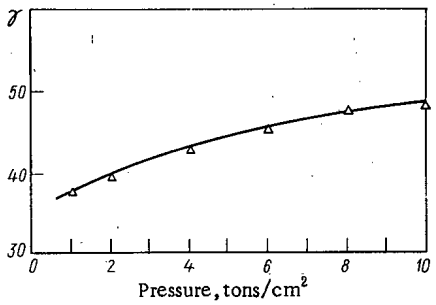

Fig. 6

Fig. 5. Temperature dependence of the change in CO content of the effluent gases in the reaction between uranium dioxide, carbon, and nitrogen.

Fig. 6. Change in the density of the pressed moldings as a function of pressing pressure (γ is the density expressed in percents of the theoretical value).

a sieve with a mesh size of 250 μ. This operation increased the bulk weight of the monocarbide and mononitride powders to 3.3-3.8 and 4.5-5.0 g/cm^3, respectively, improved their pouring characteristics, and facilitated volumetric dosing. Figure 6 shows the change in the density of the uranium monocarbide moldings due to the pressing pressure. The pressing of blocks in nondemountable molds (stamp and automatic presses) using the above-mentioned amount of binder is only permissible up to a pressure of 2.3-2.5 tons/cm^2. On raising the pressure further, the proportion of wastage increases sharply owing to overpressing. At a pressure of 1.3-1.5 tons/cm^2, mechanically strong samples are obtained in the form of bushings and tablets, with a 95-96% yield of usable products. The use of demountable molds enables the pressing pressure to be increased to 10-13 tons/cm^2 without overpressing the samples. The density of the monocarbide moldings then only increases substantially with rising pressure as far as 5-6 tons/cm^2. The diameter of the tablets extracted from the molds increases by 3.5-4%; their density equals 6.3-6.6 g/cm^3.

Sintering. The uranium monocarbide and carbonitride samples (containing up to 50% UN) are more appropriately sintered in vacuum in order to accelerate the compaction process. Carbonitride (over 50% UN) and mononitride samples are better sintered at up to 1500-1700°C in vacuum and then at a higher temperature in a nitrogen atmosphere.

It follows from the data relating to the sintering of the monocarbide (Figs. 7-11) that the compaction process takes place at a considerable rate and the sintering temperature is the decisive factor. Thus the density of the cores rises from 6.6 (original molding) to 12.3-12.6 g/cm^3 (90.5-92.5% of the theoretical density) in the first 30-40 min sintering at 1900°C. Increasing the period of sintering from 1 to 10 h raises the density of the cores by 4-5%. The specific pressing pressure (between 1.5 and 13 tons/cm^2) has hardly any effect on the density of the resultant samples if the sintering time is over 1.5 h (at 1700-2000°C). Increasing the height/diameter ratio from 0.35 to 2.1 reduces the density of the cores by 3-5%.

Sintering carbonitride (all compositions) and mononitride samples at 1900-2000°C in an argon and nitrogen atmosphere for 2-3 h gives finished articles with a density of 93-95% theoretical. Cores sintered above 1650°C usually exhibited no open porosity. In most cases there were fine pores 1-3 μ in diameter distributed uniformly both inside the crystals and along the grain boundaries (Fig. 11).

We see from a consideration of the microstructures that, on varying the composition of the cores from the stoichiometric uranium monocarbide, through the carbonitride, to the mononitride, the mean grain size changes from 20-50 to 20-30 μ (1900°C, 3 h). This may be explained by the slightly smaller surface activity of the mononitride powders. Even so, the surface activity of the powders of all the uranium compounds studied is fairly high, and ensures the formation of high-density cores (92-95% theoretical) in 2-4 h at 1800-1900°C, without any introduction of the amounts of surface-active additives usually employed

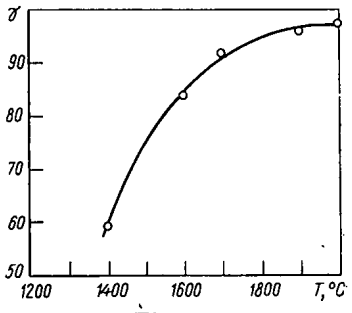

Fig. 7

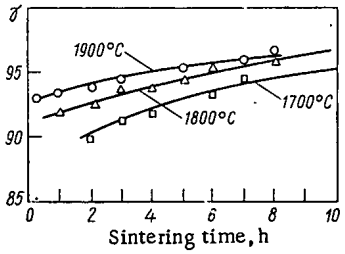

Fig. 8

Fig. 7. Change in the density of uranium monocarbide cores in relation to the sintering temperature.

Fig. 8. Change in the density of uranium monocarbide cores in relation to sintering time at 1700, 1800, and 1900°C.

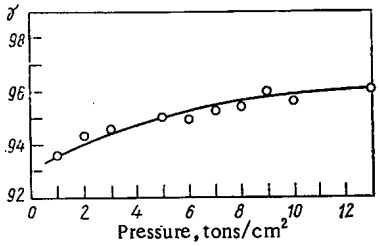

Fig. 9

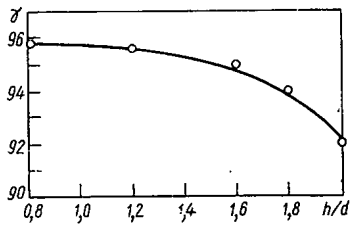

Fig. 10

Fig. 9. Change in the density of uranium monocarbide cores in relation to pressing pressure (1800°C, 5 h).

Fig. 10. Change in the density of the uranium monocarbide cores (1900°C, 3 h) in relation to the height/diameter ratio h/d.

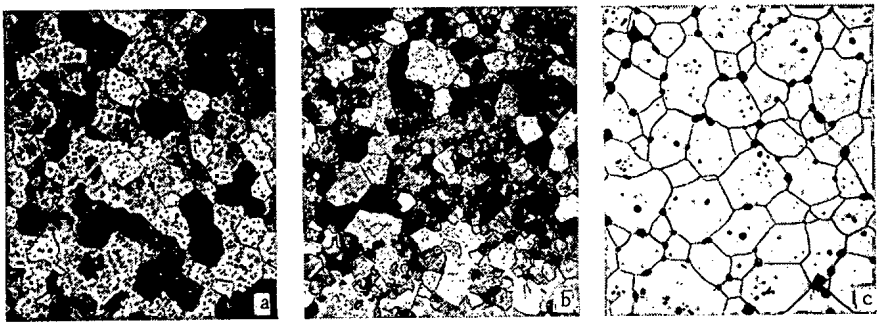

Fig. 11. Microstructure of monocarbide (a), carbonitride $UC_{0.75}N_{0.25}$ (b), and mononitride (c) cores. Magnifications (×200), (×200), and (×500), respectively.

in powder metallurgy or artificial activation of the sintering. As the amount of mononitride increases, the microhardness of the compound falls from 800-840 for the stoichiometric monocarbide to 730-760 kg/mm² for the pure mononitride. The amount of oxygen in the sintered samples is 0.05-0.1%.

On the basis of the foregoing investigations we made a decision regarding the methods to be used in preparing cores for radiation tests in the BOR-60 and SM-2 reactors. High-density uranium monocarbide cores were obtained in the form of tablets by pressing the charge at a pressure of 1.35-1.5 tons/cm² and then sintering in vacuum at 1800°C for 4 h. Before pressing, the charge was granulated by the method already described. The bulk weight of the granulated powder was 3.7 g/cm³. As a binder we used paraffin (0.03%). The diameter deviation of the cores fluctuated over the range ±0.05 mm.

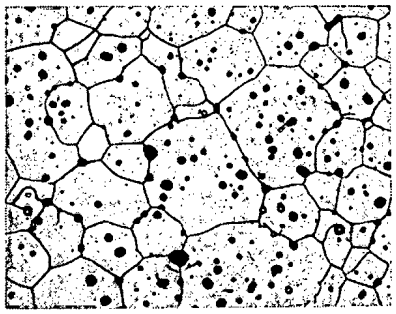

Fig. 12. Microstructure of uranium carbonitride $UC_{0.5}N_{0.5}$ rod cores. (×500).

Manufacture of Cores by Die Extrusion and Sintering

One of the most promising methods of making cores is die extrusion, which enables us to obtain rod-shaped cores with a high length/diameter ratio and with a constant diameter along the whole length.

As original material for the rod-shaped cores we used uranium carbide, sesquinitride, and carbonitride obtained from metallic uranium or uranium dioxide (Tables 1 and 5).

The powders of the original materials were mixed with a plasticizer, this being a solution of paraffin and raw rubber (60 and 40 wt. %) in trichloroethylene. The quantity of paraffin and rubber mixture so introduced equalled 5% of the weight of the mixture. From the air-dried, homogenized mass, cylindrical samples 7 mm in diameter were produced by die extrusion. The extrusion pressure for a pressed-mass temperature of 42-48°C was 480-500 kg/cm^2 and the extrusion velocity 1.2 m/min.

In order to obtain rod samples of satisfactory geometrical shape without any cracks, the arrangements for removing the plasticizer had to be carefully organized. For the corresponding experiments we used a thermal balance with a high-sensitivity quartz spring. The plasticizer was removed in vacuum at various heating rates; it was only completely eliminated at 800°C. For samples of the diameter indicated above, the permissible maximum evaporation rate of the binder components was 0.4 mg/cm^2 · min.

The original moldings were cut into rods of the desired length, stacked on graphite substrates covered with tantalum carbide, and placed in a furnace, in which they underwent low-temperature heat treatment as follows: heating in vacuum $1 \cdot 10^{-4}$ mm Hg at 100 deg/h up to 300°C, then at 50 deg/h to 500°C. This arrangement removed 80-85% of the plasticizer. Subsequent heating in order to sinter the cores was carried out at 400-500 deg/h. The optimum sintering temperature for the carbonitride rods was 0.85 T_m (T_m being the melting point of the material). No serious contortion of the rod cores occurred, and a density of 91-93% theoretical was obtained in a sintering time of 1 h. The sintering was carried out in specially pure nitrogen at a pressure of 1 atm. This form of heat treatment enabled us to obtain rods of uranium carbonitride of various compositions with an oxygen content of no greater than 0.02 wt. %, the sag in rods 100 mm long not exceeding 0.2 mm. The core samples usually had a single-phase structure (Fig. 12).

The foregoing experiments lead to the following brief conclusions: we have demonstrated the possibility of producing uranium sesquinitride from metallic uranium by a continuous process; we have determined the conditions for producing quality-standardized uranium monocarbide, mononitride, and carbonitride from the dioxide in a fluidized bed; we have determined the optimum conditions for manufacturing uranium carbonitride cores by static pressing and die extrusion, followed by sintering.

LITERATURE CITED

1. F. Gorle et al., Symp. on Thermodynamics of Nuclear Materials with Emphasis on Solution System, SM-98/48, IAEA, Vienna (1967).
2. O. Knacke et al., ibid., SM-98/14.
3. T. Sano et al., "Research on the production of uranium monocarbide," AERE-836 (1961).
4. T.S. Men'shikova et al., The Fourth Geneva Conference, USSR paper No. 454 (1971).
5. I. S. Golovnin et al., "Study of promising fuel composites based on uranium and plutonium carbide for fast reactors," At. Énerg., 30, No. 2, 211-216 (1971).
6. T. Lindemer et al., J. Amer. Ceram. Soc., 52, No. 5, 233 (1969).
7. R. B. Kotel'nikov et al., High-Temperature Nuclear Fuel [in Russian], Atomizdat, Moscow (1969).

R. I. Plotnikov and G. A. Pshenichnyi

FLUORESCENT X-RAY RADIOMETRIC ANALYSIS*

A NEW BOOK ON X-RADIOMETRIC ANALYSIS

Reviewed by Yu. M. Gurvich

x-Ray radiometric analysis has already been in use for two decades. It was first proposed as a variant of x-ray spectral analysis in which a high-level x-ray generator would be replaced by a low-level radioisotope source, and later on the appropriate instrumentation was developed, putting this line of work on an independent practical footing.

The portability and simplicity of the equipment, the wide range of elements subject to determination, the high precision and accuracy, ease of proximate analysis, and the low cost of carrying out analyses render the x-radiometric method both versatile and economical. To date, however, the x-radiometric method has not met with the widespread acceptance one might expect. The book by R. I. Plotnikov and G. A. Pshenichnyi, Fluorestentnyi Rentgenoradiometricheskii Analiz, V. A. Meier and N. I. Komyak (editors), published by Atomizdat must help to a certain extent in removing this shortcoming.

The book is in five chapters. The basic components of x-ray radiometric equipment are analyzed and discussed in detailed fashion (but electronic recording devices generally included in this line of equipment are not covered in the text), as well as techniques for eliminating factors disturbing the analysis (variations in the physical and chemical properties of specimens under analysis, and variations in the geometrical conditions of the measurements), and the discussion extends to cases of application of various methods of analysis in the solution of production problems. The equipment described gives some idea of the level of development of this domain of equipment and instrument design; tables of performance characteristics of both Soviet and foreign analyzers are provided.

A separate chapter deals with the physical fundamentals of the x-radiometric method. There is a definite interest in the material relating to effects of interaction between x-ray or γ-ray emission and matter. But the topics covered in this chapter are not readily accessible to analysts who constitute the natural reader audience of this book, because of their complexity. Moreover, there is lacking a rigorous analysis of the errors in the method and of the reasons for those errors. The appendix should have included a table of absorption coefficients, which would have been useful in practical applications.

Earlier books devoted to x-ray radiometric analysis (e.g., by A. L. Yakubovich et al., by N. N. Shumilovskii et al.), discussed the x-radiometric method and the conventional variant of x-ray spectroscopic analysis (using a dispersing crystal) as competing techniques. This book by R. I. Plotnikov and G. A. Pshenichnyi makes an attempt to delimit the ranges of application of both those modifications, and to map out the most promising areas of application of the x-radiometric fluorescent method. These areas of application include above all sampling of ore and rock in strip mining and underground mining, mass analysis of a restricted number of elements in a stream of material (moving on the conveyor belt, or conveyed through pulp lines or pipelines) or in samples, determination of coating thickness, and some cases where analysis of small absolute quantities of material is involved. The crystal diffraction method is more convenient for simultaneous or sequential multicomponent analysis of such complex objects as alloyed steels, many types of ores and products of ore beneficiation, and also materials to which silicate analysis has to be applied, and so forth. Even when we make use of semiconductor detectors capable of handling simultaneous determination of a large number of elements, reliance on the x-ray radiometric equipment for these problems is limited because of overloading of the amplifier circuitry by the radiation of the principal components. Hence the high threshold sensitivity of the x-ray radiometric method (10^{-3} to 10^{-4}%)

* Atomizdat, Moscow, 1973.

Translated from Atomnaya Énergiya, Vol. 35, No. 6, p. 386, December, 1973.

mentioned in the book can be actually realized only in isolated instances, in contrast to what is possible with the crystal diffraction method.

The x-radiometric method of analysis could achieve widespread acceptance only when simple and inexpensive equipment is produced in mass quantities. The book under review takes note of the modular design principle now gaining a foothold in Soviet and foreign x-ray equipment and instrument design in concepts of instruments backed up by a set of interchangeable sensors for analysis of a variety of objects.

On the whole, the book reviewed is of substantial interest since it provides the reader with a view of the development of the x-radiometric method and of the implementation of that method in industry. Unfortunately, the limited printing (total of 1650 copies) may leave the book inaccessible to workers in the numerous analytical laboratories who might otherwise be interested.

E. M. Lobanov, A. O. Solodovnikov,
B. I. Nudel'man, B. E. Krylov,
R. I. Gladysheva, N. S. Matveev,
R. M. Garaishin, I. I. Gulin,
and V. S. Chernukhina

RADIOISOTOPE BEARINGS IN INDUSTRIAL BUILDING MATERIALS*

Reviewed by A. Pugachev

The book goes into the solution of entirely new problems in the area of radioisotope monitoring and radioisotope-assisted automatic control of manufacturing and technological processes in the manufacture of building materials. The authors cite their original research and development work aimed at finding solutions to the most outstanding production problems. More specifically, the authors present the reader with their research findings and data on implementation of the γ-transmission method in inspection of the refractory lining of rotating kiln.

Attention is centered on monitoring the technological variables of the materials being processed in a given situation. The solution of problems of this type opens the way for automating fabrication processes, improving product quality, and achieving optimum control over the process. The research findings show that radioisotope techniques can be used successfully in ascertaining the degree of decarburization of materials directly within a rotating cement kiln, in measuring the permeability to gas of materials to be fired and sintered (sinter pyrite, sinter cake, clinker brick, pellets, etc.).

The present unavailability of instruments for such monitoring jobs puts difficulties in the way of controlling firing and sintering processes in some branches of the national economy. The results arrived at by these authors are therefore of wider interest than just the building materials industry.

A new technology, fluidized-bed firing, has not been lagging, and has been winning increasing favor. The research findings proved that the degree of firing of building materials in a suspended state or in a fluidized bed can indeed be monitored with the aid of ionizing radiations.

The readers will be able to familiarize themselves with the investigative procedures, with laboratory facilities and pilot plants developed by the authors. The physics topics covered in the text are well coordinated with topics in technology and production, all of which only adds to the value of the book.

The book is written in easy-to-read language, and will unquestionably be of definite interest both to specialists on the building materials industry and to specialists in other branches of the national economy.

* Atomizdat, Moscow, 1973.

Translated from Atomnaya Énergiya, Vol. 35, No. 5, p. 404, December, 1973.

E. Bujdoso (editor)

HEALTH PHYSICS PROBLEMS OF INTERNAL CONTAMINATION

PROCEEDINGS OF THE IRPA SECOND EUROPEAN CONGRESS ON RADIATION PROTECTION*

Reviewed by O. M. Zaraev

This compendium of articles contains the proceedings of the second European congress on radiation protection, which was held May 3-5, 1972. The physics society of the Hungarian Peoples Republic, in collaboration with the International Radiation Protection Association, sponsored the gathering (see Atomnaya Énergiya, 33, No. 4, 872 (1972)).

The compendium opens with an introductory report by the IRPA president W. Marley. The remaining 105 reports are broken down by subject matter into 11 sections: "Internal dosimetry" (9 papers), "Maximum permissible doses from some naturally occurring radioisotopes" (7 papers), "Estimates of internal exposure doses for some artificially produced radioelements" (6 papers), "Metabolism of radioelements" (17 papers), "Radiodetoxicological procedures and biological effects of internal exposure" (15 papers), "Protecting the population from internal exposure in connection with the operation of nuclear power plants and facilities" (6 papers), "Protecting the population from internal exposure to radioisotopes of natural origin and global fallout" (10 papers), "Spectrometry of human radiations" (7 papers), "Plutonium radiometry in vivo, analysis of secretions, measurement of aerosol activity" (10 papers), "Protection of professional workers against internal exposure" (15 papers), and "Various topics in internal dosimetry" (3 papers).

Close attention is given to analysis of the present state of the art and trends of further development in normalizing exposure levels for the population as a whole and for personnel in particular, to in-depth validation of the maximum permissible dose concept, and to improved calculation of absorbed dosage with due attention given to the microdistribution of radioisotopes in the organs and tissues of the human organism. In addition to the theoretical topics, methods and instruments for practical internal dosimetry are also discussed. Reliable estimates of internal contamination and exposure levels relying on direct measurements of human body radiation, and also on indirect data including the results of long-term analysis of body secretions, parameters of the metabolism, information on actual environmental pellution at the instant radioisotopes gain access to the organism.

Experimental data are furnished in abundance not only on the metabolism and kinetics of turnover of the radioisotopes of greatest importance in industry and scientifically, but also on estimates of the biological effects of small doses of those isotopes, as well as on stimulation of secretions and lessening of deposition of various radioactive elements through reliance on strong chelating complexing agents. Organization of radiation safety monitoring and inspection, and development of practical measures in the design and operation of enterprises and institutions utilizing radioactive materials were also discussed.

The wide scope of the various aspects of internal dosimetry covered, and the high level of scientific work reported on in the articles, are due in large measure to the work done by scientists of the socialist countries.

This collection of articles will be of great interest to research scientists, engineering physicists, physicians, and other specialists working in the field of radiation safety.

* Akademiai Kiado, Budapest, 1973.

Translated from Atomnaya Énergiya, Vol. 35, No. 6, p. 422, December, 1973.

N. Danila

NUCLEAR ELECTRIC POWER STATION*

Reviewed by Yu. Klimov

This book is a monumental monograph encompassing a broad range of topics in the engineering and costs aspects of nuclear power generation. The nine chapters of the text cover the state of power fuel resources on a worldwide basis, discuss the fundamentals of the theory of nuclear power reactors, thermal arrangements in various types of nuclear power stations, designs of nuclear reactors currently in service, layouts and special features of power generating and power handling equipment in nuclear power stations. Optimization of flowsheets and of the thermodynamical parameters of nuclear power stations, reactor monitoring and control and monitoring and control of the nuclear power station as a whole, biological shielding and the makeup of power station equipment, and also power station economics and economic optimization of power station parameters, are among the topics discussed.

The monograph is of a review nature, and cites a list of literature containing 431 reference titles, most of them works by Soviet specialists.

The very broad range of topics that the author decided to cover meant some sacrifice of detailed treatment, and of depth of treatment to a certain extent, so that the principal quality of the monograph, precisely the broadness of the subject matter, renders it particularly useful to those specialists who lack sufficient experience in the nuclear power field or are only beginning to specialize in that field.

* Editura Academiei Republicii Socialiste Romania, Bucuresti, 1973.

Translated from Atomnaya Énergiya, Vol. 35, No. 6, p. 446, December, 1973.

LIFE TESTS OF A THERMIONIC CONVERTER

E. S. Bekmukhambetov, V. I. Berzhatyi,
V. P. Gritsaenko, Yu. I. Danilov,
A. A. Dzhaimurzin, Sh. Sh. Ibragimov,
A. S. Karnaukhov, V. P. Kirienko,
I. M. Kuznetsov, O. I. Lyubimtsev,
V. A. Maevski, M. V. Mel'nikov,
V. K. Morozov, V. N. Ryzhikh,
V. V. Sinyavskii, and Zh. S. Takibaev

UDC 621.36

Reference [1] has described the basic results of reactor tests, of duration 220 h, of the two six-element thermionic ÉS-6-1 and ÉS-6-2 experimental assemblies, at an average electrical power density of 5 to 10 W/cm^2.

We have at least as great a problem in testing the similar ÉS-6-3 assembly, i.e., to check its operation and investigate its output characteristics at constant thermal reactor power over 1000 h.

The Experimental Assembly. In the form subjected to life tests the experimental assembly consisted of six thermionic electrical generator elements connected in series with the following parameters: the emitter material is a tungsten–rhenium alloy (27% Re); the collector material is niobium; the fissile material is uranium dioxide; the collector insulating material is aluminum oxide; and the interelectrode gap (in the cold state) is 0.3 mm.

To increase the probability of the interelectrode gap remaining sealed, the ES-6-3 included a vacuum guard cavity containing a distributed heat rejection system. The rest of the construction of the assembly and elements was the same as in [1].

Test Results. Life tests of the ÉS-6-3 were carried out on the general-purpose closed-loop facility of a water–water reactor with the following basic stages: operational outgassing of the assembly materials at reactor power giving maximum emitter temperature of $T_{e,\max} \approx 1700°C$; opening of a liquid cesium thermostat ampule and increase of thermal power q_F to attain an average electrical power density of $\overline{W}_{sp}$ = 5 to 10 W/cm^2 at $T_{e,\max}$ = 1800 to 1900°C, with the necessary investigations being performed at intermediate power levels; investigation of the assembly characteristics with q_F = const and with periodic smooth (smooth reduction) and abrupt (removal of reactor safety rods) changes of reactor power.

The ÉS-6-3 assembly was brought to a thermal power for which $\overline{W}_{sp}$ reached ~7 W/cm^2, and was subjected to life testing. Its static and dynamic volt–ampere characteristics were taken periodically; for the rest of the time it operated at an average current density of $\bar{j}$ = 6 to 10 A/cm^2. The total ÉS-6-3 test time was 2670 h.

The static volt–ampere characteristics obtained at the start of the life tests with q_F = const correspond to the discharge operating condition for all the six elements and agree well with the characteristics of similar assemblies tested earlier [1]. A comparison of the characteristics of the three assemblies for the initial test period is shown in Fig. 1.

The ÉS-6-3 assembly was operated for about 450 h at practically constant $\overline{W}_{sp}$. During that time a smooth change in the volt–ampere characteristics was observed, with an increase in the short-circuit current and a very slight reduction of W_{sp} at the optimum points; the rate of this process gradually diminished, and towards the end of the period in question the change in slope was arrested. There was a smooth increase in the optimum temperature of the cesium thermostat (by about 10°C). We can assume that these

Translated from Atomnaya Énergiya, Vol. 35, No. 6, pp. 387-390, December, 1973. Original article submitted February 28, 1973.

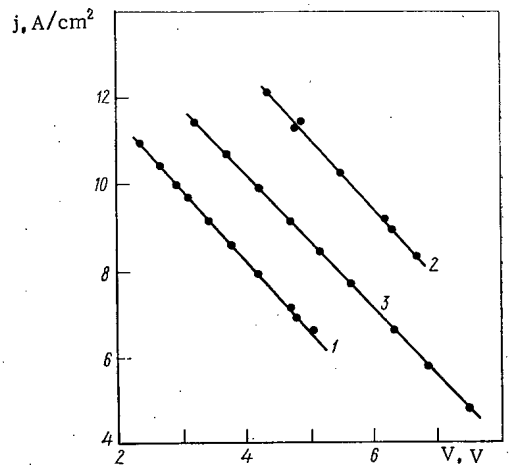

Fig. 1. Static volt–ampere characteristics of the three six-element assemblies: 1) ÉS-6-1, $\bar{q}_F$ = 53 W/cm²; 2) ÉS-6-2; $\bar{q}_F$ = 90 W/cm²; 3) ÉS-6-3, $\bar{q}_F$ = 68 W/cm². The cesium vapor pressure is optimum.

phenomena are interrelated and can evidently be explained by a change in the absorption of the electrodes.

During the 2670 h test period there were 16 smooth and 5 abrupt reductions of reactor power, followed by a smooth return to the previous power level. The smooth and abrupt power reductions led in almost all cases to some reduction in the output characteristics of the assembly, the volt–ampere characteristics showing both a change in slope at roughly constant short-circuit current, and also an equidistant shift.

The first type of characteristic change can be explained by short-circuiting of the electrodes of one of the elements. Short-circuiting of the first element was observed after the third removal of emergency protection after 444 h. It was established from readings of differential thermocouples that one of the central elements went out of action. After 1150 h there was apparently a short-circuit of a second element, and simultaneously a shift in the characteristics.

Later, after reactor shutdown, there occurred only an equidistant shift in the volt–ampere characteristics for q_F = const. Only during the last 600 h was no change observed in the output power. In this period there was also no drop in power between shutdowns of the reactor.

The variation in the volt–ampere characteristics for q_F = const during the life tests is shown in Fig. 2. Over the 2670 h the electrical power of the assembly decreased from 560 to 75 W.

The variation in the total power of the assembly during the tests is shown in Fig. 3. The arrows show the times of the smooth (PO_1, . . . , PO_{16}) and abrupt (AZ_1, . . . , AZ_5) reductions of thermal reactor power, as well as the variation in the support tube temperature T_{st}.

In the first 400 h of the tests the activity of gases evacuated from the interelectrode gap showed periodic sharp increases (Fig. 4), and then gradually decreased, stabilizing after 500 h of tests. This is evidence that in the first phase of the tests there is a breakdown in the sealing of the individual emitters, with subsequent spontaneous decrease in the leakage channels.

Discussion of Results. The main result of the tests is the long operating time (2670 h) of the ÉS-6-3 six-element thermionic assembly with sealed emitter subassemblies of the electrical generator elements, during which time a discrete reduction was observed in the electrical power of the assembly following any of the reactor shutdowns.

Besides short-circuiting of the elements, the main cause of assembly power reduction accompanying the equidistant shift in the volt–ampere characteristics must be an increase in the collector temperature T_C considerably above the optimum value T_C^{opt}. Theoretical investigations using the method described in [2] have shown that a deviation of T_C from T_C^{opt} shifts the volt–ampere characteristics at q_F = const essentially in an equidistant manner; for W_{sp} = 5 to 10 W/cm² an excess of T_C over T_C^{opt} of 200°C reduces the assembly power by roughly 25%.

The quantity T_C was not measured during the tests, but was determined by

$$T_C = T_{st} + \Delta T(q_{rej}),$$

where ΔT is the temperature drop at the collector stack, which depends on the heat flux q_{rej}. The introduction of an additional evacuated cavity in the ÉS-6-3 increased T_{st}, which was ~550°C at the start of the life tests. For ΔT = 250 to 300°C at the start of the tests $T_C \gtrsim T_C^{opt}$ for T_E = 1800 to 1850°C. During the tests T_{st} increased smoothly by 100°C (see Fig. 3), while $\Delta T(q_{rej})$ increased owing to the change in the thermal resistance of the multilayer collector stack. This resistance increase may be associated with plastic deformation of the stack materials and subsequent stratification during changes in the thermal conditions in the reactor shutdown periods. A similar explanation was given in [3] for the reduction by almost a factor of three in the electrical power of the thermal emission assembly tested for 1700 h in a reactor.

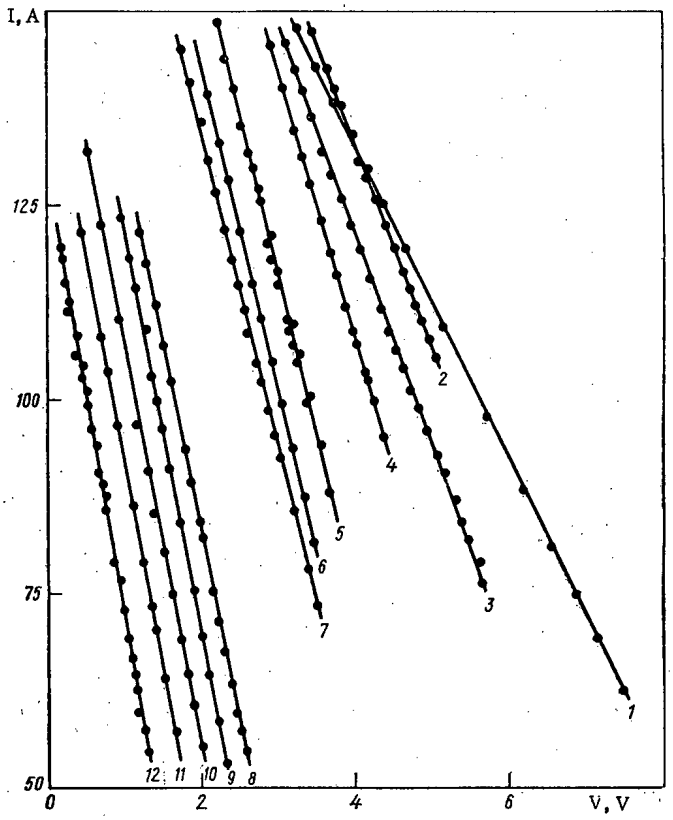

Fig. 2. Variation of the static volt–ampere characteristics of the ÉS-6-3 assembly during life tests at constant reactor power: 1) 45; 2) 178; 3) 295; 4) 395; 5) 440-823; 6) 1061; 7) 1145; 8) 1268-1438; 9) 1535-1644; 10) 1933; 11) 2045; 12) 2215-2672 h.

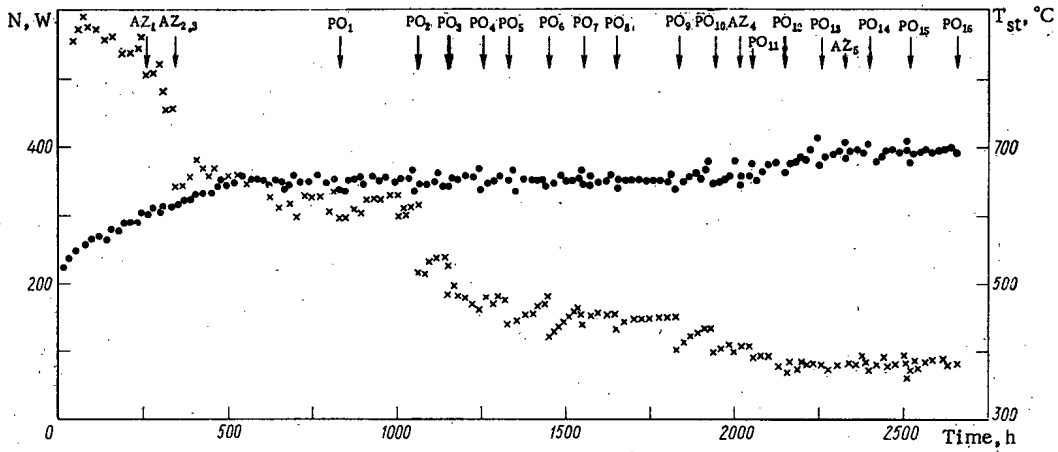

Fig. 3. Variation of the electrical powers (×) and of support tube temperature (•) during tests of the ÉS-6-3 assembly.

The reduction of assembly power due to increase in T_C is confirmed by the dependence of $\overline{W}_{sp}$ on q_F obtained during the initial and subsequent rises in reactor power. While $\overline{W}_{sp}$ increases linearly with q_F during the first power rise, i.e., analogous to [1], during subsequent upward steps in reactor power (beginning with a certain value q_F^*) the increase in $\overline{W}_{sp}$ with increase in q_F slows up noticeably because of the effect of T_C not being optimum (Fig. 5).

An evident possible additional cause for the reduction in the assembly output characteristics accompanying the equidistant shift is an increase of thermal loss from the emitter during the tests. This can be due to an increase of the surface area of contact when the spacers become imbedded in the electrode material, to an increase in the emittance of the electrodes because of condensation of nontransparent films on

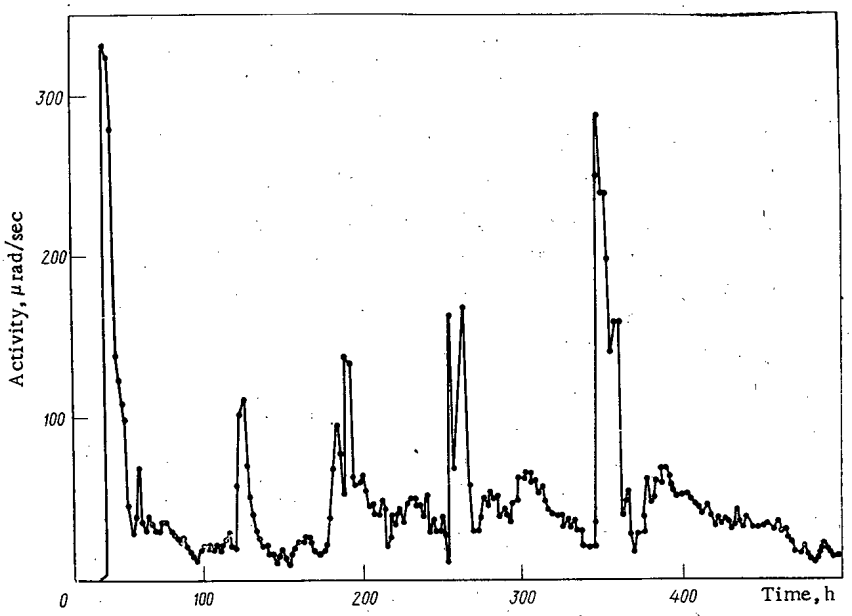

Fig. 4. Variation of the activity of gases at the assembly outlet in the first 500 h of tests of the ÉS-6-3 assembly.

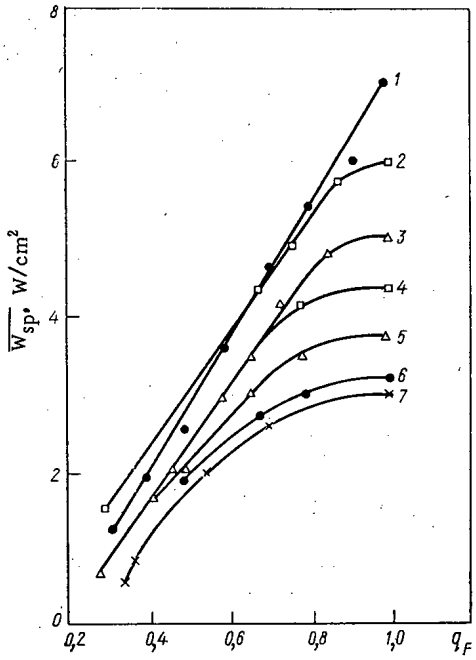

Fig. 5. Variation of the electrical power of the assembly during the increase in reactor power during the first 1000 h of tests: 1) first rise of reactor power; 2, 3) power rise after the first and second AZ removals; 4-7) power rise after the first, second, third, and fourth smooth reactor shutdowns, respectively.

the collector, and to an increase in loss of heat through the cesium vapor and other gases when the interelectrode gap decreases because of expansion processes.

The partial reduction of assembly power can be explained by the arisal and development of shunt resistances (of magnitude 10^{-2} to 10^{-3} Ω) between the element electrodes, coupled with simultaneous increase in leakage current through the collector insulation.

All these factors can evidently be coming into play (to different degrees at different times) during the life tests. Postreactor investigations of the test assembly will refine our knowledge of causes of variations in $\overline{W}_{sp}$.

Because the nonuniformities of energy production over the height of the assembly are larger than in [1], the value of $T_{e,\,max}$ is larger than in the ÉS-6-1 and ÉS-6-2 tests, and in fact in the first period of the tests $T_{e,\,max}$ = 1900-1950°C. For peripheral elements $T_{e,\,max}$ is 200°C lower, and for intermediate elements it is ~50°C lower than for the central elements. The departure from temperature uniformity of individual elements ($T_{e,\,max} - T_{e,\,min}$) is also greater than for previous assemblies.

The variation of $T_{e,max}$ during the tests depends on the reason for decrease in $\overline{W}_{sp}$: an increase of T_C with decrease of $\overline{j}$ would lead to an increase of $T_{e,max}$, whereas an increase in thermal losses from the emitter would decrease $T_{e,max}$. A final conclusion regarding the variation in $T_{e,max}$ requires special investigations.

CONCLUSIONS

The ÉS-6-3 six-element thermionic assembly has been tested in a reactor for 2670 h. During the tests the electrical power of the assembly decreased from 550 W, corresponding to a specific power of ~7 W/cm^2, to 75 W. A stepwise decrease in assembly power was observed following any reduction in reactor power; this is attributed to short-circuiting of individual elements, to irreversible increase in temperature of the collectors, and to possible increase in heat loss from the emitter.

LITERATURE CITED

1. V. I. Berzhatyi et al., Atomnaya Énergiya, 31, No. 6, 585 (1971).
2. Yu. A. Broval'skii et al., Report of the Second International Conference on Thermionic Energy Conversion [in Russian], Izd. VNIIT, Moscow (1969), p. 281.
3. M. Yaters et al., The Third International Conference on Thermionic Electrical Power Generation, Jülich FRG (June, 1972), Session C-34.

SPECTRA OF FILTERED NEUTRON BEAMS FROM THE OBNINSK REACTOR

E. N. Kuzin, S. P. Belov,
V. G. Dvukhsherstnov, V. M. Furmanov,
and N. N. Shchadin

UDC 539.125.5.18

The need for more precise nuclear physics data for fast reactor calculations has led to the creation of new methods for measuring various neutron interaction cross sections or their ratios. In recent times, filtered beams [1-3] based on the use of thick filters of various elements which have deep interference minima in the total cross section are being widely used along with methods which employ accelerators and the time-of-flight technique. Such filters, located in a well-collimated neutron beam from a high-power reactor, make it possible to produce a definite neutron spectrum at the end of the beam with the predominant neutron flux in a rather narrow energy range in the neighborhood of the interference minimum of the total cross section. By using this method, one can obtain sufficiently intense beams of quasimonochromatic neutrons which often have a low γ-ray background. Filters of scandium, iron, and silicon are most widely used in the energy region 1-1000 keV. Neutron spectra produced by means of such filters have strong peaks at 2, 24.5, 55, and 144 keV, respectively. To increase the monochromaticity of the filtered beams, supplementary filters are usually used which are made of materials that slightly change the intensity of the main peak and which remove neutrons of other energies from the beam. The value of filtered beams has been increased considerably by the development of a method for neutron spectroscopy using proton-recoil proportional counters [4, 5] which allows a detailed study of beam spectral characteristics and thus a determination of the optimal shape of the neutron spectrum.

This paper prevents measurements of neutron spectra from one of the horizontal beams of the reactor at the Obninsk atomic power station filtered with scandium, iron, and silicon; it also presents optimal sets of main and supplementary filters suitable for reactors such as that at the Obninsk atomic power station.

EXPERIMENTAL METHOD

Experimental Geometry. Spectra of neutrons filtered with scandium, iron, and silicon and with supplementary filters of sulfur, aluminum, titanium, manganese, and boron were measured at the uranium–graphite reactor of the Obninsk atomic power station for a thermal power of ~12 MW. The experimental geometry is shown in Fig. 1. The neutron beam emerges from the core-reflector boundary along a horizontal channel 50 mm in diameter and 5 m long through the graphite reflector and the reactor shield. The neutron beam emerging from the reactor shield is shaped by two iron-and-water collimators with openings 30 and 20 mm in diameter. Filters of scandium (99.85%), iron (Armco steel), and silicon (99.9%) are located in the 30-mm opening of the steel insert in the first collimation tank. Supplementary filters of titanium, manganese, cobalt, sulfur, and aluminum are set up ahead of the 20-mm opening in the second collimation tank, and a filter of ^{10}B is installed at the point where the neutron beam emerges into the experimental room. To decrease the γ-ray background, the collimation tanks are filled with an aqueous solution of boric acid and several lead collimators are installed along the beam.

Detectors. Cylindrical proportional counters filled with mixtures of hydrogen and methane were used to measure the neutron spectra. The counters were set up at the exit from the last lead collimator so that the axis of the beam was perpendicular to the axis of the counter. The counters are cylinders 32 mm in diameter with walls of stainless steel 0.5 mm thick; the collecting electrode is a tungsten wire 0.03 mm in diameter; the length of the sensitive volume (~100 mm) is bounded by field tubes; counter insulators are

Translated from Atomnaya Énergiya, Vol. 35, No. 6, pp. 391-395, December, 1973. Original article submitted April 11, 1973.

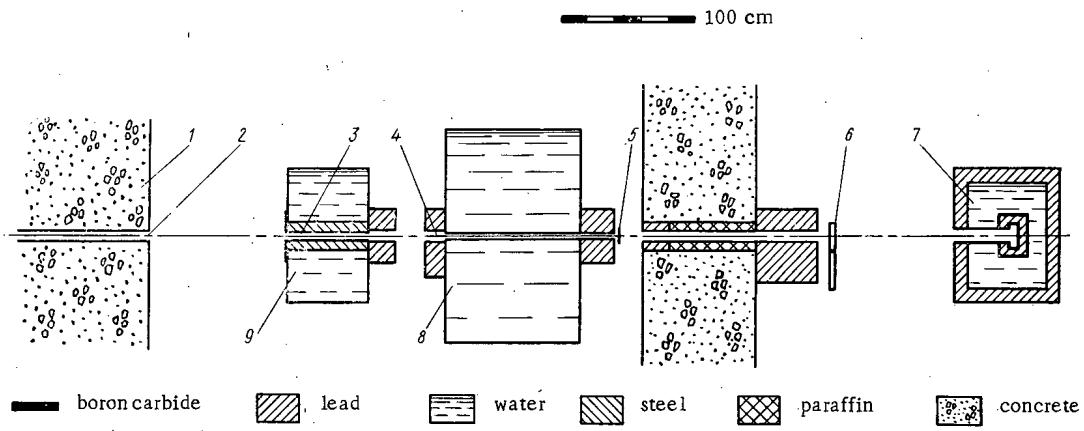

Fig. 1. Experimental geometry: 1) reactor shield; 2) neutron beam; 3) Sc, Fe, and Si filters; 4) Ti, Mn, Co, Al, and S filters; 5) ^{10}B filter; 6) neutron detector; 7) neutron "trap"; 8, 9) collimation tanks containing borated water.

TABLE 1. Characteristics of Proportional Counters

Counter	Gas mixture pressure, atm	Mixture composition	Collecting electrode operating voltage, V	Field tube voltage, V	Gas amplification factor	Useful energy region, keV
CHM-47	1	90% H_2 + 9,8% CH_4 + 0,2% ^3He	2200	1560	1500	1—15
CHM-38	3	90% H_2 + 9,5% CH_4 + 0,5% ^3He	2600	2300	80	10—300
CHM-39	4	95% CH_4 + 5% N_2	3400	3010	10	200—1300

made of glass. Other counter characteristics are shown in Table 1.

To amplify counter pulses, a fast, low-noise, charge-sensitive preamplifier with field-emission transistors at the input was used; the circuit is similar to that described in [6]. To reduce noise level and high-frequency pickup, great attention was paid to thorough shielding and careful arrangement of preamplifier parts.

The noise level of the preamplifier was estimated to be 20-40 keV for a gas amplification factor of one. Pulses from the preamplifier were then fed into a spectrometric nonoverloading amplifier with integration and differentiation time constants of 0.5 and 7.5 μsec. The energy scale of the spectrometer was calibrated in a thermal neutron beam by means of the peak resulting from the absorption of the total kinetic energy of the products of the reaction $^3He(n, p)^3H$ + 765 keV for hydrogen counters and of the reaction $^{14}N(n, p)^{14}C$ + 627 keV for the methane counter; it was also calibrated by means of pulses from an NZ-256 precision pulse generator. Generator pulses were fed into the preamplifier input which made it possible to monitor the stability of the entire amplification channel of the spectrometer. The pulse-height distributions from recoil protons were recorded with an NTA-512 analyzer. (Construction of the counters and preamplifier has been described in detail [7].)

Instrumental distributions of recoil-proton pulses were converted into neutron energy spectra by "sliding strip" differentiation [8]. Corrections for wall effect were not introduced into the neutron energy spectra since few high-energy neutrons were contained in the measured spectra. It is assumed that inclusion of this effect would lead to corrections of no more than 5-10% in the spectra.

RESULTS

Scandium Neutron Beam at 2 keV. To produce a neutron spectrum with an intense peak at 2 keV, a neutron beam from the uranium–graphite reactor at the Obninsk atomic power station was sent through a metallic scandium filter 219 g/cm^2 thick. It turned out that a large number of neutrons with energies from 8 to 100 keV were present in the neutron spectrum in addition to the strong peak at 2 keV. In such a situation, the problem of monochromatization is solved in two ways: either one increases the thickness of the main filtering element or one selects additional filters made of elements which have peaks in their total neutron cross sections at those energies where the total cross section of the nuclei in the main filter has a minimum.

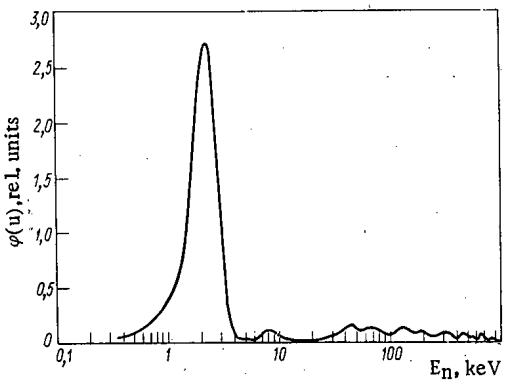

Fig. 2

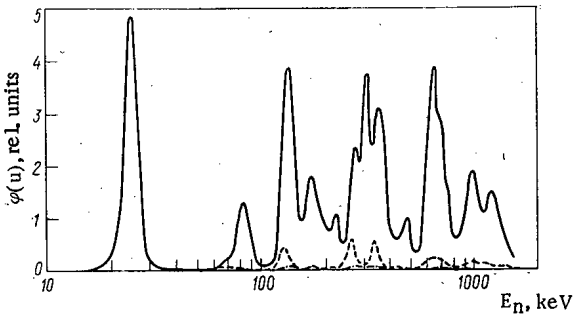

Fig. 3

Fig. 2. "Signal" neutron energy spectrum for scandium beam.

Fig. 3. Neutron energy spectrum of iron beam at the Obninsk atomic power station reactor. Filter thicknesses (in parentheses), g/cm^2: ———) Fe(240); – – –) Fe(240), Al(40.5), S(5.7), ^{10}B(0.2); – . – . –) neutron "signal" spectrum.

TABLE 2. Neutron Groups in Scandium Beam

Energy range, keV	Relative intensity	Energy range, keV	Relative intensity
0,6—4,0	1,00	200—400	0,02
4,0—20	0,03	400—800	0,02
20—100	0,07	>800	0,00
100—200	0,04	>4,0	0,18

However, increase in the thickness of the main filtering element inevitably leads to a loss of intensity in the selected neutron peak; in selecting supplementary filters, it is also necessary to take care that the total cross sections of the nuclei in these filters are small in the energy region of the selected peak.

In this work, the problem of monochromatization was solved by a basically different means: the neutron spectrum emerging from the filters is not monochromatized but rather a certain "signal" spectrum. The "signal" spectrum for any beam is defined as the difference between the "signal + background" (S + B) spectrum and the "background" (B) spectrum, where the "signal + background" is the neutron spectrum after the filter set with a selected peak, the intensity of which is comparable to the total intensity of all neutrons of other energies; "background" is the neutron spectrum measured after the same set of filters plus one or more additional filters which most efficiently absorb neutrons in the selected peak. Thin filters of ^{142}Ce and Mn, which have total cross-section maxima in the region of 1.3 and 2.38 keV, can be recommended as supplementary filters for the measurement of background in the scandium beam.

Figure 2 shows the "signal" neutron spectrum for the scandium beam with scandium and titanium filters 219 and 6.7 g/cm^2 thick, respectively. The "background" spectrum was measured with a supplementary manganese filter 4.5 g/cm^2 thick; the titanium filter was used to suppress a strong neutron peak at ~8 keV. In Fig. 2, the scandium peak is shifted somewhat to the high-energy side; however, if one takes into account the behavior of ion-formation energy in hydrogen in the region below 10 keV [9], the peak is displaced to an energy of 2 keV. The width of this peak at half-height is 1.3 keV (the natural width of the scandium peak is ~0.7 keV) and the intensity of the neutron flux is $\sim 5 \cdot 10^4$ N/cm^2 · sec. Table 2 gives the relative intensities of various neutron energy groups in the "signal" spectrum of the scandium beam.

It was established that there are practically no γ-rays in the scandium beam through an evaluation of the γ-ray background in the experiments by replacement of the manganese filter with a cobalt filter having the equivalent γ-ray attenuation which attenuated the 2-keV neutron flux very little (~10%).

Iron Neutron Beam. Figure 3 shows the energy spectrum of neutrons filtered by a comparatively small thickness of iron (Armco steel), aluminum, and sulfur, and also one of the "signal" neutron spectra. All spectra shown in Fig. 3 are normalized with respect to the peak intensity at 24.5 keV. The energy location of spectral peaks and also the nature of the spectral changes resulting from the introduction of supplementary filters for monochromatization of the beams corresponds to the structure in the total cross section. The intensity of the peak at 24.5 ± 1.0 keV is $2 \cdot 10^4$ N/cm^2 · sec at the detector position for an iron filter 240 g/cm^2 thick. Table 3 gives the relative intensities of various neutron energy groups in the iron beam spectrum from the reactor of the Obninsk atomic power station.

TABLE 3. Neutron Groups in Iron Beam

energy interval, keV	Relative neutron intensity, beam 1	2	3	4	5	6	7
17—30	1	1	1	1	1	1	1
30—100	0,231	0,032	0,004	0,013	0,000	0,037	0,003
100—200	0,941	0,167	0,021	0,068	0,008	0,131	0,009
200—500	1,615	0,413	0,040	0,158	0,022	0,171	0,025
500—800	0,784	0,180	0,019	0,057	0,004	0,080	0,012
> 800	0,907	0,248	0,017	0,052	0,002	0,105	0,014
> 30	4,478	1,04	0,101	0,348	0,036	0,524	0,063
Relative intensity of 17-30 keV group	1	0,74	0,58	0,52	0,40	0,98	0,82

Note. Composition of filters used (numbers before symbols for elements indicate filter thickness in g/cm^2):
Beam 1: 240 Fe.
Beam 2: 240 Fe + 18.9 Al + 5.7S + 0.2 ^{10}B.
Beam 3: S = (S + B) − B; (S + B) = 240 Fe + 18.9 Al + 5.7S + 0.2 ^{10}B; B = 240 Fe + 18.9 Al + 5.7S + 0.2 ^{10}B + 3.4 Ti.
Beam 4: 240 Fe + 40.5 Al + 5.7S + 0.2 ^{10}B.
Beam 5: S = (S + B) − B; (S + B) = 240 Fe + 40.5 Al + 5.7 S + 0.2 ^{10}B; B = 240 Fe + 40.5 Al + 5.7S + 0.2 ^{10}B + 3.4 Ti.
Beam 6: 162 Fe + 40.5 Al + 5.7S + 0.2 ^{10}B.
Beam 7: S = (S + B) − B; (S + B) = 162 Fe + 40.5 Al + 5.7S + 0.2 ^{10}B; B = 162 Fe + 40.5 Al + 5.7S + 0.2 ^{10}B + 3.4 Ti.

TABLE 4. Neutron Groups in Silicon Beam

Energy interval, keV	Neutron ("signal") beam at 55±5 keV	Neutron ("signal") beam at 134±14 keV	Neutron beam at 144±15 keV
	relative intensity		
20—40	0,041	0,000	0,002
40—65	1	0,008	0,064
65—100	0,145	0,001	0,020
100—200	0,047	1	1
200—600	0,001	0,002	0,006
600—1000	0,024	0,008	0,012
> 1000	0,077	0,019	0,036

It is clear from Table 3 that a "signal" spectrum without marked loss of intensity in the main peak at 24.5 keV but with noticeable improvement in the degree of monochromatization is obtained by the introduction of a supplementary titanium filter 3.4 g/cm^2 thick for measurement of the "background" spectra of the iron beam.

Silicon Neutron Beam. Figure 4 shows the neutron spectrum from a silicon filter 118 g/cm^2 thick and a supplementary titanium filter 7.9 g/cm^2 thick for suppressing neutrons with energies of 50-60 keV. The positions of the peaks correspond to neutron energies of 144 and 50 keV where there are deep minima in the total cross section of the silicon nucleus. The difference in the position of the 50-keV peak from the data of [3] is caused by the supplementary titanium filter; the behavior of the total cross section in titanium at 50-60 keV explains the shift. Measurement of the "background" spectrum for the neutron beam at 144 keV by means of a sulfur filter 5.7 g/cm^2 thick made it possible to obtain a "signal" spectrum with a neutron peak at 134 keV and a high degree of monochromaticity. Neutron fluxes at 144 ± 15 and 134 ± 14 keV are $8 \cdot 10^4$ and $4 \cdot 10^4$ N/cm^2 · sec.

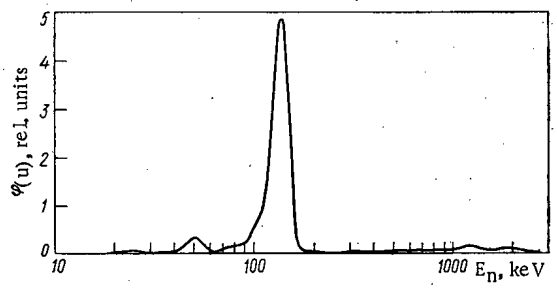

Fig. 4

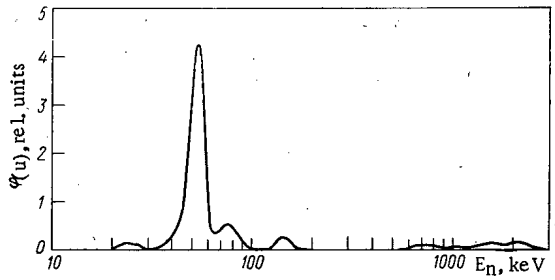

Fig. 5

Fig. 4. Energy spectrum for neutrons in 144-keV silicon beam. Filter thicknesses, g/cm^2: Si(118), Ti(7.9), ^{10}B(0.2).

Fig. 5. Energy spectrum of neutrons in silicon beam ("signal") at 55 keV. Filter thicknesses, g/cm^2: "signal + background") Si(87.9), S(34.6), ^{10}B(0.2); "background") the same filters plus Ti(7.9).

Using a main filter of silicon 87.9 g/cm^2 thick, a supplementary filter of sulfur 34.6 g/cm^2 thick to suppress 144-keV neutrons, and a titanium filter 7.9 g/cm^2 thick to measure the "background" spectrum (i.e., to suppress the peak in the region of 50-60 keV), a "signal" neutron spectrum was obtained with good separation of the peak at 55 ± 5 keV and an intensity of ~10^4 N/cm^2 · sec.

The energy spectrum of neutrons in the silicon beam at 55 keV is shown in Fig. 5. Table 4 shows the relative intensity of various neutron energy groups for the peaks at 55 ± 5 and 134 ± 14 keV, which were obtained as "signal" spectra, and for the 144-keV neutron beam.

For the silicon neutron beams, the γ-ray background was taken into account by means of measurements with an additional thin water filter and calculation of γ-ray and neutron attenuation by this filter.

In conclusion, the authors express their gratitude to Yu. A. Kazanskii for valuable advice and discussions of the results and also to A. F. Gamal for kindly supplying the silicon filter.

LITERATURE CITED

1. O. Simpson and L. Miller, Nucl. Instrum. and Methods, 61, 245 (1968).
2. D. L. Broder et al., Preprint FÉI-200 [in Russian], Obninsk (1971).
3. O. Simpson et al., Proceedings of the Third Conference on Neutron Cross Sections and Technology, CONF-710301, Vol. 2, Knoxville (1971), p. 598.
4. E. Bennett, Nucl. Sci. and Eng., 27, 16 (1967).
5. P. Benjamin et al., Nucl. Instrum. and Methods, 59, 77 (1968).
6. R. Letourneau et al., Nucl. Instrum. and Methods, 70, 106 (1969).
7. E. P. Kuzin et al., Preprint FÉI-291 [in Russian], Obninsk (1971).
8. K. Lantsosh, Practical Methods of Applied Analysis [in Russian], Fizmatgiz, Moscow (1961), p. 327.
9. H. Werle et al., Nucl. Instrum. and Methods, 72, 111 (1969).

OPERATION OF A COLD TRAP FOR SODIUM IMPURITIES

L. G. Volchkov, M. K. Gorchakov,
F. A. Kozlov, V. V. Matyukhin,
Yu. P. Nalimov, and B. I. Tonov

UDC 621.039.534

Studies [1, 2] have shown that one should know the effects of various parameters, including those dealing with structural design, on the distribution of impurities precipitated throughout a trap in order to guarantee optimal performance of a cold trap for sodium impurities (impurity content, productivity). However, the investigation of this distribution has been conducted after the testing of the traps and only for certain operations.

In this paper, particular consideration is given to this problem and to the study of heat exchange processes. The studies are conducted on a gas-cooled cold trap. During the tests, the sodium was "contaminated" with sodium peroxide.

An experimental trap is represented in Fig. 1a. An internal regenerator for the trap is achieved in the form of coils of tubes 25 × 2 mm in size with an average diameter of 150 mm and a 52 mm pitch. The coils are located in the dump tank and the final cooling zone. The density of the packing (stainless steel chips) in the absorbers, embedded in parallel, increased in the direction of flow of the metal: 70, 140, and 200 kg/m^3.

The air cooling the trap was distributed through three chambers embedded in parallel (zones I, II, and III below, counting from the absorber). In order to intensify heat transfer to the air [3], 5 × 2 mm transverse, rectangular fins are arranged 7 mm apart on the casing of the trap.

The coefficients of heat transfer in the different zones, the temperature distribution along the height and diameter, the diffusion characteristics, and the oxide content and its distribution along the height and diameter of the trap were determined.

The distribution of the oxides along the height of the trap were measured periodically in proportion to the accumulation of impurities in it. For these purposes, the trap was examined using γ-rays. The absorption of γ-rays by the oxides accumulating in the trap was determined in the following manner. Initially, when the trap is filled with pure sodium, measurements were conducted at selected points. At the same time, we recorded the signal with a second instrument and a combined thickness of a specially selected stack of steel plates guaranteeing the maximum possible absorption of the γ-rays.

The absorption of γ-radiation by a trap increases in proportion to the accumulation of oxides in it. Compensation of this absorption is achieved by decreasing the number of plates in the stack placed at the outlet for the beam of γ-rays from the collimator of the source assembly. The difference in the total thicknesses of the plates (h mm of steel) for these measurements and the readings of the second instrument is a measure of the variation in the concentration of the oxides in the volume being examined with the γ-radiation. In order to eliminate errors connected with the occurrence of cavities in the trap and with a variation in the temperature, we measured the absorption of the γ-rays during continuous circulation of the sodium through the trap under stationary temperature conditions.

The source assemblies and ionization chambers were moved lengthwise along the trap and across its diameter by special apparatus with traversing equipment (precision of apparatus is ±2 mm). We utilized a special instrument for continuous measurement of the hydrogen in the sodium [4]. During contamination

Translated from Atomnaya Énergiya, Vol. 35, No. 6, pp. 396-400, December, 1973. Original article submitted April 7, 1973.

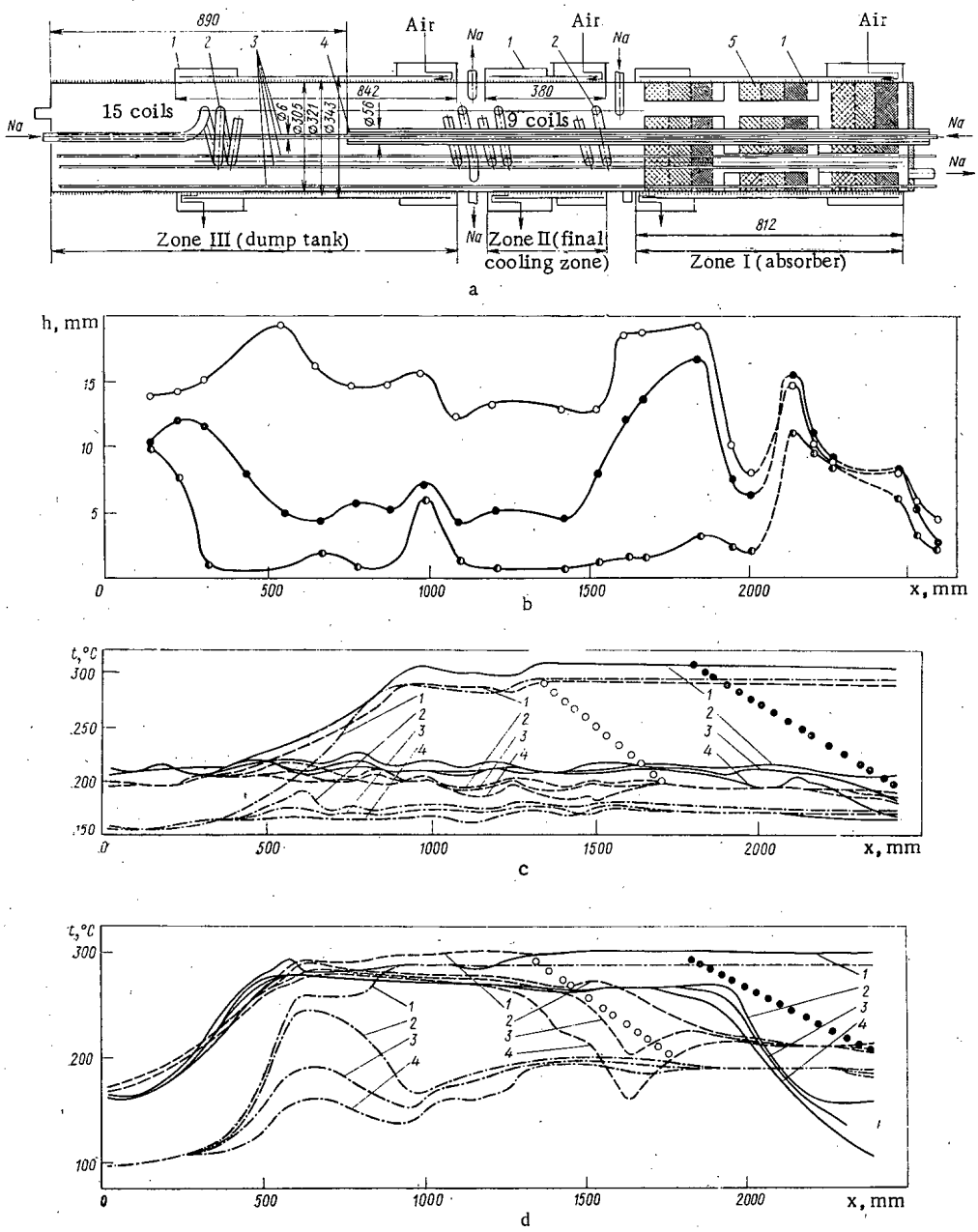

Fig. 1. Diagram of cold trap and distribution of temperature and sodium oxide along its height. a) Diagram of cold trap: I) air-cooling chamber; 2) regenerator coil; 3) mobile thermocouple containers; 4) 18 mm diameter center pipe; 5) absorber. b) Distribution of sodium oxide G_{Na_2O} along the height of the trap: ◑) 14; ●) 63; ○) 111 kg. c) Temperature fields inside the trap for $G_{Na_2O} = 0$ and $G_t = 0.9$ m^3/h: ———) temperature for $Re_{aI} = 5.3 \cdot 10^4$, $Re_{aII} = Re_{aIII} = 0$; – – –) temperature for $Re_{aII} = 5.6 \cdot 10^4$, $Re_{aI} = Re_{aIII} = 0$; – · – · –) temperature for $Re_{aIII} = 4.5 \cdot 10^4$, $Re_{aI} = Re_{aII} = 0$; 1, 2, 3, 4) thermocouples located 0, 54, 100, and 144 mm, respectively, from the axis of the trap; ●) behavior of the theoretical average temperature of the sodium for cooling only in the absorber; ○) the same for cooling only in the final cooling zone. d) Temperature fields in the trap: ———) temperature inside the trap for $G_{Na_2O} = 35$ kg: – – –, – · – · –) temperature inside the trap for $G_{NaO_2} = 87$ kg (remaining conditions and symbols as in c).

of the coolant by sodium peroxide, the plugging temperature T of a plugging meter did not exceed 540°K. Otherwise, the method of testing is similar to that described in [2].

In addition to the coefficients of heat transfer, we calculated the total amount of heat in the sodium carried off by the air:

$$Q_t = [GC_p\rho\,(t'-t'')]_t - [GC_p\rho\,(t''-t')]_{u.\,cl} - [GC_p\rho\,(t''-t')]_{l.\,cl}$$

where Q is the heat flow, W; G is the flow rate, m^3/h; t is the temperature of the sodium, °C; C_p is the specific heat at constant pressure, J/kg·deg; ρ is the density, kg/m^3. The distribution of the heat-flow relative to the cooling zones occurred in proportion to the flow rates and heating of the air:

$$Q_i = Q_t \frac{[GC_p\rho\,(\theta''-\theta')]_{ai}}{\sum_i [GC_p\rho\,(\theta''-\theta')]_{ai}},$$

where θ is the temperature of the air, °C. The indexes in the equations here and below denote: t) trap; l. cl, u. cl) lower and upper coils; a) air; m) mobile thermocouple; one prime) inlet; two primes) outlet; i = I, II, III) zone number.

An exact determination of the average temperature of the sodium is impossible due to the strong influence of longitudinal heat overflows (low Pe = wd/a numbers), the complex hydrodynamics, and the thermal interaction of the zones. In this connection, we took the reading of the mobile thermocouple (t_m), located 54 mm from the axis, for the average calorimetric temperature of the sodium at a given cross section of the trap in zones I and II, i.e., it was assumed that $\bar{t}_i = \bar{t}_{mi}$ (i = I, II). The approximation $t'_{III} \approx t'_t$ is utilized in the dump tank for determining the temperature of the sodium. The coefficients of heat transfer were calculated from the equations:

$$k_i = \frac{Q_i}{F_i(\bar{t}_{mi} - \bar{\theta}_i)}, \quad i = \text{I, II};$$

$$k_{III} = \frac{Q_{III}}{F_{III}(t'_t - \bar{\theta}_{III})},$$

where k is the coefficient of heat transfer, $W/m^2 \cdot deg$; F is the heat exchange area, m^2; for the contaminated surfaces F_i, we took an equal surface, free from impurities.

The diffusion characteristics obtained for a cold trap (the time dependence of the plugging temperature of the plugging meter on the operating conditions) were used for finding

$$\beta = \ln\frac{C_0 - C_f}{C - C_f} \Big/ \frac{G}{V}\tau,$$

where V is the volume of sodium in the loop at the temperature of the inlet to the trap, m^3; τ is the decontamination time, reckoned from the moment of measurement of C_0; C_0, C are the initial and instantaneous concentrations of oxygen in the sodium, wt. %; C_f is the final saturation concentration of oxygen in the sodium at the temperature of the air from the trap, wt. %. The transformation from the plugging temperature to the oxygen concentration was achieved by means of the equation

$$\lg C = 1{,}2 - \frac{1900}{T}.$$

During the testing of the trap, we measured the distribution of the oxides in its volume five times in three planes: along the diameter of the trap and at distances of 80 and 100 mm from the axis (Fig. 1b). The initial oxide deposits were distributed, primarily, in the absorber and the bottom of zone III. Subsequently, the oxides were distributed in zone II, in the first and second sections of the absorber, and in the middle of zone III. Thus, after approximately 14 kg of oxide had accumulated in the trap, only two of the three sections of the absorber functioned, and the accumulation of oxides in them practically ceased after that, as a significant amount of impurities settled in the outlet of zone II (the trap accumulated 63 kg of Na_2O). The location of high impurity precipitation was then shifted downwards in zone II, moving away from the absorber, and rose in zone III. The concentration of precipitate formed at the beginning of the tests varied little afterwards.

Let us consider the time dependence of the temperature distribution in the trap. It follows from Fig. 1c, d that the combined action of free and forced convection appears to be the principal phenomenon determining the processes in the trap. In a "clean" trap, natural convection results in an equalizing of the temperature field along its height. An increase in the temperature at the wall during removal from the bottom of the trap (see Fig. 1c) indicates that the motion of the metal is directed downwards just at the wall. Only in this manner can one explain the downward buildup of a cold layer in zone II and its gradual thinning in zone III, where surface cooling under the given conditions was absent.

It is obvious that the flow rate for the metal moving upward through the interior of zone II must be higher than the average flow rate through the trap. One can estimate its value using the equation

$$G_1 = G_t\,(t_t' - t_2)/(t_1 - t_2),$$

which is obtained from the conditions for the heat balance and the flow-rate balance for the rising (G_1, t_1) and falling (G_2, t_2) flows in zone II ($G_1 t_1 \approx G_t t_t' + C_2 t_2$; $G_1 = C_2 + G_t$). In accordance with the experimental results, if the readings of the second and fourth mobile thermocouples are taken at t_1 and t_2 ($t_2 \approx 195°C$, $t_t' = 297°C$, $t_1 = 206°C$), then $G_1 \approx 9G_t$.

The wall flow falls below the heat-transfer region and is mixed with the hot sodium entering the trap; as a result, the temperature of the metal falls sharply at the inlet to the dump tank irrespective of the point of heat removal by the air.

The results of the tests show that natural convection develops during the cooling of every zone; however, its effect is reduced in those regions where a significant quantity of oxides is precipitated.

A hot "jet" is located just below the inlet for the metal in zone III. The greater its penetration depth, the higher the inlet velocity of the sodium and the lower the sodium–air temperature difference [5]. A region of practically stationary cooled metal, which is formed because of the heat losses and the descent of the cold metal at the wall of the trap, is found beneath the "jet" as far as the bottom. The hydrodynamics of the upper part of zone III has an extremely complex character and is distinguished by an intensive mixing of cold and hot flows. The fact that the range of the fluctuations in the temperature of the region between the "jet" and the downward flow at the wall reaches 30°C attests to this.

The temperature fields vary substantially during the accumulation of oxides in the trap (see Fig. 2d). Their analysis shows that the oxides are distributed nonuniformly in the trap. The effect of the composite convection on the temperature distribution diminishes longitudinally; the longitudinal temperature gradient in the sodium flow approaches the theoretical value.

From an analysis of the temperature distribution in the trap, it follows that under testing conditions the precipitation of the oxides could occur in practically the entire volume of the trap, with the exception of the hot "jet" region. An intensive accumulation of oxides in zone I and the bottom of the dump tank during the initial period of testing is explained by the divided mass exchange surfaces in the absorber and the sedimentation processes in the dump zone. Hence, the region of intensive circulation is confined to zone II in proportion to the accumulation of oxides in the inlet section of the absorber; its permeation of the latter is inhibited. As a result, the region of intensive mass exchange is distributed near the inlet to the absorber at the end of zone II. The accumulation of impurities in this region results in a further shift downwards of the region of intensive circulation, and the layer of oxide formed at the end of zone II begins to function as the absorber. Thus, the coolant, whose concentration of impurities is close to saturation at a given temperature, enters the absorbers and the further accumulation of impurities in them takes place very slowly. At the same time, the retention coefficient for oxygen in a contaminated trap (the weight of $Na_2O > 63$ kg) with by-passing of the absorber by the sodium is approximately one. After 14 kg of sodium oxide has accumulated in the trap, only two of the three sections, arranged in parallel, of the absorber were actually functioning; this is explained by the clogging of the bypass tubes with impurities. This was verified upon sectioning the trap in order to analyze its contents after the tests.

The slight increase in the concentration of impurities in the lower part of the dump zone (~250 mm from the bottom) with further accumulation of them in the superincumbent regions is explained by cessation of the circulation of the coolant in this region after formation of the deposit and the absence of temperature gradients in it. Consequently, the impurities are not carried upward into this zone by the sodium flow and the deposit formed is concentrated because the distillation process occurs very slowly.

The results of the measurements of the coefficients of heat transfer in the various zones of the trap are shown in Figs. 2 and 3. The coefficients of sodium-wall heat transfer were not calculated because of the absence of accurate data for heat-exchange involving air.

During the operation of only zone II, its coefficients of heat transfer attain 465 $W/m^2 \cdot deg$ (see Fig. 2). The inclusion of cooling zone I reduces k_{II}. This is explained (the reduction of k_{III} with the inclusion of cooling zones I and II is also found from the tests) by the unusual shielding of the wall by a cold flow of metal, descending from above. The inclusion of an internal regenerator did not cause an appreciable change in k_{II} and k_{III}. Apparently, this is explained by the insignificant heat removal by the coil in view of the small temperature difference. The values of k_I in a clean trap reach 290 $W/m^2 \cdot deg$ (see Fig. 2). In

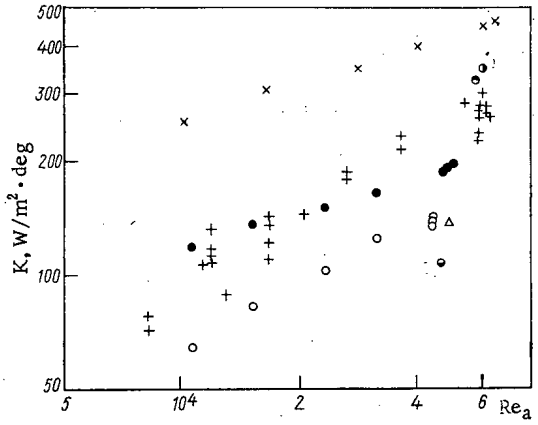

Fig. 2

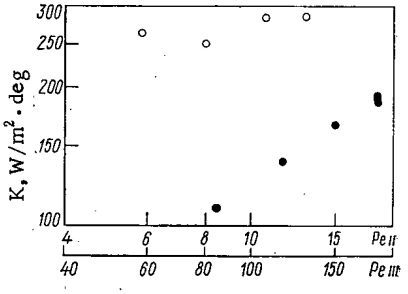

Fig. 3

Fig. 2. Dependence of the coefficients of heat transfer on Re_a. When G_t = 0.9 m^3/h and G_{Na_2O} = 2.4 kg: ×) k_{II}, Re_{aI}, Re_{aIII} = 0; ◑) k_{II}, $Re_{aI} = 6 \cdot 10^4$; ◓) k_{II}, $Re_{aI} = 6 \cdot 10^4$, $Re_{aIII} = 5 \cdot 10^4$; ●) k_{III}, $Re_{aI} = Re_{aIII}$ = 0; ○) k_{III}, $Re_{aII} = 6 \cdot 10^4$, Re_{aI} = 0; △) k_{III}, $Re_{aI} = 6 \cdot 10^4$, Re_{aII} = 0; ◒) k_{III}, $Re_{aI} = Re_{aII} = 6 \cdot 10^4$. When G_t = 0.41; 0.9; 1.67 m^3/h and G_{Na_2O} = 0-35 kg: +) k_I, $Re_{aII} = (0-6) \cdot 10^4$, $Re_{aII} = (0-5) \cdot 10^4$.

Fig. 3. Dependence of the coefficients of heat transfer on Pe. ●) k_{II}, G_{Na_2O} = 2.4 kg, $Re_{aIII} = 5 \cdot 10^4$; ○) k_{II}, G_{Na_2O} = 14 kg, $Re_{aII} = 2.8 \cdot 10^4$, $Re_{aIII} = 2.4 \cdot 10^4$-$5 \cdot 10^4$.

zones I and II, the coefficients of heat transfer are weakly dependent on the flow rate of the sodium through the trap (see Figs. 2 and 3). Therefore, one can assume that $k_I < k_{II}$ due to restriction by the chips and by the baffles in the transfer section of zone I.

The values of k_{III} are shown in Figs. 2 and 3. The increase in k_{III} with an increase in Pe_{III} (Pe_{III} is calculated from the inlet pipe parameters) occurs primarily because of an increase in the penetration depth of the "jet," i.e., in fact, because of an increase in the heat-exchange area. On the basis of the data presented, one can assume that k_I = 290, k_{II} = 350, and k_{III} = 115 $W/m^2 \cdot deg$ for a 0.9 m^3/h sodium flow rate and $Re_{aI} = Re_{aII} = 6 \cdot 10^3$ and $Re_{aIII} = 5 \cdot 10^3$ during the combined operation of all of the zones in a "clean" trap.

During the accumulation of 87 kg of oxides in the trap, the coefficient of heat transfer in zone III dropped from 195 to 150 $W/m^2 \cdot deg$ when G_t = 0.9 m^3/h and $Re_a = 5 \cdot 10^4$. One can explain such a small decrease by the relatively low accumulation of sodium oxide in the zone where the flow of hot sodium, entering the trap, develops, i.e., in the zone of the most intensive heat exchange. A significant decrease in k_{II} (from 465 to 315 $W/m^2 \cdot deg$, when G_t = 0.9 m^3/h and $Re_a = 6 \cdot 10^4$) during the accumulation of 111 kg of sodium oxide in the trap is explained by the fact that zone II contains the most oxide. An appreciable change in the coefficient of heat transfer did not occur in the absorber after the accumulation of 35 kg of sodium oxide in the trap, when G_t = 0.9 m^3/h and $Re_a = 6 \cdot 10^4$.

Analysis of the dependence of the oxygen retention coefficient β in the trap on the parameters showed that β = 0.7-1 for G_t = 0.245-0.9 m^3/h and broad ranges of Re_a numbers in the zones, during which the spread in the experimental data is reduced with an increase in the amount of oxide accumulated in the trap and $\beta \rightarrow 1$. The maximum air pressure differentials in chambers I, II, and III equal 520, 445, and 520 mm H_2O for flow rates of 1870, 1750, and 1550 m^3/h, respectively. Using this data, the conventional hydraulic resistance coefficients for the air chambers together with the local resistances are calculated: ξ_I = 0.12; ξ_{II} = 0.24; ξ_{III} = 0.17.

During the testing of the trap, a periodic accumulation of impurities (including hydrogenous impurities as well) is found in its outlet line. This resulted in an increase of the hydraulic resistance of the trap. The precipitated impurities were easily washed out during the pumping of the hot sodium out of the loop through this line and were then collected by the trap. This effect vanishes for large accumulations of sodium oxide in the trap. The sodium oxide capacity of the trap (i.e., the ratio of the weight of accumulated oxide to the weight of sodium in a clean trap) comprised 64 wt. %.

Thus, examination of the trap by γ-rays proved to be an effective way of investigating the oxide distribution in the zones of the trap, which is a heat-mass exchange system. The deficiencies discovered (the precipitation of impurities in the outlet line during the initial period of operation, the clogging of the array of bypass pipes, and the accumulation of impurities near the absorber) can be eliminated by design measures and by the utilization of procedures for removing local obstructions. The periodic flushing of the outlet line and the feeding of hot, pure sodium into the region of accumulation are related to the above, which allows one to transport the impurities to the dump tank.

LITERATURE CITED

1. V. I. Subbotin and F. A. Kozlov, in: Alkali Metal Coolants, IAEA, Vienna (1967), p. 535.
2. Yu. E. Bagdasarov et al., Technological Problems of Fast Neutron Reactors [in Russian], Atomizdat, Moscow (1969).
3. Yu. V. Petrovskii and V. G. Fastovskii, New Effective Heat Exchangers [in Russian], Gosénergoizdat, Moscow–Leningrad (1962).
4. V. I. Subbotin et al., in: Sodium-Cooled Fast Reactor Engineering, IAEA, Vienna (1970), p. 471.
5. V. I. Subbotin et al., Proceedings of the Council for Mutual Economic Aid Symposium on Fast Reactors [in Russian], Vol. 1, Obninsk (1968), p. 534.

EMISSION OF IMPURITIES WITH WASTE PRODUCTS OF SODIUM COMBUSTION

Yu. V. Chechetkin, I. G. Kobzar',
and G. I. Poznyak

UDC 621.039.534.63:536.46

In the seal failure of the first loop of a fast reactor in which sodium is used as the coolant, the high temperature of the sodium leads to the spontaneous ignition of the sodium in an oxygen-containing atmosphere, while the radioactivity results in contamination of the station premises. The experience which has been gathered in the operation of sodium systems has shown that failure involving considerable losses of the coolant are little likely, but that even small outflows of sodium can lead to a substantial deterioration of the radiation conditions on the premises of a reactor station. Thus, though large-scale failures are not very likely, one cannot simply disregard possible small outflows resulting from a failure.

Model experiments on the outflow of hot sodium in sudden full-cross-section breaks of conduits have revealed that the ejection of the sodium takes place without extensive atomization of the sodium, whereupon a quiet burning follows.

It has been shown in [1] that without thermal isolation, the temperature of the main mass of hot sodium stabilizes at 650-700°C. The maximum temperature on the surface of the hot mass reaches 870-980°C. During the burning of the sodium, aerosols in the form of oxides with a sodium concentration of 30-40% of the initial material are emitted into the air. The corresponding value was 7-19% in [2]. Similar values were obtained in [3]. According to the data of [4, 5], when sodium burns in air, about 20% of the oxidized sodium is emitted in the form of aerosols into the atmosphere.

The emission of fission products and other sodium admixtures with the aerosol during the combustion of sodium has been considered to a lesser extent in the literature. Mainly the emission of ^{131}I has been reported in the papers published. For example, the maximum ^{131}I emission in [6] amounted to 10% of the initial value, and the emission did not exceed 3.4% in some experiments. It was shown that the iodine is emitted from the sodium while adsorption to the sodium oxide takes place. It was established in [2, 3, 6, 7] that when sodium is burnt, iodine is present in the aerosols mainly in the form of sodium iodide NaI (65%) and sodium iodate $NaIO_3$ (35%).

Only qualitative information has been provided on the removal of fission products, nuclear fuel, corrosion products, and initial admixtures from sodium. It was shown in [3] that when iodine and cesium are present in equal concentrations in burning sodium, the concentration of ^{137}Cs in the aerosols is more than 10 times greater than the ^{131}I concentration in the aerosols, after the combustion of the sodium. Since the majority of fission products (strontium, bromine, lanthanum, mercury, ruthenium, zirconium, and niobium) and the nuclear fuel are present in sodium mainly in the form of oxides, the emission of these oxides in aerosols must be insignificant [6]. In experiments in which sodium and plutonium were burnt [6], it was found that the plutonium–sodium ratio in the aerosols varied between 0.34 and 0.008% and less. A high initial value of the ratio is observed in the first moment of the ignition of sodium. One must bear in mind that the majority of the data were obtained when small sodium samples (up to 150 g) were burnt.

Summarizing, the existing data on the outflow of sodium and its admixtures into the surrounding atmosphere during the burning of sodium are, if available at all, inconsistent. But the data are of great importance for the planning of emergency measures in which the aftereffects of possible discharges of the coolant are taken into consideration, or for setting requirements for shielding means.

Translated from Atomnaya Énergiya, Vol. 35, No. 6, pp. 401-404, December, 1973. Original article submitted February 14, 1973.

TABLE 1. Emission of Impurities in the Aerosol When Sodium Is Burnt

Expt. No.	Element	Compound	Isotope	Activity, μCi	Fraction of the isotopes in the aerosol, % of the initial amount in the oxidized sodium	Fraction of sodium in the aerosol, % of oxidized sodium	Weight of sodium sample, kg
1	Sodium	—	—	—	—	13	40
2		NaCl	^{22}Na	0,15—11	12,5—14,5	12,5—14	0,15—0,165
3		Coolant	^{22}Na	10—22	12,6—14,9	11,5—14,1	0,104—0,15
4	Silver	$AgNO_3$	^{110m}Ag	2,3	11,3	12,5	0,158
9		Coolant	^{110m}Ag	3,5—8,6	8,1—12,5	11,5—14,1	0,104—0,15
10	Iron	$FeCl_3$	^{59}Fe	0,01	2,1	13,6	0,165
11	Cobalt	$Co(NO_3)_2$	^{60}Co	0,01	1,1	14	0,15
12	Zinc	$Zn(NO_3)_2$	^{65}Zn	0,014	23,5	14	0,15
13		Coolant	^{65}Zn	1,7—2,1	28,1—30,7	11,5—12,3	0,104—0,15
14	Iodine	NaI	^{131}I	22	8,8—9,3	11—12,6	0,128—0,119
15		NaI	^{131}I	200	11,6	12,6	40
16		NaI	—	—	10,6	11,6	44
17	Barium	$BaCl_2$	^{140}Ba	2,8	1,4	13,6	0,163
18	Lanthanum	$LaCl_2$	^{140}La	1,7	0,9	13,6	0,163
19	Cesium	$CsNO_3$	^{137}Cs	19—40	52—56,3	11—14,6	0,11—0,163
20	Cerium	$CeCl_3$	^{144}Ce	170	42,8	14,6	0,11
21	Strontium	$SrCl_2$	^{90}Sr	23	3,1	12	0,161
22	Zirconium	$Zr(C_2O_4)\cdot 2Zr(OH)_4$	^{95}Zr	23	0,9	13,6	0,163
23	Ruthenium	$Ru(NO_3)_3$	^{106}Ru	9	6,6	11	0,128

Note. The O_2 concentration in the atmosphere is 21%. In experiments 1 and 16, t = 445°C; in the other experiments, t = 500-550°C. The amount of admixed NaI was 425 g in experiment 16.

The present article reports on an experimental investigation of the outflow of admixtures when sodium burns during depressurization of the coolant loop.

The experiments were made in a station having a volume of 390 m^3, natural ventilation, and a sealed test volume of about 1 m^3. In a first experiment, sodium was heated to the required temperature in a melting tank having a volume of 0.16 m^3. The sodium was discharged into a special bottom plate through a tubular duct with electrical heating and thermal isolation. In the second experiment, the sodium, along with admixed impurities, was heated in a sealed melting furnace having a volume calculated for tests with 400 g sodium. Sodium-combustion experiments were made in the normal atmosphere. Sodium which had been taken from a BOR-60 reactor was used in some experiments, whereas various compounds were introduced in some cases before melting the sodium. The corresponding elements were applied in the form of chlorides and nitrates to solid sodium carbonate and dried under an infrared lamp.

The introduced radioactivity allowed reliable recordings of the radioisotopes present in samples to be analyzed. The composition of the aerosols which were formed during the burning of sodium was determined with the aid of chemical analyses or γ-spectrometrical analyses of the oxides which settled on the surfaces. The amount of aerosol was determined by weighing. Radiochemical isotope separation methods were employed in several experiments. The activity of samples which contained ^{90}Sr was measured with rate meters and ring counters. The γ-activity was analyzed with the aid of AI-256 analyzers and NaI(Tl) detectors having a size of 70 × 70 mm and Ge(Li) detectors having a volume of 25 cm^3. The concentration of stable sodium was in all samples determined by titration with standard hydrochloric acid and with flame photometry; the concentration of sodium peroxide was determined by iodometry.

The main results obtained in the experiments are listed in Table 1. The table includes the most important information on the impurities which were introduced into the sodium before it was burnt: elements and their compounds, the radioisotopes of each element, which were used in the measurements, and the activities of these radioisotopes. The fraction of an element contained in the aerosols was determined from the ratio of the concentration (activity) of the element in the aerosols to the total concentration (activity) in the oxidized sodium mass.

The following conclusions can be drawn from the results. When sodium quietly burns, its emission in the form of oxides into the atmosphere of the station amounts to 9-15% of the oxidized sodium mass. The emission of iodine, silver, and ruthenium is close to the emission of the sodium; the emission of zirconium, barium, lanthanum, strontium, iron, and cobalt amounts to about 3% of the initial concentration in the burnt sodium. The emission of cesium and cerium in the sodium waste gases is highest and amounts to 43-56% of the initial concentration in the burnt sodium. The low emission of ^{59}Fe and ^{60}Co is also noted

in the investigations of the isotope composition of the aerosols in the gas chamber of the BOR-60 and BR-5 reactors. At the maximum concentration of aerosols in air (1 g/m^3), the following distribution of the precipitated waste gases of sodium and its impurities was observed: less than 2% precipitated on the ceiling, less than 18% on the walls, and about 80% of the total amount of sodium oxides which had gone into the atmosphere settled on the floor.

The experimental results imply the following scheme of the emission of admixtures during the burning of sodium. The oxidation of sodium on the surface of the melt greatly increases the temperature (870-980°C), and, as a consequence, sodium evaporates, oxidizes in the atmosphere, and is carried away into the surrounding space by air currents.

The sodium-combustion products, which are suspended in the atmosphere of the premises, obey the usual laws of coagulation, diffusion, and precipitation. Depending upon the amount of ejected material and the emission time, one or the other mechanism dominates. The reduction of the particle concentration in the course of time follows an exponential law when the initial concentrations are below 1 mg/liter air. At initial aerosol concentrations between 1-2 and 60 mg and more per liter [4], the behavior of the aerosols is determined mainly by coagulation. In this case, the time dependence of the precipitation of the suspended mass differs from an exponential law. When the initial concentration is much smaller than 1 mg/liter, sedimentation and diffusion on the walls predominate. The sedimentation of the aerosols is in this case practically independent of the initial concentration and occurs at a constant rate.

The total sodium concentration in the aerosols is proportional to the amount of sodium oxidized on the surface of the melt. A certain decrease in the sodium emitted into the aerosol during the burning of large amounts of sodium can be explained by the intensive flow of heat from the high-temperature zone to the rest of the outflowing sodium. Thus, the amount of evaporating sodium is reduced. This conclusion is corroborated by the results of experiments in which the emission resulting from the burning of various amounts of sodium was measured either at equal or at different temperatures.

The distribution of traces (microcomponents) between the liquid phase and the gas phase depends upon both the temperature and the vapor pressure of the compound in which the traces are embedded. When sodium burns, the emission of the admixtures is also affected by the adsorption of the oxides which are on the surface of the melt, and by mechanical removal via the flow of evaporating sodium.

The majority of the admixtures listed above are present in the form of oxides or pure elements in sodium. The formation of the oxides of iron and nickel in sodium at high temperatures has been described in [8]. The conclusions are apparently valid for cobalt, because its chemical properties are similar to those of iron and nickel. Silver and zinc readily dissolve without forming intermetallic compounds with sodium [9, 10], their oxides are reduced, and, at high temperatures, silver and zinc are probably present in the form of the elements. Easily soluble admixtures are emitted in amounts which are proportional to the weight of the evaporating sodium. This is put into evidence by the data on the emission of silver the vapor pressure of which is low at the temperature of burning sodium. The amount emitted is close to the amount of sodium emitted. The intensive emission of zinc results from the high vapor pressure of zinc, because the temperature on the surface of the melt is close to the boiling point of zinc (913°C).

In a melt of metallic sodium, cerium is probably present in the form of Ce_2O_3. When sodium burns in the presence of an oxidizing agent (oxygen, sodium peroxide), conditions for a violent oxidation of Ce_2O_3 into CeO_2 exist. The reaction can increase the emission of cerium.

The solubility of iron oxide and cobalt oxide is low, and these oxides have the tendency to interact with the sodium oxides. The removal of the oxides in the aerosol must be insignificant, which is observed in experiments. The emission figures which were measured are probably the result of a mechanical entrainment. Noteworthy is the satisfactory agreement between the removal of zinc and silver in experiments in which a sample of the coolant of the POR-60 reactor was burnt, and in an experiment in which samples with added impurities were burnt. It follows from the results of [6, 10-13] that iodine, rubidium, and cesium are fully soluble in sodium. Experiments which were made with the systems Cs–Na, Rb–Na, Cs–I–Na, and Rb–I–Na have shown that I, Cs, and Rb are independently transferred into the vapor phase. The last two elements are carried away in the form of elements. Lanthanum, zirconium, strontium, and barium are apparently capable of forming stable, nonvolatile oxides in sodium. Hence, their removal with the aerosol must be insignificant during the burning of sodium. The results of the experiments confirm these conclusions.

The following conclusions can be drawn from our data.

1. When hot sodium coolant burns quietly in a station which is under normal atmospheric conditions and has no provisions for suppressing the burning, the emission of sodium in the form of aerosols does not exceed 14% of the burnt sodium mass. The impurities which were present in the initial sodium are carried away into the atmosphere with the combustion products. The quantity of emitted silver, iodine, and ruthenium is close to the amount of sodium emitted. The emissions of zirconium, barium, lanthanum, strontium, iron, and cobalt amount to less than 3% of the initial amounts in the burnt sodium. The greatest discharge into the aerosols is observed in the case of cesium and cerium (43-56% of the initial concentrations in the burnt sodium).
2. At the maximum aerosol concentrations of about 1 g sodium per m^3, the distribution of the precipitated sodium combustion products is characterized by the following values: ceiling less than 2%, walls less than 18%, and floor about 80%.

The data on the emission of sodium impurities with the sodium combustion products into the atmosphere of a reactor station can be used in the analysis of the aftereffects of an emergency discharge of the sodium coolant in a fast reactor, in the development of measures for the liquidation of these aftereffects, and in the planning of systems for the purification of gas emissions.

LITERATURE CITED

1. C. Vates, An Appreciation of Fast Reactor Safety, AHSB(S)R-188 (1970).
2. R. Dickinson, Nucleonics, 18, No. 1, 107 (1960).
3. J. Saroul, Programme Experimental Nouveau sur l'Etude Hors-Pile de le Sodium dans les Enceintes de Reacteurs Rapides. Congres National sur la Diffusion des Produits de Fission. Saclay (Novembre 4-6, 1969).
4. R. Koontz et al., Treatment of Airborne Radioactive Wastes, Vienna, IAEA, SM-110 (1968), pp. 51-61.
5. H. Morewitz et al., Proceedings International Conference Safety Fast Reactors, Aix-au-Provence (1967), p. VI/5.
6. G. Keilholtz and G. Battle, Jr., Fission Product Release and Transport in Liquid Metal Fast Breeder Reactors, ORNL-NSIC (1969).
7. Cl. Descamps et al., Proceedings International Conference Safety Fast Reactors, Aix-au-Provence (1967), p. VI/1.
8. B. A. Nevzorov, Corrosion of Construction Materials in Sodium [in Russian], Atomizdat, Moscow (1968).
9. S. I. Drakin et al., Zh. Fiz. Khimii, 38, No. 2 (1964).
10. M. Sittig, Sodium, Its Production, Properties, and Applications [Russian translation], Gosatomizdat, Moscow (1961).
11. W. Clough, J. Nucl. Energy, 21, 225 (1967).
12. W. Clough, J. Nucl. Energy, 25, 417 (1971).
13. W. Clough, The Behavior of Barium and Strontium Fission Products in Liquid Sodium, AERE-6194 (1969).

PURIFYING AND CONCENTRATING LIQUID LOW-RADIOACTIVITY WASTE PRODUCTS WITH THE INVERSE OSMOSIS TECHNIQUE

Yu. I. Dytnerskii, A. A. Pushkov, A. A. Svittsov, D. I. Trofimov, Yu. I. Zhilin, and V. G. Grigor'ev

UDC (621.039.751.4+628.314.2).001.5

Among the new techniques developed in the last few years for purifying solutions from salts and concentrating the solutions, the inverse osmosis technique assumes a particular position. This method is advantageously distinguished from other methods by several details: no chemical agents are required, the process occurs without phase transitions, and the process can be conducted at normal temperatures. The energy consumed in this technique is close to the minimum energy for thermodynamic separation work [1].

The principle of the method is as follows: when a pressure higher than the osmotic pressure is applied to a solution which on one side is bounded by a semipermeable membrane, the solvent begins to penetrate through the semipermeable membrane, but the dissolved material remains in the solution the concentration of which increases in the course of time. When semipermeable membranes of high selectivity and permeability became available [2, 3], the inverse osmosis technique could be used in practice for the distillation of seawater. Standard blocks of desalination units making use of this method are serially produced in the US. The output is 1000 m^3 fresh water per day.

The selectivity of membranes is given by the formula

$$\varphi = \left(1 - \frac{X_2}{X_1}\right) 100\%, \quad (1)$$

where X_1 denotes the concentration of the dissolved material in the initial solution; and X_2 denotes the concentration of the dissolved material in the filtrate. The permeability characterizes the membrane efficiency which is expressed in liter/$m^2 \cdot h$.

During the last few years, the inverse osmosis method has received great attention as a method of purifying various types of sewage [4].

The liquid low-radioactivity wastes are neutral aqueous solutions of mineral salts with a small admixture of organic materials, the total concentration of which (about 0.5-1 g/liter) is 30-40 times smaller than the concentration of the organic material in seawater [5]. It therefore appeared sensible to use the inverse osmosis method for purifying and concentrating solutions of the above-specified kind [6]. The present work was undertaken for the purpose of establishing the possibilities of inverse osmosis for these goals.

We used in our work single- and multisection apparatus (Figs. 1 and 2) with semipermeable membranes on the basis of cellulose acetate. The membranes had been produced with a special technology [7]. The experiments were made on real industrial, radioactive waste waters having the following characteristics: salt concentration 0.5 g/liter; pH of the material 7-8; oxidability 25-30 mg O_2/liter; and β-activity $5 \cdot 10^{-7}$ Ci/liter. The solutions were initially coagulated and mechanically filtered. Several experiments were made on model solutions of sodium nitrate.

The operational parameters of the process were at first studied on single-section apparatus with a strongly agitated solution. Figure 3 illustrates the dependences of both permeability and selectivity of

Translated from Atomnaya Énergiya, Vol. 35, No. 6, pp. 405-408, December, 1973. Original article submitted September 13, 1972.

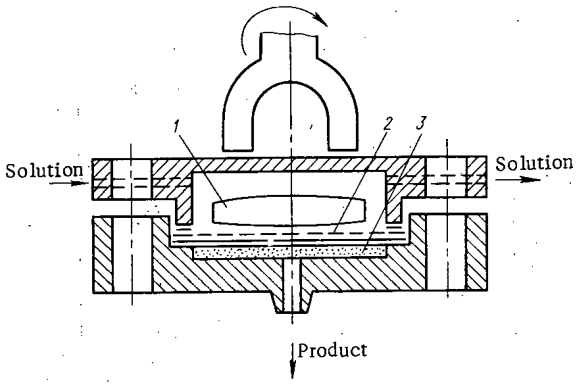

Fig. 1

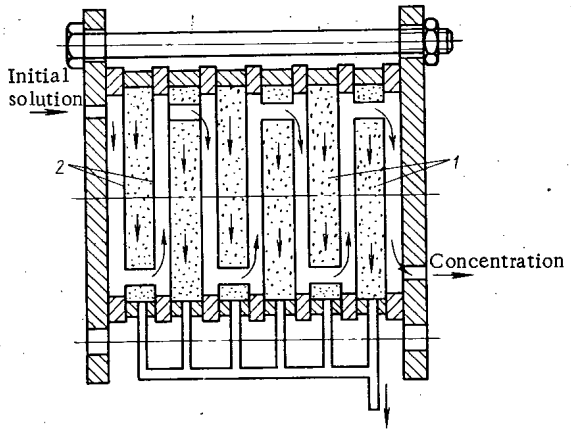

Fig. 2

Fig. 1. Scheme of the single-section laboratory cell: 1) magnetic stirrer; 2) semipermeable membrane; 3) porous drainage layer.

Fig. 2. Scheme of the multisection separator: 1) porous drainage layer; 2) semipermeable membrane.

cellulose acetate membranes upon the pressure in the treatment of various solutions.*

During the experiment, the salt concentration in the solution increased gradually. The most intensive increase in salt concentration was observed in the solution layer close to the membrane. This effect is termed concentration polarization and leads to a substantial deterioration of the efficiency of the membrane.

The rate at which water penetrates a membrane is expressed by the formula

$$G = K(P - \pi), \tag{2}$$

where K denotes the membrane constant; P is the pressure of operation; and π denotes the osmotic pressure of the solution and is proportional to the concentration of the solution. The quantity $(P-\pi)$ is termed the motive force of the process. Thus, an increase in the concentration in the layer close to the membrane reduces both permeability and selectivity of the membrane [8, 9]. The efficiency of the process increases when the solution over the membrane is agitated, as can be inferred from Fig. 4.

In research on the influence of the salt concentration of the initial solution upon the properties of cellulose acetate membranes, a decrease in both permeability and selectivity of the membrane was observed at high (up to 30%) concentrations of the solution to be separated. The reduced permeability results from a decrease in the motive force of the process (Eq. (2)), whereas the reduced selectivity is a consequence of an increased penetration of the dissolved matter by diffusion when the concentration gradient increases [10].

In order to determine the efficiency of purification from various radioisotopes, several experiments were made with aqueous solutions of sodium nitrate which was present in various concentrations and contained admixed traces of radioisotopes. The results of these experiments are listed in Table 1.

The coefficient of concentrating, i.e., the reduction of the final volume of waste products, is an important indicator of the processing of radioactive waste. The radioactive solutions were concentrated on an experimental multisection apparatus of the filter-press type which had a total useful membrane area of 0.16 m^2. Figure 5 depicts the scheme of the apparatus. The initial volume of the solution (100 liter) was reduced 400 times (to the smallest possible volume of liquid in the system). The concentration of the salts in the solution increased steadily from 0.5 to 21.0 g/liter, i.e., the salt concentration increased about 40 times. As can be inferred from the results, a significant purification of the solutions does not occur at these values, because 45 g of the 50 g of salts contained in the initial solution are transferred into the concentrate. The reason is that the selectivity of the membranes used in the experiments was relatively low (about 90%). The purification coefficient increases with increasing selectivity of the membrane, and a reduction of the concentrate volume can be obtained with the necessary salt concentration in the purified water. Improved results can be obtained when the solutions to be purified are processed several times.

* All following experiments were made at the optimum pressure of 100 atm.

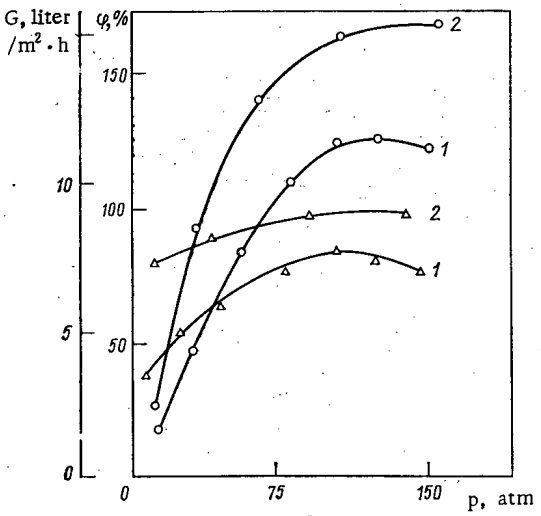

Fig. 3

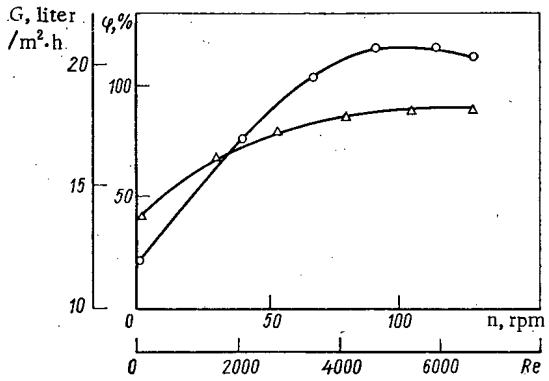

Fig. 4

Fig. 3. Dependence of the selectivity (△) and permeability (○) of cellulose acetate membranes upon the pressure: 1) $NaNO_3$ solution; 2) liquid wastes.

Fig. 4. Dependence of the selectivity (△) and permeability (○) of cellulose acetate membranes upon both the rate of stirrer rotation and the quantity Re.

Figure 6 illustrates the variation of both permeability and selectivity of the membranes during the process of concentrating the solutions.

The selectivity of the cellulose acetate membranes was constant in the entire variability range of the concentrations. The permeability of the membranes (and, hence, the capacity of the apparatus) decreased during the experiments from 9.8 to 3.5 liter/$m^2 \cdot h$. This reduction of the output results from the precipitation of iron hydroxides on the membrane surface (the iron hydroxides are present in the form of suspended matter in the solutions). The precipitate was removed after disassembly of the apparatus, and the permeability of the membranes could be restored to the initial level.

Additional experiments were made with solutions which had not gone through the coagulation stage. The results of two experiments are compared in Table 2: treatment of the solutions before and after coagulation with the technique adopted. The results led to the assumption that a treatment of the liquid wastes before their introduction into the inverse osmosis apparatus can be restricted to filtration, which means a substantial simplification of the purification technique. However, the coagulation stage cannot be excluded from the scheme adopted, because it is then necessary to reduce the amount of organic admixtures in the waste waters, to retain all colloids present, and to reduce the concentrations of metals such as Ce, Zr, Nb, and rare-earth elements. All this is obtained during the purification process based on inverse osmosis.

When radioactive wastes were treated in a single-step process, the salt concentration decreased in both cases from 0.46 to 0.08 g/liter, while the specific β-activity decreased from $6.4 \cdot 10^{-8}$ to $2.4 \cdot 10^{-9}$

TABLE 1. Results of Experiments in Which Model Solutions Were Purified from Various Radioactive Isotopes

Isotope	Initial solution		Filtrate		Selectivity		Permeability, liter /$m^2 \cdot h$
	concentration of $NaNO_3$, g/liter	activity, Ci/liter	concentration of $NaNO_3$, g/liter	activity, Ci/liter	$NaNO_3$,%	radioisotopes,%	
^{131}I	0,56	$3,56 \cdot 10^{-7}$	0,058	$4,39 \cdot 10^{-9}$	89,7	98,9	11,7
	24,97	$2,53 \cdot 10^{-7}$	2,55	$1,24 \cdot 10^{-8}$	90,2	95,4	
^{144}Ce	0,70	$6,49 \cdot 10^{-6}$	0,098	$3,37 \cdot 10^{-8}$	86,0	99,5	10,9
	25,20	$5,66 \cdot 10^{-5}$	3,13	$3,29 \cdot 10^{-7}$	87,5	99,2	
^{137}Cs	0,67	$5,18 \cdot 10^{-6}$	0,067	$3,32 \cdot 10^{-8}$	90,2	99,5	11,2
	21,40	$3,42 \cdot 10^{-5}$	2,19	$1,16 \cdot 10^{-6}$	90,0	97,0	
^{95}Zr	0,67	$1,07 \cdot 10^{-5}$	0,109	$9,46 \cdot 10^{-8}$	84,2	99,2	10,7
	29,50	$7,68 \cdot 10^{-5}$	3,72	$2,06 \cdot 10^{-7}$	87,4	99,7	
^{83}Sr	0,63	$4,09 \cdot 10^{-6}$	0,064	$7,40 \cdot 10^{-8}$	90,0	98,6	10,9
	32,25	$7,80 \cdot 10^{-5}$	3,97	$1,83 \cdot 10^{-6}$	88,0	97,7	
^{60}Co	0,66	$3,83 \cdot 10^{-5}$	0,087	$2,28 \cdot 10^{-7}$	87,0	99,5	11,0
	25,00	$7,70 \cdot 10^{-4}$	2,79	$1,29 \cdot 10^{-6}$	89,0	99,8	

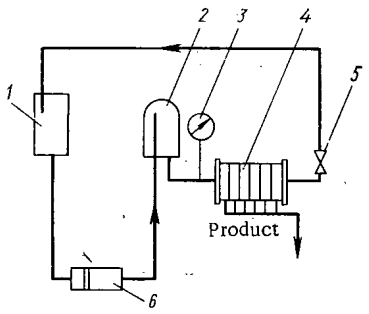

Fig. 5

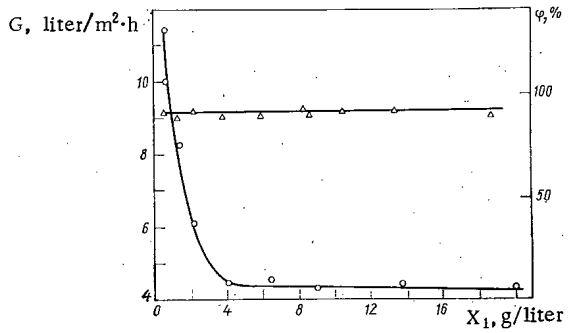

Fig. 6

Fig. 5. Scheme of the experimental apparatus for the separation of solutions by inverse osmosis: 1) initial volume; 2) hydraulic accumulator; 3) manometer; 4) separator; 5) valve for pressure adjustment; 6) pump and metering device.

Fig. 6. Change of both selectivity (△) and permeability (○) of cellulose acetate membranes during the concentrating process.

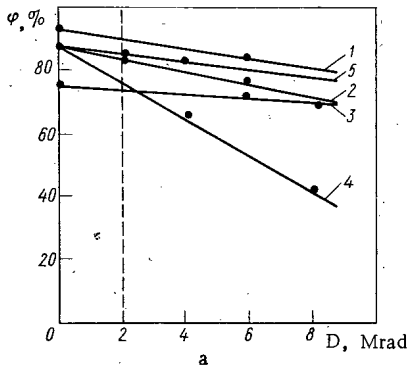

a

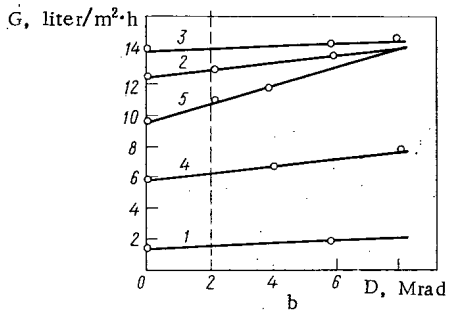

b

Fig. 7. Change of both selectivity (a) and permeability (b) of five cellulose acetate membranes tested during irradiation with γ-rays (the numbers at the curves correspond to the number of the membrane); – – –) minimum of the γ-radiation.

TABLE 2. Change of the Permeability of Membranes during the Treatment of Solutions before and after Coagulation

Solution to be treated	Initial concentration, g/liter	Initial permeability, liter /m²·h	Final concentration, g/liter	Final permeability liter /m²·h	Decrease in permeability, liter /m²·h
Before coagulation	0,46	12,7	1,23	11,8	0,9
	0,46	9,8	1,30	7,5	2,3

Ci/liter. This corresponds to a decrease of 80% in the salt concentration and a decrease of 96% in the β-activity. The need for a second purification step depends upon the quality of the semipermeable membrane and the economical process parameters of the various possible schemes.

During the treatment of the radioactive solutions, the radiolysis of the cellulose acetate was studied. (Cellulose acetate was the base material of the semipermeable membranes.) The change of the membrane properties was checked with a cobalt γ-source for which both selectivity and permeability were measured. The corresponding dependences are illustrated in Fig. 7. Calculations have shown that during the treatment process of liquid wastes of low radioactivity, the service life of the membranes does not impose any restrictions upon the process.

The results of the investigations have confirmed that the inverse osmosis technique is promising in purification processes of liquid waste products of low radioactivity. The results have established that larger units can be employed. The position of inverse osmosis in a scheme for the purification of radioactive solutions must be determined. A corresponding research program will provide information of the efficiency of the inverse osmosis technique used on an industrial scale.

LITERATURE CITED

1. L. S. Lukavyi et al., Teor. Osnovy Khim. Tekhnol., 4, No. 5, 763 (1970).
2. C. Reid and E. Breton, J. Appl. Polym. Sci., 1, 133 (1959).
3. C. Reid and J. Cuppers, J. Appl. Polym. Sci., 2, 264 (1959).
4. Yu. I. Dytnerskii et al., Khim. Promyshl., No. 12, 395 (1971).
5. D. I. Trofimov et al., Report Presented during the Conference "Practice of Processing Radioactive Waste Products of Low and Medium Activity," International Atomic Energy Agency, Vienna (1965).
6. B. S. Kolychev, Reports of the Symposium of the Council of Mutual Economic Aid "Research on Processing of Irradiated Fuels" (Marienske Lazne, Czechoslovakia, May, 1971) [in Russian], Vol. 1, Izd. SÉV (1971).
7. S. Manijakian and S. Loeb, First Intern. Symp. on Water Desalination, Washington (October, 1965).
8. L. S. Lukavyi and Yu. I. Dytnerskii, Khim. Promyshl., No. 12, 921 (1968).
9. L. S. Lukavyi and Yu. I. Dytnerskii, Teor. Osnovy Khim. Tekhnol., 4, No. 4, 585 (1970).
10. Yu. I. Dytnerskii et al., Teor. Osnovy Khim. Tekhnol., 2, No. 5, 651 (1968).

FRAGMENT YIELDS FROM THE SLOW-NEUTRON FISSION OF ^{241}Am AND ^{241}Pu

N. V. Skovorodkin, A. V. Sorokina,
K. A. Petrzhak, and A. S. Krivokhatskii

UDC 621.039.512.23

The study of fragment mass yields from the thermal-neutron fission of ^{241}Am is of interest for nuclear physics. The isotope $^{241}Am_{95}$ is an odd–even isotope, and according to systematics it should have a small thermal-neutron fission cross section since the fission barrier of the compound nucleus ^{242}Am is higher than the binding energy of a neutron [1]. However, measurements show that ^{241}Am occupies a special place among such isotopes since its thermal-neutron fission cross section is very large – 3.13 b [2]. In addition the compound nucleus ^{242}Am has a spontaneously fissionable isomer. Therefore it is of great interest to compare the fragment mass yield curves of the three fissionable systems having 242 nucleons but various numbers of protons in their nuclei: $^{241}Am_{95}$(n, f), $^{241}Pu_{94}$(n, f), and $^{242}Cm_{96}$ (spontaneous fission).

The fragment mass yields of ^{241}Am from neutron-induced fission were first reported by Cuninghame [3] and later by Rickard et al. [4]. Cuninghame determined the relative yields of 21 isotopes. The absolute yields were obtained by normalizing the sum of the experimental and extrapolated values of the relative yields to 200%, assuming that the absolute yield of ^{140}Ba is 6%. The authors estimate that the uncertainty in the latter value is ±15%. The neutron spectrum was 85% thermal and 15% neutrons with energies above 0.3 eV. The experiments were performed on americium free of fissionable contaminants.

Rickard et al. [4] used ^{241}Am which was not specially purified. The absence of ^{239}Pu was monitored only by the α-particle spectrum. The relative yields were normalized to absolute values by using the value of the absolute yield of ^{139}Ba [3]. The ratio of thermal to fast (≥1 MeV) neutrons was about 10.

At the time the present work was being completed an article [5] appeared reporting the yields of 23 mass chains. The thermal neutron flux was measured by the activation of gold foils ~100 μg/cm thick, and the number of fissions in the irradiated samples was calculated by using 3.13 b for the thermal-neutron fission cross section of ^{241}Am [2]. The samples were irradiated in a thermal column. The cadmium ratio for gold was ~5000. The fission fragment activity was measured with a γ-ray spectrometer using a Ge(Li) detector which was calibrated against standards supplied by MAGATÉ.

The present article reports on our measurements of the absolute yields of a number of isotopes. The number of fissions in an irradiated target was measured directly by the method described in [6].

EXPERIMENTAL METHOD

Yields of ^{241}Am Fission Fragments

Since the ^{241}Am fission cross section is several orders of magnitude smaller than the fission cross sections of such transuranic elements as ^{239}Pu and ^{241}Pu, these fissionable isotopes must be removed from the americium. Plutonium was removed by sorption on an 8 N HNO_3 anion-exchange resin [7]. The decontamination factor per cycle was ~10^3. The remaining transuranic and rare-earth elements were separated from americium by a cation-exchange resin column using ammonium α-hydroxyisobutyrate [7]. However the americium purified this way contained ^{147}Pm, as was discovered in determining the yields of the rare-earth elements. Therefore still another purification was performed using concentrated HCl on a cation-exchange resin column [8].

Translated from Atomnaya Énergiya, Vol. 35, No. 6, pp. 409–416, December, 1973. Original article submitted April 4, 1973; revision submitted July 9, 1973.

TABLE 1. Absolute Cumulative Yields Determined by Radiochemical Method

Isotope	$T_{1/2}$	Absolute yield, %	No. of experiments performed	Data from		
				[3]	[4]	[5]
^{89}Sr	50,36 days	1,07±0,07	3	0,81±0,05	1,2±0,1	—
^{90}Sr	28,1 years	1,37±10	3	1,16±0,08	—	—
^{95}Zr	65,5 days	4,03±0,15	5	3,90±0,51	2,7±0,1	4,04±0,21
^{97}Zr	17,0 h	5,37±0,21	3	3,55±0,46	—	5,16±0,04
^{99}Mo	66,96h	6,55±0,18	6	6,85±0,41	6,3±0,3	6,90±0,26
^{112}Pd	21,0 h	0,57±0,02	4	—	—	—
^{132}Te	77,7 h	4,88±0,19	3	4,48±0,31	3,9±0,3	4,70±0,02
^{139}Ba	82,9 min	6,58±0,21	3	6,22±0,31	6,22	8,68±0,27
^{140}Ba	12,8 days	6,02±0,17	8	6,0±0,36	5,2±0,1	5,63±0,11
^{141}Ce	32,51 days	4,71±0,16	6	5,04±0,66	4,7±0,2	6,29±0,31
^{144}Ce	284,3 days	3,41±0,09	8	3,15±0,41	3,2±0,2	—

Note. The yield of ^{139}Ba was computed on the basis of the relative yield ^{139}Ba/^{140}Ba found equal to 1.093 ± 0.009 in the present work.

The absolute yields of a number of fragments were determined by measuring the number of fissions in the americium sample and the absolute β-activity of each isotope in a 4π-flow counter as in [9]. The yields of other fragments were determined either relative to the yield of some reference fragment (^{144}Ce, ^{147}Nd, ^{140}Ba) with the measurement of the absolute β-activity by a 4π-counter, or by the method of R values [10] with respect to the yields of the corresponding fragments from ^{239}Pu irradiated simultaneously under the same conditions. The values of the ^{239}Pu fission fragment yields from slow-neutron fission were taken from [11]. A semiconductor γ-ray spectrometer with a Ge(Li) crystal or a scintillation γ-ray spectrometer with a NaI(Tl) crystal were used to compare the activities of the isotopes being studied.

The absolute cumulative yields of ^{89}Sr, ^{90}Sr, ^{95}Zr, ^{97}Zr, ^{99}Mo, ^{112}Pd, ^{132}Te, ^{139}Ba, ^{140}Ba, ^{141}Ce, and ^{144}Ce were obtained directly. The samples for the determination of the absolute yields and the mica detectors for measuring the number of fissions in the working samples were prepared the same way as in [6]. The samples were irradiated in a neutron flux of $\sim 3 \cdot 10^{13}$ neutrons/cm^2 · sec for 1 to 2 h so that the number of fissions due to the accumulated ^{242m}Am and ^{242}Am did not exceed 1% of the number of fission due to ^{241}Am.

The cadmium ratio for the conditions in question was more than seven. The screening of the working samples as a result of neutron absorption in them was 0.1% [6].

All subsequent operations – the unpacking of the irradiated assemblies, the etching of the mica, the measurement of the number of fission fragment tracks, the dissolving of the working samples of ^{241}Am, the radiochemical analysis, the measurement of the absolute β-activity, etc. – are described in [6, 7, 9, 12]. The results of these measurements are shown in Table 1.

The samples of ^{241}Am for the determination of the relative yields and for relative γ-ray spectrometer measurements were prepared by vacuum sputtering of americium and plutonium nitrates on thin (0.1 mm thick) disks of high-purity aluminum (AB00000). The thickness of the layer of material did not exceed 150 μg/cm^2, so that no correction had to be made for the self-absorption of fragments in the layer. The diameter of the active spot was ~8 mm. The fission fragments emerging from the sample were collected on disks of this same aluminum placed 0.1 mm from the sample. These collectors were later analyzed. The irradiation conditions were the same as in the determination of absolute yields. The remaining procedures are described in [7, 9, 12].

The relative and absolute yields of isotopes of rare-earth elements and yttrium are shown in Table 2, and the absolute yields determined by the R-value method are given in Table 3.

The mean-square errors of the direct determination of the absolute yields are made up of the error in measuring the number of fissions in the sample, the error in measuring the absolute β-activity, and the error in determining the chemical yield of the carriers.

The errors of the absolute yields obtained by relative methods include, in addition to the errors indicated above, the errors of measuring the β- and γ-activities, and in the case of the R values, the errors in measuring the absolute yields of the ^{239}Pu fission fragments.

TABLE 2. Yields of Isotopes of Rare-Earth Elements and Yttrium

Isotope	$T_{1/2}$	No. of experiments performed	Yield (our data)		Data from		
			relative	absolute	[3]	[4]	[5]
^{91}Y	58,8 days	5	0,505±0,007	1,73±0,06	1,16±0,08	1,9±0,05	1,48±0,43
^{92}Y	3,52 h	3	0,568±0,029	1,94±0,11	—	2,3±0,1	2,09±0,04
^{93}Y	10,18 h	3	0,779±0,017	2,66±0,10	—	3,0±0,2	—
^{140}La	40,0 h	3	1,752±0,103	5,98±0,38	6,0±0,36	5,2±0,1	5,63±0,11
^{141}La	3,85 h	3	1,206±0,051	4,12±0,20	—	—	—
^{141}Ce	32,51 days	6	1,343±0,012	4,59±0,15	5,04±0,66	4,7±0,2	6,29±0,31
^{143}Ce	33,4 h	3	1,018±0,018	3,48±0,12	—	3,4±0,1	3,48±0,15
^{143}Pr	13,59 days	7	1,077±0,013	3,68±0,12	3,32±0,46	—	—
^{144}Ce	284,3 days	8	1,000	3,41±0,09	3,15±0,41	3,2±0,2	—
^{145}Pr	5,98 h	3	0,957±0,026	3,27±0,13	—	—	—
^{147}Nd	11,06 days	7	0,610±0,006	2,08±0,07	2,08±0,33	—	1,81±0,20
^{149}Nd	1,8 h	2	0,378±0,020	1,29±0,08	—	—	—
^{149}Pm	53,09 h	5	0,434±0,015	1,48±0,07	—	—	—
^{151}Pm	28,40 h	5	0,237±0,012	0,81±0,05	—	—	—
^{153}Sm	47,1 h	6	0,167±0,003	0,57±0,02	0,76±0,12	—	—
^{155}Eu	1,815 years	2	0,090±0,008	0,30±0,03	—	—	—
^{156}Sm	9,4 h	3	0,0357±0,0011	0,122±0,005	—	—	—
^{156}Eu	15,21 days	6	0,0712±0,0014	0,243±0,009	—	—	—
^{157}Eu	15,15 h	5	0,0471±0,0021	0,161±0,008	—	—	—
^{159}Gd	18,0 h	6	0,0209±0,0008	0,071±0,0036	—	—	—
^{161}Tb	7,2 days	5	0,00639±0,00024	0,0218±0,0011	—	—	—

TABLE 3. Absolute Cumulative Fission Fragment Yields from the Slow-Neutron Fission of ^{241}Pu

Isotope	$T_{1/2}$	Absolute yield (our data)			No. of experiments performed	Data from		
		scintillation spectrometer	crystal spectrometer	^{239}Pu [11]		[3]	[4]	[5]
^{95}Zr	65,5 days	4,11±0,08	3,77±0,11	4,99	5+3	3,90±0,51	2,7±0,1	4,04±0,21
^{97}Zr	17,0 h	5,30±0,06	5,26±0,11	5,55	3+3	3,55±0,46	—	5,16±0,04
^{99}Mo *	66,96 h	—	6,55 *	6,17		6,85±0,41	6,3±0,3	6,90±0,26
^{103}Ru	38,6 days	—	5,32±0,16	5,63	2	—	7,7±0,2	7,65±0,23
^{105}Rh	35,9 h	—	6,71±0,18	5,50	3	—	6,6±0,2	6,85±0,29
^{109}Pd	13,47 h	2,54±0,08	—	1,40	2	—	—	—
^{111}Ag	7,5 days	0,99±0,03	—	0,27	5	0,89±0,05	0,22	1,19±0,04
^{112}Pd	21,0 h	0,57±0,02	—	0,12	1	—	—	—
^{115}Cd	53,5 h	0,047±0,002	—	0,038	4	0,046±0,003	—	0,075±0,008
$\sum$ Cd + ^{m}Cd †		0,050±0,002	—	0,041		0,050±0,004	—	0,080±0,009
^{127}Sb	91,2 h	0,51±0,02	—	0,378	3	—	—	0,66±0,03
$\sum$ ^{129}Je		1,26±0,11	—	1,15	1	—	—	—
^{131}I	8,05 days	3,69±0,13	3,44±0,19	3,75	3+3	3,71±0,19	2,1±0,1	4,01±0,14
^{132}Te	77,7 h	—	4,85±0,14	5,13	3	4,48±0,31	3,9±0,3	4,70±0,02
^{133}I	20,8 h	—	6,48±0,1	6,90	3	—	4,0±0,2	7,46±0,30
^{135}Xe	9,2 h	—	7,32±0,20	7,25	2	—	4,8±0,3	6,09±0,30
^{136}Cs ‡	13,5 days	0,266±0,014	—	0,0835	5	0,288±0,032	0,16	—
^{137}Cs	30 years	6,21±0,27	—	6,48	6	9,2±1,84	5,6	—
^{140}Ba *	12,8 days	6,02 *	6,05±0,16	5,58 *		6,0±0,36	5,2±0,1	5,63±0,11
^{141}Ce *	32,51 days	—	4,65 *	5,13 *		5,04±0,66	4,7±0,2	6,29±0,31
^{143}Ce	33,4 h	—	3,71±0,10	3,99	2	3,32±0,46	3,4±0,2	3,48±0,15

*Reference isotopes with which yields were compared. The values of the ^{99}Mo, ^{140}Ba, and ^{141}Ce yields in ^{239}Pu fission were taken from [6].

† Corrections to the ^{115m}Cd yield were introduced by taking account of the experimental data on the yields of cadmium isomers in the thermal neutron fission of heavy elements [13].

‡Independent value of ^{136}Cs yield in the thermal-neutron fission of ^{239}Pu taken from [14].

The mass yield curve (Fig. 1) was plotted from the yields of the final members of the mass chains. The corrections for the independent yields of these isotopes were introduced, as in [9], by using a Gaussian charge distribution.

Table 4 shows the calculated values of the cumulative yields of some of the final numbers of the mass chains which differ from the measured yields.

The sums of the yields of the masses in the heavy and light peaks are 98.5 ± 3.0 and 101.1 ± 3.4%, respectively. The total width of the heavy peak at 1/10 the maximum height of the smooth curve, $\Delta_{H1/10}$, is

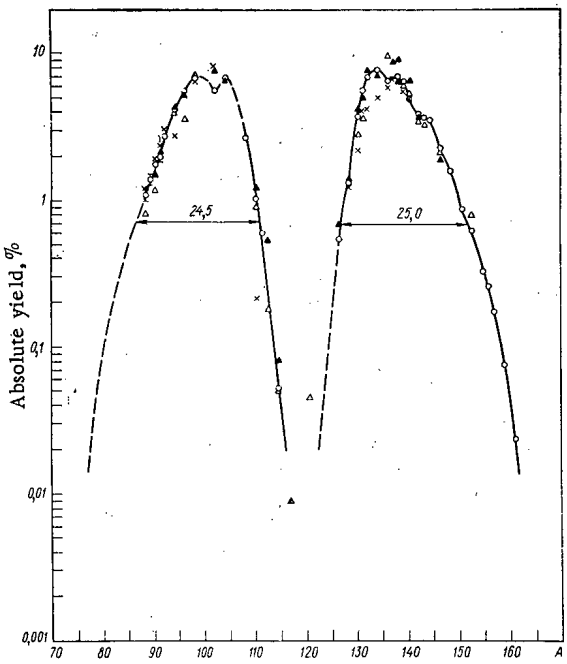

Fig. 1

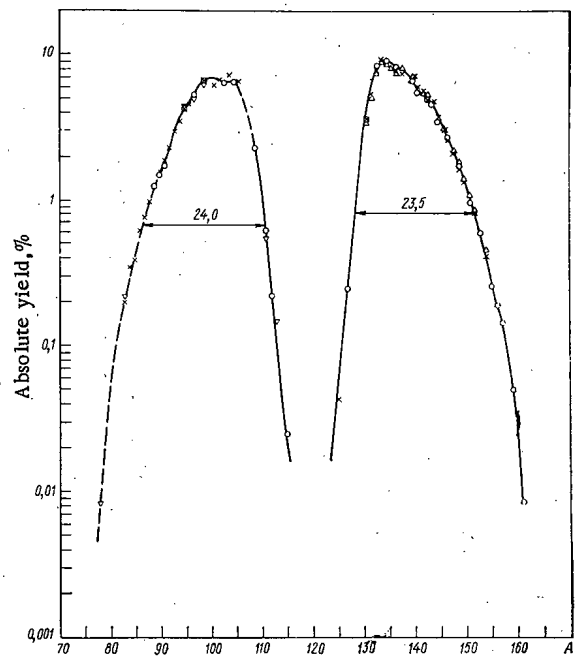

Fig. 2

Fig. 1. Fission fragment yields from the slow-neutron fission of ^{241}Am: ○) our data; △) [3]; ×) [4]; ▲) [5].

Fig. 2. Fission fragment yields from the slow-neutron fission of ^{241}Pu; ○) our data; △) [16]; ×) [17]; ▽) [18].

TABLE 4. Yields of Final Members of Mass Chains

Isotope	Average measured yield, %	Calculated yield of the final member of the chain, %
^{97}Zr	5,29±0,05	5,42±0,05
^{132}Te	4,86±0,17	5,30±0,18
^{133}I	6,48±0,17	6,54±0,17
^{135}Xe	7,32±0,20	7,36±0,20
^{140}Ba	6,03±0,16	6,07±0,16

25.0 ± 1.0 mass units (MU) and for the light masses $\Delta L_{1/10}$ is 24.5 ± 1.0 MU. The average masses in the peaks of the light and heavy fragments are M_L = 100.5 ± 0.7 MU, and M_H = 138.4 ± 1.0 MU. Hence the average number of prompt neutrons per fission is $\bar{\nu} = A_f - (\bar{M}_L + \bar{M}_H = 3.1$ ± 1.0. This value is in good agreement with the result of direct measurements ($\bar{\nu}$ = 3.219 ± 0.038) [15], but differs from the result obtained in [5] by radiochemical measurements of yields ($\bar{\nu}$ = 4.0). Fine structure is apparent on the smooth yield curve (Fig. 1) for masses 99-100, 105-106, 134-135, 139-140, and 145.

Yields of ^{241}Pu Fission Fragments

The yields of fission fragments of this isotope were determined by the same methods used for ^{241}Am. The results obtained are shown in Table 5. The yields of isotopes of the rare-earth elements and the isotopes ^{91}Y, ^{99}Mo, and ^{140}Ba were measured earlier [6]. Figure 2 shows the yields of the final members of the chains. The sums of the yields of the masses in the heavy and light peaks are 101.2 ± 3.0 and 98.2 ± 2.9%, respectively. The values of $\Delta_{H1/10}$ and $\Delta_{L1/10}$ are 23.5 ± 1.0 and 24.0 ± 1.0 MU, respectively, and the average masses of the heavy and light peaks are: $\bar{M}_H$ = 138.5 ± 1.0 MU and $\bar{M}_L$ = 100.5 ± 0.7 MU. Hence $\bar{\nu}$ = 3.0 ± 1.0, which is in rather good agreement with the value $\bar{\nu}$ = 2.874 ± 0.015 measured directly. Fine structure is evident on the mass yield curve for masses 144, 139-140, 133-134, and in the light peak, probably, for masses 99 and 105.

DISCUSSION OF RESULTS

Figure 1 shows that our data on ^{241}Am are in rather good agreement with earlier results [3, 4], but differ significantly from Nakahara's [5] values of thermal-neutron fission yields (cadmium ratio for gold $R_{Au} \geq 5000$). At the maximum of the heavy peak Nakahara's values for the ^{137}Cs and ^{138}Ba yields are much larger than ours, while the yields of heavier fragments are smaller. These differences amount for the fact that his average mass of the heavy peak ($\bar{M}_H$ = 137.3) is almost 1 MU smaller, and the average number of prompt neutrons is one larger ($\bar{\nu}$ = 4.0) than our values.

TABLE 5. Absolute Cumulative Fission Fragment Yields from the Slow-Neutron Fission of ^{241}Pu

Isotope	Absolute yield (our data), %	Method of determining yield	No. of experiments performed	Data from [16]‡	Data from [17]‡	Data from [18]
^{89}Sr	1,21±0,004	Absolute	3	—	—	—
^{90}Sr	1,46±0,04	"	3	—	1,53	—
^{95}Zr	4,08±0,12	"	3	—	3,92	4,17
	4,12±0,10	By R factor	6	—		
^{97}Zr	4,99±0,22	" " "	6	—	4,76	4,69
^{99}Mo *	6,15±0,16	Absolute	5	—	6,17	6,00
^{103}Ru	6,05±0,19	By R factor	3	—	—	—
^{105}Rh	6,08±0,16	" " "	3	—	—	—
^{109}Pd	2,26±0,12	" " "	2	—	—	—
^{111}Ag	0,59±0,02	Absolute	3	—	—	0,52
	0,56±0,02	By R factor	4			
^{112}Pd	0,223±0,007	Absolute	3			
	0,233±0,012	By R factor	3	—	—	—
^{115g}Cd	0,022±0,001	" " "	3	—	—	—
^{115}Cd	0,024±0,001	—	—	—	—	—
^{127}Sb	0,227±0,007	Absolute	3	—	—	—
	0,239±0,013	By R factor	2			
^{131}I	3,20±0,14	" " "	6	3,01	3,15	—
^{132}Te	4,49±0,12	Absolute	5			
	4,48±0,10	By R factor	6	4,47	4,64	—
^{133}I	7,23±0,25	" " "	3	6,56	6,71	—
^{135}Xe	7,80±0,19	" " "	2	7,08	—	—
^{136}Cs †	0,0175±0,0007	" " "	2	—	—	—
^{137}Cs	7,05±0,33	" " "	5	—	6,60	—
^{140}Ba *	5,64±0,15	Absolute	6	5,78	5,86	—
^{141}Ce *	4,81±0,13	"	5			
	4,78±0,18	By R factor	6	4,84	—	5,11

*Reference isotopes.

† Independent yield of ^{136}Cs.

‡In [16, 17] the values of the yields were obtained by a mass spectrometric method.

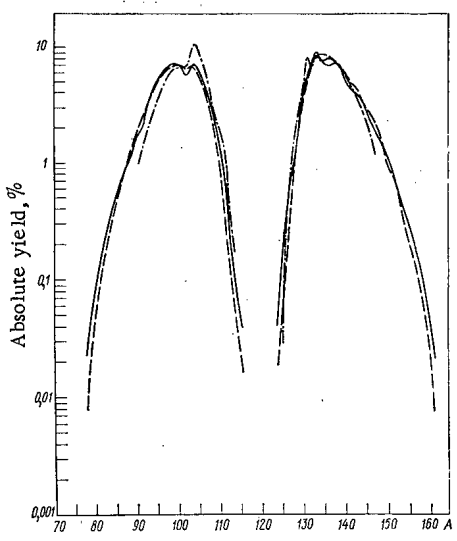

Fig. 3. Yield of fission fragment for three fissionable systems with $A_f = 242$: ——) fission of ^{241}Am by slow neutrons (our data); ----) fission of ^{241}Pu by slow neutrons (our data); -·-·-·) spontaneous fission of ^{242}Cm (data of [23]).

Our values of the fragment yields from symmetrical fission (^{111}Ag, ^{112}Pd, ^{115}Cd, ^{117}Sb) for a reactor neutron spectrum ($R_{Au} = 4$-5) agree with those in [3] within the limits of error. The yields of ^{115}Cd and the other fragments in the valley for a thermal neutron spectrum ($R_{Au} \geq 5000$) [5] are almost half again as large as those for the reactor spectrum. It is shown in [19-21] that the probability of the symmetrical fission of ^{235}U and ^{239}Pu by resonance neutrons depends not only on the excitation energy but also on the spin state of the compound nucleus: for resonances with higher spin values the probability of symmetrical fission is smaller than for fission by thermal neutrons, and for resonances with smaller spin values of the compound nucleus it is larger. For the actual spectrum the probability of symmetrical fission is determined by the contributions of these two groups. In our case ($R_{Au} = 4$-5), just as in the fission of ^{235}U and ^{239}Pu by resonance neutrons, the main contribution to the fission of ^{241}Am by slow neutrons comes from

TABLE 6. Some Parameters of the Mass Distribution Curves for Fissionable Systems with $A_f = 242$

Fissionable system	$\bar{M}_L$	$\bar{M}_H$	$\Delta_{L\,1/10}$	$\Delta_{H1/10}$	$\left[\frac{M_H - M_L}{A_f}\right]^2$	$\bar{\nu}$	Y_{115Cd}	Position of fine structure
$^{241}Pu + n$	100,5±0,7	138,5±1,0	24,0±1,0	23,5±1,0	0,0247	3,0±1,0	0,0237	99; 105; 133—134; 144
$^{241}Am + n$	100,5±0,7	138,4±1,0	24,5±1,0	25,0±1,0	0,0245	3,1±1,0	0,0504	99—100; 105—106; 134—135; 139—140; 145
^{242}Cm(s.f.)	102,3	137,3	21,5	21,5	0,0209	2,4	0,036	105; 132; 134

resonances with a higher value of the spin state of the comound nucleus ($I = 3^-$) for which the probability of symmetrical fission is smaller than for thermal neutrons.

In the fission of ^{241}Pu by slow neutrons (Fig. 2) the values of the yields of the final members of the chains found by radiochemistry (our data) and mass spectrometry ([16, 17]) are in rather good agreement in the region of maximum yields. However, in the region of the rare-earth elements the values of the yields found by radiochemistry are systematically lower than the results obtained by mass spectrometry, except for the yields of the reference fragments ^{144}Ce and ^{147}Nd (^{147}Pm) which are the same. Since the neutron spectra were nearly the same in all the studies (in our case $R_{Au} = 4$-5; in all the others $R_{Au} = 2.5$-3.0) this divergence cannot be explained by the effect of fast and resonance neutrons. In addition the ^{241}Pu thermal-neutron fission cross section is so large that the contribution from fast neutrons should be small.

We determined the relative yields of all the rare-earth elements in a single experiment by separating all of them from one sample. In the initial determination of relative yields by mass spectrometry the isotopes of individual elements were separated from various samples and then the individual groups were joined. Therefore the divergences mentioned can be accounted for by joining and normalization errors. For this reason our method is probably preferable. It is possible, however, that for masses with yields <1% the final members of the chains can be formed with appreciable independent yields [22].

Our results permit practically a unique comparison of the yield curves for the three fissionable systems having 242 nucleons but various numbers of protons in their nuclei and different excitation energies: the slow-neutron induced fission of ^{241}Pu and ^{241}Am (our work) and the spontaneous fission of ^{242}Cm [23]. Some characteristics of these curves are given in Table 6, and the curves are shown in Fig. 3.

Figure 3 shows that although A_f is the same for all the systems mentioned, the light peak for the spontaneous fission of ^{242}Cm is shifted toward larger mass numbers by approximately 2 MU and the heavy peak toward smaller mass numbers by approximately 1 MU relative to the peaks for the induced fission of ^{241}Pu and ^{241}Am. Therefore the spontaneous fission of ^{242}Cm is less asymmetric. The width of the curves and the number of neutrons emitted per fission generally increases with increasing excitation energy. These values are minimum for the spontaneous fission of ^{242}Cm and are significantly larger for the neutron-induced fission of ^{241}Pu and ^{241}Am. This is a consequence of the higher excitation energy in induced fission. However, the ^{241}Am yield curve is broader than that for ^{241}Pu, although the latter has a larger excitation energy than ^{241}Am. This is probably related to the large fast-neutron contribution to ^{241}Am fission since the ^{241}Pu thermal-neutron fission cross section is hundreds of times larger than the fast-neutron cross section, while the ^{241}Am thermal-neutron and fast-neutron cross sections are comparable, and the fast-neutron fission contribution will be significant, particularly for fragments of strongly asymmetric fission whose yields increase with increasing neutron energy [24].

It should be noted that according to Nakahara [5] the fragment yield curve is narrower for ^{241}Am than for ^{241}Pu, which does not agree with our results. However ^{147}Nd is the heaviest fragment whose ^{241}Am fission yield was determined experimentally by Nakahara; the yields of heavier fragments were obtained by extrapolation. Figure 3 shows that the curve for ^{241}Am begins to spread out in comparison with the curve for ^{241}Pu only after A = 151, and the yields of strongly asymmetric fragments, e.g., ^{161}Tb, are almost 2.7 times as large for ^{241}Am as for ^{241}Pu. Up to a mass of 151 the yield curve for ^{241}Am is narrower than that for ^{241}Pu. Finally there is still another factor which probably can influence the interpretation. In [5] the ^{241}Pu fission fragment yield curve plotted from a mass spectrometer analysis was chosen for comparison with the ^{241}Am fission fragment yield curve, and as we showed earlier, the wings of the ^{241}Pu curve obtained by radiochemistry are narrower than those obtained by mass spectrometry.

The probability of symmetrical fission for these systems can be compared by the ^{115}Cd yield. The probability of symmetrical fission is almost twice as large for ^{241}Am as for ^{241}Pu. This may be a consequence of the fact that the contribution from fast-neutron fission is appreciably larger for ^{241}Am than for ^{241}Pu, and the fragment yield from symmetrical fission increases rapidly with increasing neutron energy. The increased ^{115}Cd yield for ^{241}Am in comparison with ^{241}Pu can probably also be accounted for by the different effect of resonance neutrons. As shown earlier the fission of the compound nucleus ^{242}Am occurs mainly from higher spin states ($I = 3^-$), while the fission of the compound nucleus ^{242}Pu appears to occur from lower spin states ($I = 2^+$). In the fission of compound nuclei with smaller angular momenta more neutrons are emitted on the average [25]. Thus in the fission of ^{241}Pu ^{115}Cd should be obtained from the heavier primary masses which have lower yields. The ^{115}Cd yield from the spontaneous fission of ^{242}Cm is also higher than that from the induced fission of ^{241}Pu. It should be noted, however, that the average number of neutrons per fission is almost one smaller for ^{242}Cm; i.e., ^{115}Cd is farther from true symmetrical fission for ^{242}Cm than for ^{241}Pu.

The fine structure is most evident in the spontaneous fission of ^{242}Cm, and least evident in the fission of ^{241}Pu. The position of the fine-structure peaks for these fissionable systems is almost the same within ±1 MU. Unfortunately the lack of experimental data on the yields of mass numbers 136, 137, 138, and more than 140 does not permit the determination of the shape of the fragment yield curve for the spontaneous fission of ^{242}Cm in these regions. Existing data indicate, however, that the position of the fine structure for fissionable systems with $A_f = 242$ is almost independent of Z and E_{ex} and has a period of approximately 5 MU. This is particularly noticeable for ^{241}Am. This period agrees with that of the fine structure observed in the distribution of the yields of the primary masses. However, the effect of prompt neutron emission is superimposed on the secondary fine structure.

The authors thank E. I. Biryukov for performing the measurements on the crystal γ-ray spectrometer, and V. A. Yakovlev and E. I. Vystorobskaya for the use of the scintillation γ-ray spectrometer and for help with the measurements.

LITERATURE CITED

1. W. Myers and W. Swiatecki, Nucl. Phys., 81, 1 (1961); P. Seeger and R. Perisho, USAAC Report LA-3751 (1967).
2. Neutron Cross Sections, BNL-325, Vol. 3 (1965).
3. J. Cuninghame, J. Inorg. Nucl. Chem., 4, 1 (1957).
4. R. Rickard et al., Nucl. Sci. and Engng., 23, 115 (1965).
5. H. Nakahara et al., J. Inorg. Nucl. Chem., 33, 3239 (1971).
6. A. V. Sorokina et al., Atomnaya Énergiya, 31, 99 (1971).
7. N. V. Skovorodkin et al., Radiokhimiya, 12, 487-492 (1970).
8. R. Diamond et al., J. Amer. Chem. Soc., 76, 1461 (1954).
9. N. V. Skovorodkin et al., Atomnaya Énergiya, 34, 365 (1973).
10. D. Gordon et al., Nucleonics, 24, No. 12, 62 (1966).
11. H. Fickel and R. Tomlinson, Canad. J. Phys., 37, 916-926 (1959).
12. V. M. Vdovenko, A. S. Krivokhatskii, and N. V. Skovorodkin, Radiokhimiya, 13, 416 (1971).
13. Yu. A. Zycin, A. A. L'vov, and L. I. Sel'chenkov, Yields of Fission Products and Their Mass Distribution [in Russian], Gosatomizdat, Moscow (1963).
14. W. Grummit and G. Milton, J. Inorg. Nucl. Chem., 20, 6 (1961).
15. A. Jaffey and J. Lerner, Nucl. Phys., 145A, 1 (1970).
16. H. Farrar et al., Canad. J. Phys., 42, 2063 (1964).
17. F. Lisman et al., Nucl. Sci. and Engng., 42, 191 (1971).
18. I. Croall and H. Willis, AERE-6154 (1969).
19. J. Toraskar and E. Melkonian, Phys. Rev. C, 4, 267 (1971).
20. G. Cowan et al., Phys. Rev. C, 2, 615 (1970).
21. J. Toraskar and E. Melkonian, Phys. Rev. C, 4, 1391 (1971).
22. A. Wahl et al., Phys. Rev., 126, 1112 (1962).
23. E. Steinberg and L. Glendenin, Phys. Rev., 95, 431 (1954).
24. L. Bunney et al., Proceedings of the Second International Conference on the Peaceful Uses of Atomic Energy, Vol. 15, United Nations, Geneva (1958), p. 449.
25. S. Weinstein et al., Proceedings of a Symp. on Phys. and Chem. of Fission, IAEA, Vienna (1969), p. 477.

NUCLEAR METHODS AND INSTRUMENTS FOR ENVIRONMENTAL POLLUTION MONITORING

L. M. Isakov and V. V. Matveev

UDC 539.106

One of the most important problems in environment conservation is the organization of effective pollution monitoring. This is the first link in the chain of measures to be undertaken in order to prevent the disturbance of ecological equilibrium.

The atomic industry has gained much experience in organizing radiation protection services and in providing the necessary instrumentation. Because of the great attention given to the problem of radiation safety from the very beginning of atomic engineering, nuclear plants contribute very little to environmental pollution [1]. Various methods and instruments for measuring radioactive isotopes in the air, soil, plants, food, water, etc., have been developed both in the Soviet Union and abroad, and the organization of environmental radiation protection services is constantly being improved [2].

Nuclear methods of analysis (such as activation analysis and x-ray radiometric analysis) have been developed and are being successfully used in environment monitoring [3]. These methods are widely used in the Soviet Union for solving various ecological problems. However, the use of nuclear methods in large-scale analysis is still limited.

Radiation pullution is only one of the many aspects of environmental pollution and occupies rather a limited part in the overall problem of environmental control. Nevertheless, in view of the success of the atomic industry in organizing radiation safety services in nuclear plants it is natural to consider the question of taking advantage of this experience in comprehensive monitoring of the environment.

In considering the problem as a whole, one should not forget that economical aspects of environmental monitoring in many ways affect its effectiveness as the network of measuring stations can be made sufficiently widespread only if the cost of equipment and operation is reasonable. At the present stage of instrumentation development only a systematic approach to the design of suitable equipment can ensure the desirable results. Such an approach is now typical of nuclear instrument design. This approach calls for sets of nuclear instruments of a unified circuit and structural design [4, 5]. The experience gained in nuclear instrumentation can be used with advantage in the design of sets of unified instruments for environmental monitoring. Individual units and assemblies of nuclear instruments are versatile enough to be used in monitoring the nonradiation characteristics of the environment. The applicability of nuclear instrumentation to environmental pollution monitoring is the subject of this article.

Consider the structure of a system for comprehensive environmental pollution monitoring which takes into account the specific measuring problems involved (Fig. 1). The purpose of such monitoring is the determination of deviations of environmental characteristics from normal conditions, prediction of possible pollution, and the development of recommendations for controlling the discharge of various industrial wastes into the environment and for improving the operating conditions of industrial enterprises. In the diagram shown in Fig. 1 all the different kinds of pollution were divided into four major groups that cover the atmosphere, hydrosphere, and earth surface.

The group including mechanical pollution of the air and water is characterized by the content of aerosols and mechanical particles and by suspended particles, respectively. Mechanical pollution of the soil surface is characterized by changes in the elemental composition of the soil and rocks and corresponds to the second pollution group consisting of disturbances of the elemental or chemical composition of the environment. A separate group are pollutions of a biological nature which are characterized by the

Translated from Atomnaya Énergiya, Vol. 35, No. 6, pp. 417-422, December, 1973. Original article submitted May 21, 1973.

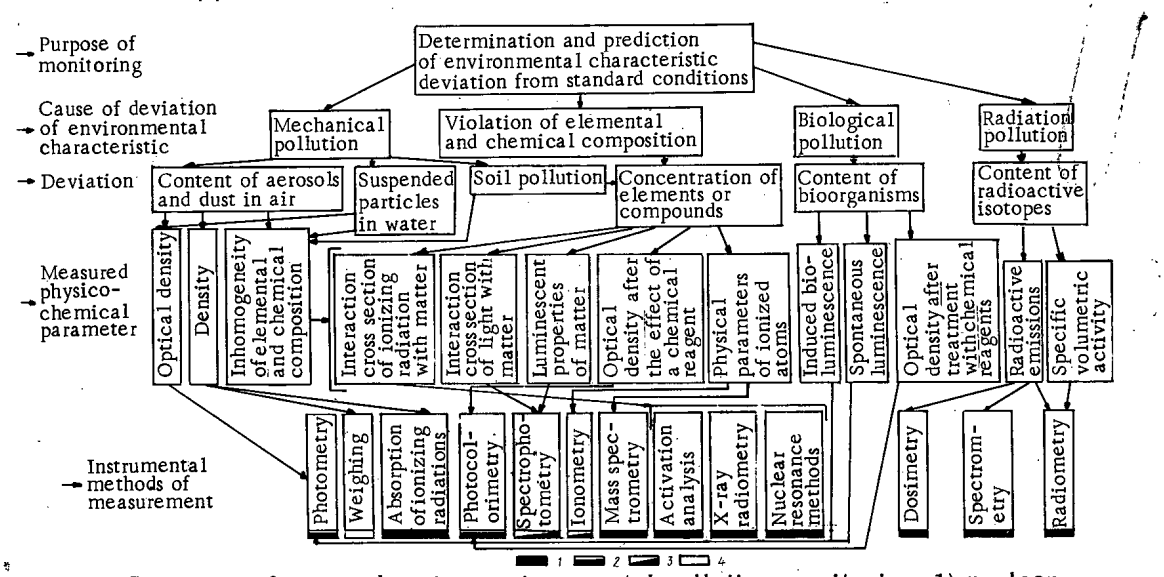

Fig. 1. Structure of comprehensive environmental pollution monitoring: 1) nuclear instruments applicable without modification; 2) nuclear instruments require modification; 3) individual units and assemblies of nuclear instruments applicable; 4) use of nuclear instruments not advisable.

content of bacteria and bioorganisms in the environment. Obviously, of some specific nature is the group of radioactive pollutions which is characterized by the content of radioactive isotopes in the tested object.

It should be noted that this classification includes only changes in material composition of the environment whereas a more general consideration should take into account also other factors that affect the environment (violation of thermal equilibrium acoustical disturbances, etc.).

The determination of the extent of pollution belonging to any of the above classification groups must be based on some specific measurable physicochemical parameter. Some such parameters are indicated in Fig. 1.

Instrumental methods based on the specific properties of these parameters can be applied to environmental monitoring. The most important of these methods are briefly discussed below.

Photometric measurements are used in the determination of water and air turbidity and of water chromaticity [6]. For example, according to the accepted methods, the turbidity of water is characterized by the content of SiO_2 found from the optical density of a water sample measured in a transmitted-light photometer with a red filter. Water chromaticity is characterized by optical density at a wavelength near the absorption peak. These measurements are made with a photometer or electrocolorimeter with the aid of a set of filters each of which tramsmits a narrow band of the visible spectrum.

Photometric methods are also used for measuring the elemental and chemical pollution. The pollution of air and water is most frequently determined by photocolorimetry [7] using either automatic or manual instruments. Photocolorimetric methods can be used for the determination of the content of any substance which has characteristic and sufficiently sensitive color reaction. The absorption of light transmitted through a stained sample gives an indication of the content of element or substance being analyzed. Photocolorimeters of various design are used as gas analyzers and water pollution monitors both in the field and the laboratory.

Various spectrometric methods are used for monitoring the pollution in environment samples (mostly under laboratory conditions); these methods are based on fluorescence spectra that characterize spontaneous or induced luminescence of matter or on absorption spectra from which the content of individual components of the sample can be determined [8]. Equipment for luminescence measurements includes light sources, spectral instruments with recording devices for plotting excitation, absorption, fluorescence and phosphorescence spectra, and various other auxiliary devices. The spectrometric method used, in particular, in atomic absorption analysis makes it possible to determine the content of individual elements in the amount of thousandths of a microgram per liter [9].

Environmental pollution (especially of the hydrosphere) is frequently monitored with instruments based on the use of ion sensitive electrodes [10].

Mass spectrometric instruments allow highly sensitive and selective determination of elemental and chemical composition of environment samples; however, these instruments are quite elaborate and costly and are used mostly in research practice.

Nuclear methods of elemental composition analysis are much faster and more sensitive than other methods of analysis. However, modern activation analysis requires sophisticated and expensive instrumentation. A much simpler and more versatile method is x-ray radiometry, although the need of high-intensity radiation sources and difficulties in preparing the sample for analysis limit its usefulness in large-scale environmental surveys. Other nuclear methods based on the interaction of ionizing radiations with matter can also be used for elemental and phase analysis. One example is the γ-resonance method [11] used in the determination of tin and iron. However, all these methods require rather specialized instruments and have a limited use in large-scale environmental testing.

A specific property of the environment is the continuous presence of bacteria and other bioorganisms which sometimes can act as a source of pollution. On the other hand, the state of certain bioorganisms depends on the conditions of their surroundings and thus can to some extent characterize their immediate environment. For example, a common procedure in sanitary hydrobiology is to determine the effect of different substances discharged into water reservoirs on the quality of water from the conditions of biological systems [8].

Of the many instrumental methods of monitoring the content of bioorganisms in the environment, the most promising are those based on the effect of bioluminescence, either spontaneous or induced, which can be excited by various means [8, 12]. One such method is, for example, the method of automatic water monitoring based on changes in the luminescence spectrum [8]. In a recently developed method the distribution of the biomass of heterotropic growing cells in the ocean is determined from the content of adenosine triphosphate in biological processes [13].

Radioactive pollution of the environment is characterized by the content of radioactive isotopes. The radiation of individual isotopes and the specific volumetric activity, which characterizes radioisotopic decay can serve as parameters for radiometric dosimetric and spectrometric measurements of radioactive pollution of the environment.

Nuclear instrumentation design methods are now quite well advanced and can be successfully applied in the field of pollution measurements [2].

The need of recording very low levels of radioactive pollution has led to widespread use of various radiochemical and physicochemical methods of analysis (isotopic dilution, isotope concentration by means of sorbents, extraction, chromatography, etc.), in radiometric measurements.

Nuclear instruments are widely used in environmental investigations with the aid of radioactive tracers. These methods are employed, for example, in studies of circulation of air masses, and water currents in rivers and reservoirs making it possible to foresee possible environment pollution and to recommend proper control of the discharge of industrial wastes.

Radiometric instruments based on absorption of ionizing radiation are used also to measure such parameters as the content of dust in air [14].

As noted above, the present stage of development of nuclear instrumentation is characterized by a systematic approach to instrument design. Such an approach requires a deep understanding of instrument utilization and a definition of a set of optimal parametric instruments, units, and assemblies covering the entire spectrum of measurements. This foresees extensive unification of instruments and the design of basic fundamental units and assemblies of devices for nuclear measurements.

The similar structure of radiometric, spectrometric, and dosimetric equipment makes it possible to develop a common unified system of nuclear instruments for monitoring environmental pollution and for elemental sample analysis. Since the problem of recording information provided by detectors of nonradiation parameters involves, in accordance with the above structural scheme, measurement of currents of the order of 10^{-12} A (ion-selective electrodes, pH meters, photometers) and the detection of light pulses (in measurements of bio- and chemoluminescence), it is possible to use for this purpose circuits and complete units similar to those used in nuclear research. On the other hand, radiation pollution can be measured by devices and instruments used in nonradiation measurements. This approach is most desirable

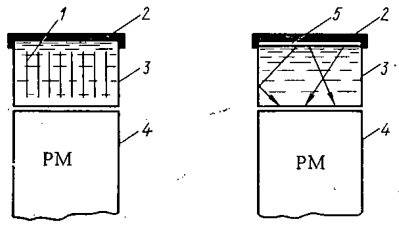

Fig. 2. Scintillation detector for water quality control: 1) scintillation detector; 2) lightproof cover; 3) test cell; 4) photomultiplier; 5) luminous compound.

in developing a unified system of pollution measuring equipment.

Since many of the methods of nonradiation parameter measurements are in the final analysis based on the measurement of light fluxes, suitable modification of scintillation detection devices based on photomultipliers can help to solve some measuring problems. For example, the role of radiometric instruments based on scintillation counters in water quality control can be significantly broadened.

Figure 2 shows one possible version of such a detector. For specific volumetric activity measurements a scintillation detector (scintillation granules, platelets fibers, or powder) are placed into the test cell. If the cell is covered by a lightproof cover (facing the liquid) coated with a luminous compound mixed with a radioactive emitter, the compound will produce scintillations which can be counted with a photomultiplier. Absorption of scintillations as a result of photon interaction with particles suspended in water is a measure of turbidity of the tested water sample. By varying the spectral composition of the scintillations (for example, using a light filter) and measuring the transmission of photons of definite wavelengths through the analyzed medium one can also measure the chromaticity of water.

Such a detector can be used in photocolorimetric measurements which, as noted before, are most widely used for monitoring the elemental and chemical composition of environment samples. The advantages of such a detector are quite obvious. The light source, a luminous compound producing scintillations under the action of radioactive emission, is very stable and does not consume energy which is of primary importance in field measurements. Moreover, discrete measurements are as a rule more accurate than analog measurements (employed in conventional photometers).

Bioluminescence and chemoluminescence measurements used for monitoring biological pollution and partially also in monitoring variations of the elemental and chemical composition are based on the detection of weak light flashes emitted by the medium being analyzed. After satisfying certain specific conditions, these measurements can be combined with the determination of the radioactivity of environment samples with the aid of scintillation detector units. Radiochemical measuring methods can supplement purely chemical methods of monitoring the content of specific substances in samples. In particular, the radioisotope dilution method is successfully used for determining the abundance of certain nonradioactive elements (for example, mercury [15]).

Instrumental methods of radioactivity measurements based on preliminary isotopic enrichment can be applied to the determination of nonradioactive impurities. For example, the sample selection and enrichment devices used in radiometric aerosol and liquid measuring instruments can be used also for nonradioactive pollution measurements (e.g., in automatic photocolorimetric gas analyzers) in which the reagent providing the color reaction is deposited on paper or cloth tape.

In monitoring atmospheric pollution the samples are taken as a rule by aspiration, i.e., suction through absorption filters. Sampling devices used in aerosol and gas radiometers are suitable for these purposes.

The widening scope of nuclear instrumentation in pollution monitoring systems has changed the approach to the application of nuclear methods of sample analysis, as the spectrometric and radiometric information recording and processing devices used in analysis must be considered in terms of broad application possibilities (including the measurement of radioactive as well as nonradioactive pollution parameters). In applying nuclear methods of sample analysis one has to consider the addition of only certain auxiliary devices (irradiation devices, sample preparation and positioning devices) which makes the application of nuclear methods relatively less costly.

An important aspect of monitoring is also the problem of optimal acquisition and processing of information provided by pollution control devices. The experience of nuclear instrumentation design can be useful also here. Nuclear instrumentation includes devices for continuous automatic measurements, portable devices for field surveys, as well as laboratory instruments for comprehensive detailed analyses. The

large volume of data provided by these instruments can be brought together in a single central system for operational monitoring of the overall radiation situation.

With some modification such information processing systems designed for nuclear research can be successfully used in comprehensive monitoring of environmental pollution. An example of such a system is the multichannel telemetering system [4] which allows remote monitoring of radiation and transmits the measuring results through 99 radiochannels. The information provided by remote sensors is collected either automatically or manually by interrogation from a central control board. The information is recorded on an electroluminescent display panel and on digital printer tape.

Thus, even a brief discussion of the subject indicates that nuclear methods and instruments can be effectively used in the organization of environmental pollution monitoring.

LITERATURE CITED

1. Yu. A. Izraél', At. Énerg., 32, 273 (1972).
2. Rapid Methods for Measuring Radioactivity in the Environment. Proceedings of International Symposium, Neuherberg (July, 1971).
3. Modern Trends in Activation Analysis. Proceedings of International Conference, College Station, Texas, USA (April, 1965).
4. V. V. Matveev, in: Nuclear Instrument Design [in Russian], Atomizdat, Moscow (1970).
5. L. M. Isakov, V. V. Matveev, and G. I. Él'tsin, in: Nuclear Instrument Design [in Russian], No. 15, Atomizdat, Moscow (1971), p. 50.
6. Yu. Yu. Lur'e (editor), Standard Methods of Water Analysis [in Russian], Khimiya, Moscow (1971), p. 31.
7. Meteorological Aspects of Atmospheric Pollution [in Russian], Gidrometeoizdat, Leningrad (1971), p. 261.
8. V. E. Sinel'nikov, Luminescence Analysis of Sea and Land Waters [in Russian], ONTI Obnisk. Otd. Gidromettsentra SSSR, Obninsk (1971).
9. B. V. L'vov, Atomic Absorption Spectral Analysis [in Russian], Nauka, Leningrad (1966).
10. Dust (editor), Ion-Selective Electrodes [Russian translation], Mir, Moscow (1972).
11. V. I. Gol'danskii et al., in: Nuclear Geophysics [in Russian], No. 3, Nedra, Moscow (1968).
12. Extremely Weak Luminescence in Biology [in Russian], Nauka, Moscow (1972).
13. E. Bowen, Luminescence in Chemistry, Van Nostrand, London–Princeton (1968).
14. V. G. Babich et al., Proceedings of the Fourth Conference on Radiometry and Dosimetry of Ionizing Radiation [in Russian], Atomizdat, Moscow (1972), p. 5.
15. Mercury Contamination in Man and His Environment, Vienna, IAEA (1972), Technical Reports Series No. 137.

OPTIMAL DISTRIBUTION OF NUCLEAR FUEL IN A CYLINDRICAL FUEL ELEMENT

Yu. V. Milovanov, É. E. Petrov, and V. Ya. Pupko

UDC 621.039.617.5

In [1] using the Pontryagin maximum principle [2] the problem of the optimal distribution of nuclear fuel in a laminated fuel element was solved for the reduction of the temperature drop in it. In the present article we solve a similar problem for a cylindrical fuel element.

The functional that describes the temperature drop in a cylindrical fuel element with arbitrary drop in a cylindrical fuel element with arbitrary distribution of concentration of fuel $\varepsilon(r)$ has the form

$$\Delta T = \frac{AR^2}{\lambda_m} \int_0^1 \frac{\int_0^\rho \varepsilon(\rho')\,\rho'\,d\rho'}{\rho\,[1-B\varepsilon(\rho)]}\,d\rho, \tag{1}$$

where $\rho = r/R$ is the dimensionless radius of the fuel element; λ_m is the thermal conductivity of the matrix; $B = 1-\lambda_f/\lambda_m$ (λ_f is the thermal conductivity of the fuel); A is a coefficient of proportionality in the assumed linear dependence $q_v(r) = A\varepsilon(r)$ between the heat release and the concentration of the fuel. It is assumed that the thermal conductivity of the mixture of the matrix and the fuel has an additive character: $\lambda(r) = \lambda_m-(\lambda_m-\lambda_f)\varepsilon(r)$.

Taking $\bar{\varepsilon} = 2\int_0^1 \varepsilon(\rho')\rho'd\rho'$; $\rho = 1/t$ (owing to the divergence of the factor $1/\rho$ in Eq. (1)); $x^0(t) = \int_1^t \frac{x^1(t')\,dt'}{t'\,[1-Bu(t')]}$; $x^1(t) = \int_t^\infty u(t')\frac{dt'}{t'^3}$ and $\varepsilon(1/t) = u(t)$, we obtain, instead of the functional, the system of equations

$$\frac{dx^0}{dt} = \frac{x^1(t)}{t\,[1-Bu(t)]}; \quad \frac{dx^1}{dt} = -\frac{u(t)}{t^3} \tag{2}$$

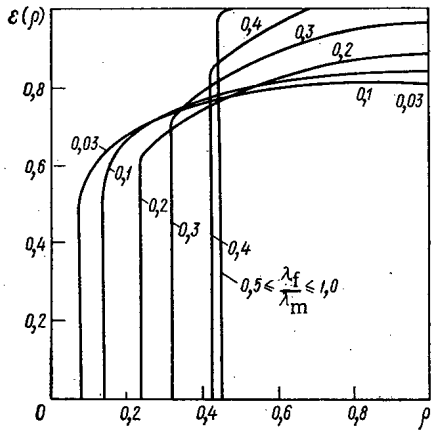

Fig. 1. Optimal distribution of concentration of fuel over the radius of the fuel element for $\varepsilon = 0.8$ for various values of λ_f/λ_m.

Translated from Atomnaya Énergiya, Vol. 35, No. 6, pp. 423-425, December, 1973. Original article submitted October 27, 1972; abstract submitted August 8, 1973.

with boundary conditions $x^0(1) = 0$; $x^1(t) = \bar{\varepsilon}/2$; $x^1(\infty) = 0$. In terms of the work [2] for the solution of the problem we must find a control u(t) such that we obtain a minimum value of the phase coordinate $x_0(\infty)$. The problem is nonautonomous, with fixed ends and time.

In accordance with the theorem on the maximum principle we construct an auxiliary function

$$H = \Psi_0(t)\frac{x^1}{t(1-Bu)} - \Psi_1(t)\frac{u}{t^3}.$$

In order to find the optimal process [u, x^0, x^1] we need the following solution of the system:

$$\frac{d\Psi_0}{dt} = -\frac{\partial H}{\partial x^0}, \quad \frac{d\Psi_1}{dt} = -\frac{\partial H}{\partial x^1} \tag{3}$$

for the functions Ψ_0 and Ψ_1, so that at each point t of the interval [1, ∞] the condition of the maximum

$$\sup_{0 \leq v \leq 1.1} H(\Psi_0, \Psi_1, x^1, v, t) = H(\Psi_0, \Psi_1, x^1, u, t) \tag{4}$$

is satisfied, where the interval [0, 1] is the region of admissible controls.

In the analysis of the derivative ∂H/∂u together with condition (4) we establish that at the center of the fuel element there is always an interval $[0, \rho_0]$, where the fuel is completely absent, and at the point ρ_0 the control varies in a jump for $\lambda_f/\lambda_m \leq 0.5$ by an amount 1/2B, and for $\lambda_f/\lambda_m > 0.5$ by 1 (generally for these values of λ_f/λ_m, the control takes two boundary values: 0 and 1). For $\lambda_f/\lambda_m \leq 0.5$ the function u(t) is found by the method of successive approximations, applied to the systems (2) and (3). Figure 1 shows how the variation in optimal distribution of the fuel along the radius of the fuel element depends on the values of λ_f/λ_m.

In the article we present solutions of the problem for the entire range of parameters $\bar{\varepsilon}$ and λ_f/λ_m. It is shown that the reduction of the temperature drop ΔT for optimization of ε(r) can be considerable. Thus, for $\bar{\varepsilon} = 0.3$ and $\lambda_f/\lambda_m = 0.03$–0.1, it is about 50%.

LITERATURE CITED

1. Yu. V. Milovanov, É. E. Petrov, and V. Ya. Pupko, Inzh.-Fiz. Zh., 24, No. 3, 533 (1973).
2. L. S. Pontryagin et al., Mathematical Theory of Optimal Processes [in Russian], Fizmatgiz, Moscow (1961).

INTERACTION OF THORIUM TETRACHLORIDE WITH CHLORIDES OF THE ALKALI METALS

A. N. Vokhmyakov, V. N. Desyatnik, and N. N. Kurbatov

UDC 541.126.2

To determine the possibility of using alkali metal chlorides with thorium tetrachloride as electrolytes in the production of thorium, as well as the behavior of thorium tetrachloride in molten alkali chlorides, the binary systems $MeCl-ThCl_4$ (where Me represents Li, Na, K, Rb, and Cs) were studied.

The fusibility of the systems was studied by differential thermal analysis. As a result of the highly hygroscopic character of thorium tetrachloride and the number of alkali metal chlorides, the experiments were conducted in an atmosphere of argon. As a result it was established that thorium tetrachloride interacts with lithium chloride, forming the compound $4LiCl \cdot ThCl_4$, which melts incongruently at 450 ± 2°C, and a eutectic with composition 38 mole % $ThCl_4$ with mp 408 ± 2°C.

Original article submitted February 23, 1973.

Thorium tetrachloride with sodium chloride forms the compound $2NaCl \cdot ThCl_4$, which melts congruently at 435 ± 2°C, and two eutectics. The eutectics formed by sodium chloride and by the compound $2NaCl \cdot ThCl_4$ correspond to the composition 26.5 mole % $ThCl_4$ at 360 ± 2°C. The eutectic formed by the compound $2NaCl \cdot ThCl_4$ and by thorium tetrachloride melts at 375 ± 2°C and contains 45 mole % $ThCl_4$. In the interaction of thorium tetrachloride with potassium chloride, two compounds $2KCl \cdot ThCl_4$ and $KCl \cdot ThCl_4$, which melt congruently at 705 ± 2 and 430 ± 2°C, and three eutectics with the compositions 25, 42, and 54 mole % $ThCl_4$ with mp 630 ± 2, 395 ± 2, and 420 ± 2°C, respectively, are formed. In the binary system $RbCl-ThCl_4$, two incongruently melting compounds $2RbCl \cdot ThCl_4$ and $RbCl \cdot ThCl_4$ were established at 710 ± 2 and 495 ± 2°C, and three eutectics with compositions 16, 44, and 58 mole % $ThCl_4$, with mp 625 ± 2, 410 ± 2, and 435 ± 2°C. Correspondingly, thorium tetrachloride interacts with cesium chloride, forming two compounds $2CsCl \cdot ThCl_4$ and $3CsCl \cdot 2ThCl_4$ and two eutectics. The compound $2CsCl \cdot ThCl_4$ melts congruently at 710 ± 2°C, $3CsCl \cdot 2ThCl_4$ incongruently at 567 ± 2°C. The eutectic formed by cesium chloride and by the compound $2CsCl \cdot ThCl_4$ melts at 576 ± 2°C and corresponds to the composition 19 mole % $ThCl_4$. The eutectic formed by the compound $3CsCl \cdot 2ThCl_4$ and thorium tetrachloride contains 60 mole % $ThCl_4$ at 460 ± 2°C. Since the radius of the alkali metal cation influences the stability of the chemical compound $2MeCl \cdot ThCl_4$ (where Me represents Na, K, Rb, and Cs), the transition from lithium to cesium is accompanied by a complication of the fusibility diagrams. The data obtained are compared with those published previously.

TRIPLE BACK-SCATTERING (REFLECTION) OF ELECTRONS IN THE USE OF $^{90}Sr - ^{90}Y$, $^{144}Ce - ^{144}Pr$, AND $^{106}Ru - ^{106}Rh$ β-SOURCES

L. M. Boyarshinov

UDC 539.124:539.121.72

In the study presented here we investigated how the characteristics of triple reflection of electrons vary with the maximum energy of a β-source in the 0.765-3.53 MeV range.

The measurements were carried out by the method described in [1]. Attenuation curves for targets made of six different elements were plotted with the $^{90}Sr-^{90}Y$ source, and curves for a lead target were plotted with the $^{144}Ce-^{144}Pr$ and $^{106}Ru-^{106}Rh$ sources. All the curves except the one for aluminum exhibited break-points, which in the case of measurements made with ^{204}Tl [2] had been observed only with heavy-element targets. It is assumed that these break-points were due to the superposition of triply reflected electrons on the flux, and even of electrons which had been reflected five or seven times, which also occur in this apparatus. In Fig. 1 we show the attenuation curve obtained with a $^{106}Ru-^{106}Rh$ source; the curve is graphically subdivided [3] into the attenuation curves for electrons emitted by the ^{106}Rh which have been reflected three, five, and seven times. In the case of the other sources, we can distinguish only the attenuation curves for the triply reflected electrons emitted by the daughter isotopes (^{90}Y, ^{144}Pr) and the curve of attenuation of the soft component, which is interpreted by superimposing the curve on the spectrum of electrons reflected five times and seven times (emitted by the daughter isotopes) and also the

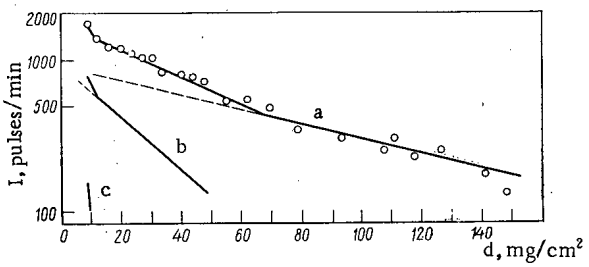

Fig. 1. Curves showing the attenuation of the intensity of electrons scattered three (a), five (b), and seven (c) times in aluminum filters of thickness d (the vertical scale is logarithmic; the source used was $^{106}Ru-^{106}Rh$).

Original article submitted April 4, 1973.

triply reflected electrons emitted by the soft mother isotopes (^{90}Sr, ^{144}Ce).

The intensity I_3 (after subtraction of the soft component) of the triply reflected electrons emitted by the isotope ^{90}Y varied with Z, the atomic number of the target, in the same way as in the case of single reflection of electrons [4]; the relation can be satisfactorily described by a power function

$$I_3 = AZ^n, \quad (1)$$

where A is a constant which depends only on the measurement geometry and on the power of the source. The exponent n varies between 2.29 and 3.04 for filters ranging from 9 mg/cm^2 (air layer) to 50 mg/cm^2 in thickness. Formula (1) is also applicable to the total intensity and the soft component. (For the total intensity the exponent n varies from 2.56 to 3.04 as the filter thickness varies from 9 to 50 mg/cm^2; for the soft component the exponent n varies from 2.94 to 3.50 as the filter thickness varies from 9 to 14 mg /cm^2.)

The variation of the maximum energy (E_3 and E_5) of the triply and quintuply reflected electrons, ascertained by the absorption method [3], as a function of the maximum energy E_0 of the source and the atomic number Z of the target, can be expressed as follows:

$$E_3 = 0.056Z^{0.45}E_0; \quad (2)$$

$$E_5 = 0.0064Z^{0.72}E_0. \quad (3)$$

We studied the variation in the characteristics of the triple reflection as a function of the β-source energy.

LITERATURE CITED

1. L. M. Boyarshinov, Dokl. Akad. Nauk SSSR, 178, No. 3, 573 (1968).
2. L. M. Boyarshinov, Dokl. Akad. Nauk SSSR, 186, No. 3, 545 (1969).
3. V. B. Luk'yanov, Measurement and Identification of β-Radioactive Specimens [in Russian], Gosatomizdat, Moscow (1963).
4. L. M. Boyarshinov, At. Énerg., 21, No. 1, 42 (1966).

CALCULATION OF GREULING – GOERTZEL ELASTIC SLOWING-DOWN PARAMETERS FOR ANISOTROPIC HIGH ENERGY SCATTERING

V. N. Gurin

UDC 621.039.51

An algorithm for a detailed 250-group calculation of a fast neutron spectrum at high energies (above 1 keV), in which anisotropic, elastic slowing down by neutrons is treated within the confines of the Greuling–Goertzel approximation, is proposed in [1]. In this algorithm, the anisotropy in the angular distribution of elastically scattered neutrons is taken into consideration for each isotope in terms of the average scattering angle and the energy-dependent Greuling–Goertzel elastic slowing-down parameters ξ and λ_0. Problems involving the calculation of the elastic slowing-down parameters are considered in [2]. Furthermore, the results of the calculations of $\xi(E)$ and $\lambda_0(E)$ for ^{16}O are also given in [3]. However, this kind of data for other important moderators is lacking in the literature. In this paper, this omission is partially remedied. Equations are proposed for calculating the elastic slowing-down parameters associated with an arbitrary elastic scattering law. The results of calculating $\xi(E)$ and $\lambda_0(E)$ for ^{12}C, ^{16}O, and ^{23}Na in the 1 keV to 10 MeV energy range are given.

Original article submitted April 19, 1973.

LITERATURE CITED

1. V. N. Gurin, V. S. Dmitrieva, and G. Ya. Rumyantsev, Preprint FÉI-223 [in Russian], Obninsk (1970).
2. H. Amster, in: Naval Reactors Physics Handbook, DIT-7030, Vol. 1, USAEC (1970), p. 89.
3. W. Stacey, Trans. Amer. Nucl. Soc., 13, 726 (1970).

A POLYTETRAFLUOROETHYLENE CHEMICAL DOSIMETER

B. K. Pasal'skii, V. A. Vonsyatskii,
Ya. I. Lavrentovich, and A. M. Kabakchi

UDC 53.07/08:53.001.5

The action of ionizing radiation on polytetrafluoroethylene (PTFE) has been investigated in [1, 2]. It was shown that radicals which are stable at room temperature are produced in the irradiated polymer. This property has been used for determining absorbed doses of γ-rays and electrons [3-5].

In the study reported here, in order to expand the possibilities for using PTFE in chemical dosimetry, we investigated the influence of parameters, of the type of radiation acting on the PTFE, and of various other factors on the character and degree of radical formation in this polymer.

We used PTFE ($d = 2.19$ g/cm^3, degree of crystallinity 60%) in the form of films 40 μ, 100 μ, and 200 μ thick which were irradiated with γ-quanta from ^{60}Co, electrons (0.23 MeV and 1 MeV), protons (5.7 MeV), deuterons (13 MeV), and α-particles (23 MeV),* which enabled us to vary the LET from ~0.2 to 55 keV/μ. The procedures used in the irradiation and in determining the absorbed energy are described in [6]. The irradiation was carried out in a vacuum (10^{-3}-10^{-4} torr) and in air at dose rates ranging from 0.4 to 20 krad/sec and specimen temperatures not exceeding 50°C.

The ESR spectra of the radicals were recorded on an RÉ-1301 radiospectrometer. The standard used was a single crystal of $CuCl_2 \cdot 2H_2O$; the number of unpaired electrons in the crystal was determined more accurately by the method described in [7]. After the irradiation we recorded chiefly the ESR spectra of the peroxide radicals, which formed an asymmetric singlet. The shape of the ESR spectra remained unchanged when the PTFE was irradiated with heavy charged particles.

We found that the concentration of the radicals increased linearly with the dose in the range from 0.5 to 80 Mrad (Fig. 1). The values of the radiation yield of radicals after exposure to various kinds of ionizing radiation are shown in Table 1.

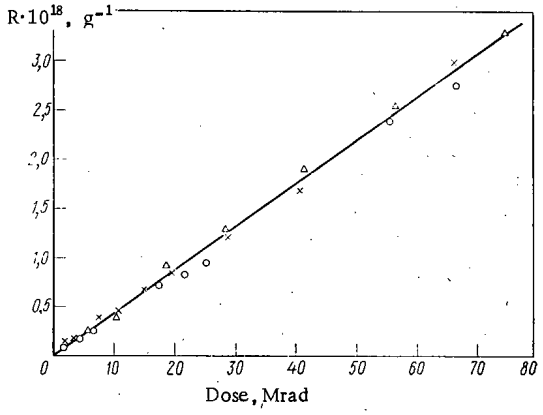

Fig. 1. Concentration of peroxide radicals as a function of dose upon exposure to: ^{60}Co γ-rays (○); protons (×); and γ-particles (△).

It can be seen from Table 1 that as the LET increases by more than two order of magnitude, the yield of radicals remains almost unchanged. It may be assumed

*Irradiation with heavy charged particles was carried out on the cyclotron of the Nuclear Research Institute of the Academy of Sciences of the Ukrainian SSR.

TABLE 1. Radiation Yield of Peroxide Radicals in Irradiated PTFE

Type of radiation	Energy, MeV	LET_∞, keV/μ	Radiation yield, 1/100 eV
^{60}Co gamma rays	1,25	0,2	0,07±0,01
Protons	5,7	14	0,07±0,02
Alpha particles	23,0	55	0,07±0,01

Translated from Atomnaya Énergiya, Vol. 35, No. 6, pp. 427-428, December, 1973. Original letter submitted October 11, 1972; revision submitted May 21, 1973.

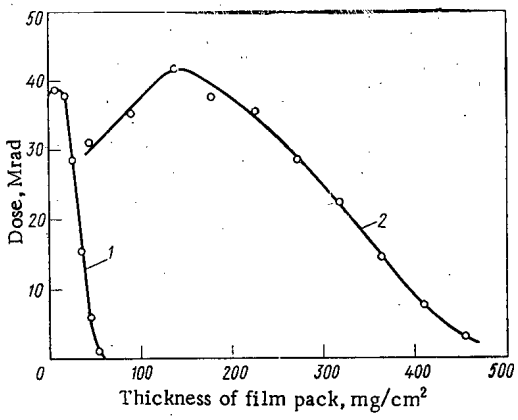

Fig. 2

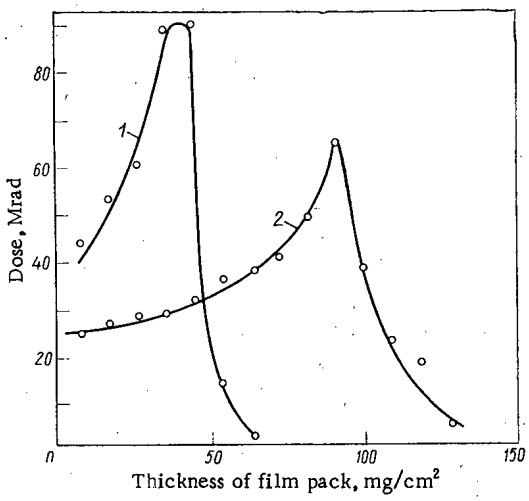

Fig. 3

Fig. 2. Distribution of absorbed doses as a function of the thickness of a pack of PTFE films irradiated with electrons having energies of 0.23 MeV (1) and 1 MeV (2).

Fig. 3. Distribution of absorbed doses in packs of PTFE films irradiated with γ-particles (1) and neutrons (2).

that the track effects do not have any influence on the rate of accumulation of radicals when PTFE is irradiated; this is apparently because the energy is absorbed uniformly throughout the entire irradiated volume.

The concentration of radicals remains unchanged when the specimens are stored for 20 days at room temperature, and after 55 days the concentration decreases by only 10%. When the temperature is raised to 70°C, the concentration of radicals remains constant, and only at 150-200°C do the radicals die at an appreciably rapid rate. The values we obtained for the effective energy of activation of the process of death of the radicals in the 160-250°C range were 13 kcal/mole for the amorphous phase of the polymer and 29 kcal/mole for the crystalline phase, which agrees with the data of [2].

Special tests showed that the radiation yield of radicals was unaffected by the oxygen in the air and by variation of the dose rate from 0.4 to 20 krad/sec; it also remained constant when films of different thickness were irradiated.

Thus, in its dosimetric characteristics PTFE satisfies fairly well the requirements for a chemical dosimeter. The fact that the radiation yield of radicals remains unchanged when the LET and dose rate are varied over wide ranges suggests that PTFE can be used for determining not only absorbed doses of γ-rays and electrons but also absorbed doses of heavy charged particles. No special calibration of the dosimeter is necessary; this is an advantage over alanine dosimeters [8, 9], for which the rate of accumulation of radicals was found to depend substantially on the LET.

The absorbed dose in the interval from 0.5 to 80 Mrad can be calculated by the following formula:

$$= 2.306 \cdot 10^{-17} \cdot [R],$$

where [R] represents the concentration of peroxide radicals per gram.

By using PTFE films of different thicknesses, we can determine (to within several microns) the spatial distribution of absorbed doses of charged particles in the layers. We obtained curves showing the distribution of absorbed doses (Figs. 2, 3) as a function of the depth of the irradiated material for the case of beams of electrons (0.23 MeV and 1 MeV), deuterons (13 MeV), and α-particles (23 MeV). It can be seen from the figures that the dose reaches a maximum at the beginning of the trajectory in the case of electrons and at the end of the trajectory in the case of heavy charged particles.

It should be noted that the range of doses measurable with a PTFE dosimeter can be considerably expanded. For example, the sensitivity of the dosimeter is multiplied more than a hundredfold when the concentration of radicals is measured in large specimen weights with highly sensitive spectrometers. Using a PTFE dosimeter, we can determine doses for values above 100 Mrad; however, in this region, as the present study shows, the rate of radical formation is no longer a linear function of the absorbed

energy. Using PTFE in the form of a powder or very thin films, we can determine the absorbed dose and the extrapolated paths of low-energy charged particles. For radiation dosimetry we can use PTFE of a different degree of crystallinity from the one investigated in the present study, since according to [1, 2], the initial concentration of radicals in the irradiated polymer is independent of the degree of crystallinity.

The relative error in the determination of the absorbed dose by means of a PTFE dosimeter in the 0.5-80 Mrad range is about 10-15%. In some cases the measurements can be made considerably more accurate.

LITERATURE CITED

1. L. A. Blyumenfel'd, V. V. Voevodskii, and A. G. Semenov, The Use of ESR in Chemistry [in Russian], Izd. SO AN SSSR (1962).
2. V. V. Voevodskii, Physics and Chemistry of Elementary Chemical Processes [in Russian], Nauka, Moscow (1969).
3. H. Judeikis et al., Radiation. Res., 35, No. 2, 247 (1968).
4. H. Judeikis and S. Siegel, IEEE Trans. Nucl. Sci., No. 6, 237 (1967).
5. N. Tamura et al., J. Appl. Phys., Japan, 9, 1148 (1970).
6. Ya. I. Lavrentovich et al., Khim. Vys. Énerg., 3, 147 (1969).
7. D. Smith and F. Dierroni, Canad. J. Chem., 43, No. 4, 876 (1965).
8. W. Bradshaw et al., Radiation Res., 17, No. 1, 11 (1962).
9. P. Ebert et al., Radiation Res., 26, No. 2, 178 (1965).

ANALYTIC DETERMINATION OF SUBGROUP PARAMETERS

V. V. Sinitsa and M. N. Nikolaev

UDC 539.125.52:621.039.51.12

The method of subgroups [1] is at present the most effective way of calculating neutron resonance fields in heterogeneous systems in a region where an approximation by narrow resonances is applicable, i.e., in a region of low-lying, broad and intermediate resonances, the calculations can be performed by an alternative method, which takes into account the detailed structure of the cross sections. A subgroup is defined as a set of a given group of neutrons having similar total cross sections and characterized by the fraction of the subgroup in the group and by the subgroup total and partial cross sections. Until now, the subgroup parameters were determined using the method of least squares [2, 3], which, as a result of the nonlinearity of the problem, required a large expenditure of computer time and resulted in a distortion of significant average characteristics. The method under discussion here ensures exact conservation of the most important moments of the cross sections and is much simpler from the calculational point of view.

It follows from [4] that for an accurate calculation of the constants for the P_1-approximation in a medium consisting only of the isotope under consideration (i.e., when the resonance self-screening is especially great), it is sufficient to calculate the cross-section moments $\langle\sigma_x\rangle$, $\langle\sigma_x/\sigma\rangle$, $\langle 1/\sigma\rangle$, $\langle 1/\sigma^2\rangle$. In order to take into account the effect of the self-screening on the concentration of the isotope in the medium, one must also define the moments $\langle\sigma_x/\sigma^2\rangle$ etc. and $\langle\sigma_x\sigma\rangle$ etc. for high and low concentrations, respectively.

Let us utilize as the fundamental conserved quantities the cross-section moments:

$$\langle\sigma_x\sigma^n\rangle=\int_{E_1}^{E_2}\sigma_x(E)\,\sigma^n(E)\,\varphi(E)\,dE\Big/\int_{E_1}^{E_2}\varphi(E)\,dE, \tag{1}$$

where $\sigma(E)$, $\sigma_x(E)$ are the total and partial cross sections; $\varphi(E)$ is the neutron spectrum; E_1, E_2 are the limits of the group interval. The quantities $\langle\sigma_x\sigma^n\rangle$ can be obtained from the detailed energy dependence of the cross sections, by means of the parameters for the allowed resonances [5], from experimentally determined transmission functions [6], or calculated using the average resonance parameters [7]. The problem involves approximating by subgroup parameters the moment sequences:

$$\langle\sigma_x\sigma^n\rangle=\sum_{i=1}^{N}a_i\sigma_{xi}\sigma_i^n,\quad n=0,\pm1,\pm2,\ldots;\qquad x=1,2,\ldots,M, \tag{2}$$

where N is the number of subgroups in the group interval $[E_1, E_2]$; a_i is the fraction of the subgroup i in this interval; σ_i, σ_{xi} are the subgroup total and partial cross sections.

Let us introduce the basis moments $t_n(\alpha)$ in the following manner:

$$t_n(\alpha)=\sum_{x=1}^{M}\alpha_x\langle\sigma_x\sigma^n\rangle;\quad \alpha_x\geqslant 0,\quad \sum_{x=1}^{M}\alpha_x=1. \tag{3}$$

The sequence of basis moments is positive for every position of the vector α (since $\sigma_x(E) > 0$ [8]); hence, one can represent uniquely the finite subsequence $\{t_n(\alpha)\}_{n=n_1}^{n_1+2N-1}$, consisting of 2N elements [9], in the form

Translated from Atomnaya Énergiya, Vol. 35, No. 6, pp. 429-430, December, 1973. Original letter submitted December 6, 1972.

$$t_n(\alpha)=\sum_{i=1}^{N} b_i(\alpha)\,\lambda_i^n(\alpha),$$
$$n=n_1,\ n_1+1,\ \ldots,\ n_1+2N-1, \tag{4}$$

where $b_i(\alpha) > 0$; $\lambda_i(\alpha)$ are real and distinct for every α. The values of $\lambda_i(\alpha)$ are roots of the polynomial

$$P_N(\alpha,\lambda)=\sum_{k=0}^{N} z_k(\alpha)\,\lambda^k, \tag{5}$$

whose coefficients depend on α and are determined from the system of linear equations:

$$\sum_{k=0}^{N-1} t_{k+j}(\alpha)\,z_k+t_{N+j}(\alpha)=0;$$
$$z_N=1,\ j=n_1,\ n_1+1,\ \ldots,\ n_1+N-1. \tag{6}$$

One can show that if $\sigma(E) > 0$, the roots of the polynomial $P_N(\alpha, \lambda)$ are strictly positive for every α [8]. We shall take the subgroup total cross sections $\sigma_i = \lambda_i(\alpha_0)$ for some as yet arbitrary $\alpha = \alpha_0$. Let us select equations from the system (2) for every x corresponding to an N and let us substitute the already known σ_i into them. We shall obtain M systems of linear equations in the unknowns $a_i\sigma_{xi}$. We shall determine from these equations, using the physically manifest condition $\sigma_i = \sum_{x=1}^{M} \sigma_{xi}$, the subgroup fractions and the partial cross sections:

$$a_i=\sum_{x=1}^{M}(a_i\sigma_{xi})/\sigma_i,\quad \sigma_{xi}=(a_i\sigma_{xi})/a_i. \tag{7}$$

The subgroup parameters obtained in this manner for N subgroups conserve exactly N cross-section moments for each reaction x, notably, those moments which entered into the system of equations for determining the $a_i\sigma_{xi}$. We shall calculate the rest of the moments using the parameters found. It can be shown that the accuracy of the reduction in the moments is unsatisfactory for certain reactions, i.e., the structure of the cross sections is reflected in insufficient detail. As a consequence of this, the quantities $a_i\sigma_{xi}$ can be negative, resulting in negative parameters, which do not have a physical meaning. At the same time, for each reaction x', there certainly exists an α_0' ($\alpha_x = 0$, $x \neq x'$; $\alpha_{x'} = 1$), for which $a_i\sigma_{x'i} > 0$ for every i [see (3), (4)], but the number of cross-section moments accurately reduced for a given reaction x' is a maximum equal to 2N. This indicates a possibility for formulating the problem of the search for a vector α_0, which would satisfy to the maximum the requirements of accuracy in the reduction of the moments and the positiveness of the subgroup parameters. Generally speaking, one can simultaneously satisfy these two requirements, when the functions $\sigma_x(E)$ behave in an arbitrary manner, only for a sufficiently large number of subgroups N. With an increase in N, the roots $\lambda_i(\alpha_0)$ of the polynomial become all the less sensitive to the choice of α_0, and the number of moments accurately reduced approaches the maximum possible value 2MN for a given number of subgroups. At the same time, all of the subgroup parameters will certainly be positive.

Let us assume as a zeroth approximation the vector α_0, whose components are all equal: $\alpha_x = 1/M$; $x = 1, 2, \ldots, M$. In this case, the 2N total cross-section moments $\langle\sigma^n\rangle$ are conserved exactly (since $\sigma(E) = \sum_{x=1}^{M} \sigma_x(E)$, $\langle\sigma^n\rangle = \sum_{x=1}^{M} \langle\sigma_x\sigma^{n-1}\rangle$), and even for a minimum number of subgroups (N = 2), it is possible to conserve exactly all of the most significant cross-section moments: $\langle\sigma_x\rangle$, $\langle\sigma_x/\sigma\rangle$, $\langle 1/\sigma\rangle$, $\langle 1/\sigma^2\rangle$. If the subgroup parameters for N = 2 do not satisfy the requirements of positiveness and the accuracy of the reduction in the moments $\langle\sigma_x/\sigma^2\rangle$, $\langle\sigma_x\sigma\rangle$, one must pass to a large number of subgroups. The upper limit N' of the number of subgroups is determined by the number of moments whose conservation must be guaranteed by the given system of subgroup constants. One can show that for N = N', the structure of the cross sections is, nevertheless, reflected in insufficient detail; for example, not all of the $a_i\sigma_{xi}$ are positive. In this case, one should utilize the possibilities implied by the selection of the vector α. Let us assume that for some reaction x', $a_i\sigma_{x'i} < 0$. Increasing the corresponding component $\alpha_{x'}$ (at the same time, one should reduce all of the remaining components so that the condition $\sum_{x=1}^{M} \alpha_x = 1$ should not be violated), one can make all of the $a_i\sigma_{x'i}$ positive for a given reaction x'. Obviously, for N = N', it is also advisable to minimize by means of α the error in the reduction of bordering moments.

Finally, let us discuss the problems concerning the selection of n_1 (the minimum order of the basis moments in the subsequence $\{t_n(\alpha)\}$) and the system of linear equations for the determination of $a_i\sigma_{xi}$. When N = 2, it is advisable to take $n_1 = -2$ since, in this case, the moments necessary for the calculation of the coefficient of diffusion and the group-averaged, blocked cross sections for a homogeneous medium of the isotope under consideration are conserved exactly. The quantities $a_i\sigma_{xi}$ must be determined from equations involving moments with n = −1 and n = 0, which guarantees accordingly the exact normalization of the probability ($\sum_{x=1}^{M} \langle\sigma_x/\sigma\rangle = \sum_{i=1}^{N} a_i = 1$) and the conservation of the average cross section. If N = 3, the choice of $n_1 = -3$ and the inclusion of an equation with the moment $\langle\sigma_x/\sigma^2\rangle$ permits one to take into account more precisely the dependence of the group-averaged coefficient of diffusion and the reaction cross sections on the isotope concentration in the medium. If N = 4, n_1 should equal −4 and the moment $\langle\sigma_x\sigma\rangle$ should be introduced into the system of equations. This choice provides a possibility for varying the vector α since the exact conservation of all of the most significant moments is already guaranteed.

With the derivation of the subgroup constants for neutron cross sections, at least up to the present time, one succeeded in guaranteeing the positiveness of the subgroup parameters and reasonable accuracy for a reduction in the bordering moments when the number of subgroups does not exceed four.

The selection of moments and equations described is directed towards obtaining the subgroup constants intended for the calculation of neutron diffusion in media. For other purposes (for example, approximations of transmission functions by an exponential sum), this choice can be different. The algorithm for obtaining the subgroup parameters is achieved by a program written in the ALGOL-60 language. A combination with a series of programs, which calculate the moments from the detailed behavior of the cross sections, the parameters for the allowed resonances, and the average resonance parameters, is accomplished.

LITERATURE CITED

1. M. N. Nikolaev et al., At. Énerg., 29, No. 1, 11 (1970); 30, No. 5, 426 (1971).
2. M. N. Nikolaev and V. F. Khokhlov, in: Information Bulletin of the Nuclear Data Center [in Russian], No. 4, Atomizdat, Moscow (1967), p. 420.
3. M. N. Nikolaev and V. F. Khokhlov, in: Nuclear Constants [in Russian], No. 8, Izd. TsNIIatominform, Moscow (1972), Part 2, p. 119.
4. L. P. Abagyan et al., Group Constants for the Design of Nuclear Reactors [in Russian], Atomizdat, Moscow (1964).
5. L. P. Abagyan et al., see [2], p. 392.
6. R. Bramblett and J. Czirr, Nucl. Sci. and Eng., 35, 350 (1969).
7. M. N. Nikolaev et al., "Calculational methods for group cross sections in a region of forbidden resonances." Proceedings of the Trilateral Soviet–Belgian–Dutch Symposium on Certain Problems in Fast Reactor Physics [in Russian], Vol. 1, Izd. TsNIIatominform, Moscow (1970).
8. N. I. Akhiezer, The Classical Moment Problem [in Russian], Fizmatgiz, Moscow (1961), Chap. 1, p. 2.
9. R. Bellman, Introduction to Matrix Analysis, McGraw–Hill, New York (1960).

RADIATION LOOP WITH ACTIVITY GENERATOR MADE OF FLAT TUBULAR ELEMENTS: IRT REACTOR OF THE TOMSK POLYTECHNIC INSTITUTE

E. P. Gefsimanskii, S. A. Kuznetsov,
Yu. G. Kulagin, E. S. Sakharov,
A. G. Skorikov, and I. P. Chuchalin

UDC 621.029.573

It is generally acknowledged that the efficiency of absorber is higher in homogeneous absorber–moderator systems than in heterogeneous ones, because of the reduced self-shielding of the absorber nuclei and because of the increased values of the resonance integral. By extending this phenomenon to the activity generator in radiation loops, we can manage to set up quasihomogeneous systems of alternating layers of absorber working material and moderator in those systems so as to substantially raise the efficiency of the expensive γ-carrier and to obtain power parameters of the radiation loop which would be an improvement over the parameters obtained in loops with modular generators [1]. Starting in 1967, an indium–gallium–tin radiation loop in which a two-layer activity generator is used [2] has been in operation at the IRT reactor of Tomsk Polytechnic Institute. Even though the two-layer system fails to provide such a high degree of homogenization of the γ-carrier and moderator as would be expected when a larger number of layers is relied upon, nevertheless the parameters of the radiation loop with the two-layer activity generator are substantially higher than in a similar radiation loop with a one-layer system [3]. A radiation loop with a four-layer activity generator proved even more efficient [4]. The concept of quasihomogeneous activity generator systems using tubular elements of γ-carrier has also been dealt with in [5-6].

The Tomsk Polytechnic Institute (TPI) two-layer generator was replaced in 1970 by a multilayer activity generator consisting of flat tubular elements. This loop has been in constant service since 1971. Figure 1a shows a cartogram of the core loading pattern responsible for the loop characteristics cited below, and Fig. 1b shows the flowsheet of the radiation loop.

The new activity generator (Fig. 2) also makes it possible to attain a still higher degree of "homogenization" of the absorber in the moderator medium, so that a higher γ-radiation dose rate is obtained with a smaller volume of γ-carrier (1350 cm^3 as against 1550 cm^3 in [2]). The generator coil, formed by 22 flat elements (500 mm in length, 62 mm in width, 2 mm in thickness; volume of γ-carrier in an element 61.5 cm^3) lying perpendicular to the face of the core and pitched 22 mm apart on the average are placed within an enclosure with an independent cooling system. When the reactor is operated at normal levels (2 to 3 MW), there is no need for forced cooling, and water inside the cooling enclosure mixes by convection with the reactor pool water.

The decrease in the reactivity margin due to the operation of the loop is not greater than 0.08%, and that is accounted for by the low concentration of absorber nuclei (in turn due to the geometry of the layers) in the layers of reflector close to the core.

The elements comprising the generator are arranged in series. A parallel arrangement is deemed infeasible, since high circulation rates would have to be maintained in that case in order to attain the loop power rating, and as a way of averting stagnation (or excessive holdback) of γ-carrier in separate parallel branches as a result of the hydraulic differences and incongruities between the elements.

Changes in the arrangement concern mainly the γ-carrier receptacle. It no longer participates directly in the circulation flow conditions, but functions only as a storage for the γ-carrier when the

Translated from Atomnaya Énergiya, Vol. 35, No. 6, pp. 430-432, December, 1973. Original letter submitted December 6, 1972.

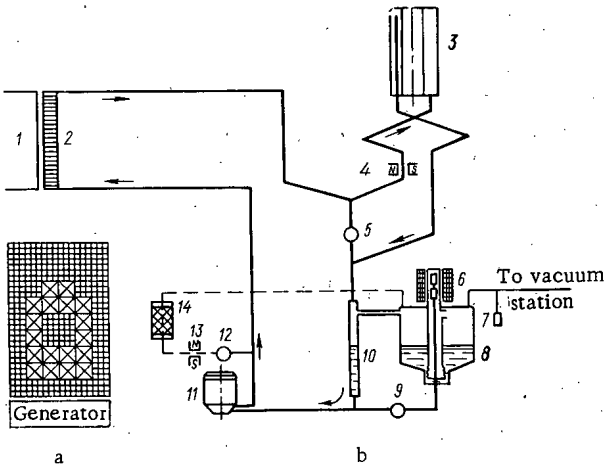

Fig. 1

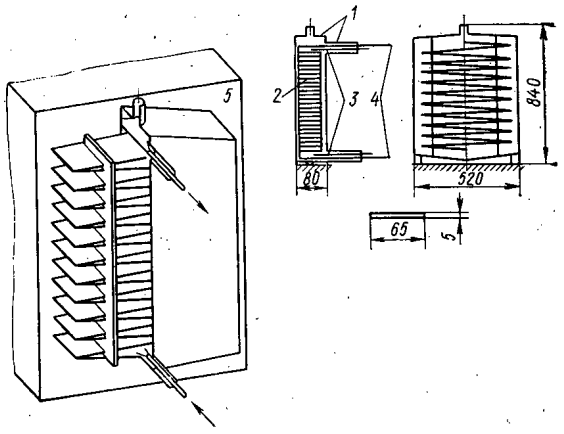

Fig. 2

Fig. 1. Working loading of core (a) and flowsheet of radiation loop (b): light hatching denotes beryllium; heavier hatching denotes fuel; 1) core; 2) activity generator; 3) mobile irradiator; 4, 13) magnetic flowmeters; 5, 9, 12) electromagnetically actuated valves; 6) level gage with bellows-actuated differential-transformer sensor; 7) LT-2 tube; 8) storage tank; 10) expander; 11) electromagnetic conductive pump; 14) filter.

Fig. 2. Activity generator consisting of flat tubular elements: 1) shielded enclosure; 2) coil; 3) thermocouples; 4) piping; 5) core.

reactor is shut down, or when the loop ceases operating. Consequently, it can contain whatever required amount of γ-carrier for irradiators of different volumes. When the loop is being filled, exactly as much alloy as needed to fill all the loop subassemblies is taken from the storage receptacle. This layout and arrangement for connecting the storage receptacle greatly simplified the job of replacing the irradiators: alloy does not have to be loaded in full (or conversely, does not have to be totally removed from the loop) in order to retain the minimum "destructive" volume. All the valves in the loop are actuated electromagnetically and controlled remotely. The irradiator can be moved about and can be enclosed in a shielded cave. The loop incorporates the filtration ducting, which functions as needed and facilitates cleaning the alloy stream periodically on a filter charged with Raschig porcelain rings.

Radiation Loop Performance Data

Activity generated	$6 \cdot 10^4$ g-eq/MW
Volume γ-carrier in generator	1350 cm^3
Volume γ-carrier in irradiator	2400 cm^3
Total volume γ-carrier in loop	4400 cm^3
Activity in irradiator	$3.3 \cdot 10^4$ g-eq/MW
Irradiator dimensions:	
height	400 mm
inner diameter	78 mm
outer diameter	118 mm
Dose rate at center of irradiator	750 R/sec·MW
Loop working γ-carrier flowrate	5 cm^3/sec
Peak temperature in generator (at reactor output level 3 MW)	75°C

Consequently, the facility now in service differs essentially from its precursor both in power output and in the simpler layout. The increase in loop power output combined with a simultaneous reduction in the amount of γ-carrier made it possible to have a high-intensity γ-field while expanding the range of research facilitated by the arrangement, particularly in the domain of radiation physics.

LITERATURE CITED

1. G. I. Kiknadze et al., Byulleten' Izobret., No. 30, 112 (1971).
2. E. S. Sakharov et al., At. Énerg., 29, No. 1, 43 (1970).

3. G. I. Kiknadze et al., At. Énerg., 19, No. 2, 176 (1965).
4. G. I. Kiknadze et al., At. Énerg., 31, No. 2, 143 (1971).
5. A. S. Dindun et al., Izv. Akad. Nauk LatvSSR, Seriya Fiz.-Tekh. Nauk, No. 6, 42 (1968).
6. A. S. Dindun et al., Izv. Akad. Nauk LatvSSR, Seriya Fiz.-Tekh. Nauk, No. 3, 53 (1969).

MUTUAL SCREENING OF γ-CARRIER LAYERS IN MULTILAYER RADIATION-CONTOUR-ACTIVITY GENERATORS

E. S. Sakharov and I. P. Chuchalin

UDC 621.039.573:621.039.553

At present in constructing radiation contours more and more use is being made of multilayer activity generators in which individual γ-carrier layers alternate with moderator layers [1, 2]. In connection with this, attempts are being made to study experimentally processes of activity generation by reactor neutron fields in such multilayer compositions [3].

If one defines the mutual-screening coefficient of the γ-carrier layers in the absorber–moderator system as the ratio of the average layer activity in the multilayer composition to the average activity of a layer when the others are absent, then

$$f_{ms} = \frac{\bar{A}}{\bar{A}_s} = \frac{\bar{\varphi}}{\bar{\varphi}_s},$$

where $\bar{A}$, $\bar{\varphi}$ are the average unit activity and the average activation-neutron flux in the γ-carrier layers located in the multilayer generator; $\bar{A}_s$ and $\bar{\varphi}_s$ are the average unit activity and the average activation-neutron flux in the case of a single layer in the same moderator and neutron field.

Knowing f_{ms}, one can calculate the value of the generated activity in multilayer generators:

$$R_{ga} = \bar{\varphi}_0 \Sigma_{act} V_{ga} f f_{ms}$$

where $\bar{\varphi}_0$ is the average unperturbed flux in the activation zone; Σ_{act} is the γ-carrier activation cross section; V_{ga} is the γ-carrier volume in a multilayer activity generator; f is the perturbation factor for a single layer; f_{ms} is the mutual-screening coefficient of the layers.

At the Tomsk Polytechnic Institute's Scientific-Research Institute on Nuclear Physics, Electronics, and Automation, experimental studies have been conducted on determining the mutual-screening coefficient of indium layers having various $\Sigma_a d$ (Σ_a is the absorption cross section; d is the layer thickness) in water in two-, three-, and multilayer activity-generator models with various spacing between layers in a thermal-neutron field.

Water was chosen as the moderator for ease in conducting the experiments, which were done on the swimming-pool type IRT research reactor [4]. The results can obviously be transferred with small errors to other moderators by taking their scattering and absorbing properties into account.

The two-, three-, and multilayer activity-generator model assemblies were plastic cells fixed to the end of a rod. Inside, indium foils, 100 mm in diameter with thickness $\Sigma_a d = 0.10$-1.1, were placed on 2-mm thick plastic backings from 0 to 30 mm apart (Fig. 1a, b). The rod with cell was lowered into the reactor pool and positioned with constant geometry over the core. The irradiation zone was chosen with primarily thermal neutrons (R_{Cd} with respect to indium greater than 10); the foils were oriented perpendicular to the upper core boundary; the neutron distribution was linear and along the assembly axis perpendicular to the foil surfaces (Fig. 1c). The exposure time in all experiments was 3 min. Irradiation took place at constant reactor power. Unperturbed-flux fluctuations in the activation zone were accounted for by using indium monitors 15 mg/cm^2 in thickness, located 10 cm from the assembly upper edge directly on the rod. All measurements were relative to the counting rate in this monitor. The flux distribution in the assembly-irradiation zone was measured by similar foils.

Translated from Atomnaya Énergiya, Vol. 35, No. 6, pp. 432-433, December, 1973. Original letter submitted December 6, 1972.

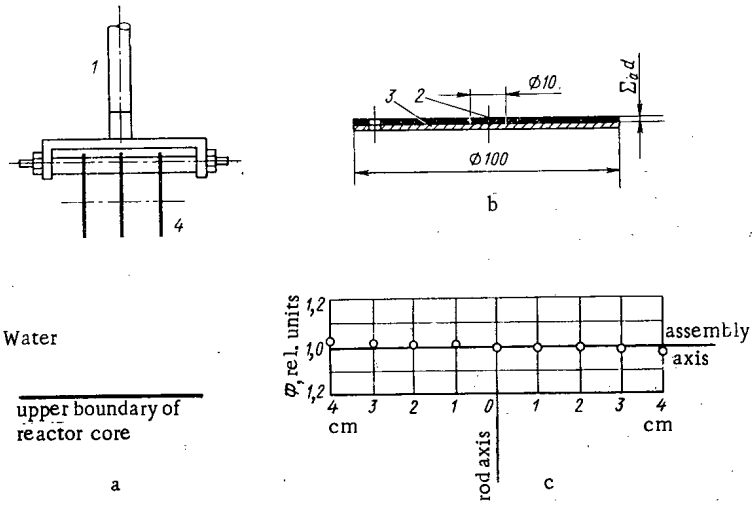

Fig. 1. a) Positions of model assemblies in swimming-pool reactor; b) assembly element; c) distribution of thermal-neutron flux in model-assembly activation zone: 1) rod; 2) detector (indium); 3) backing (plastic); 4) position of assembly elements in cell for irradiation.

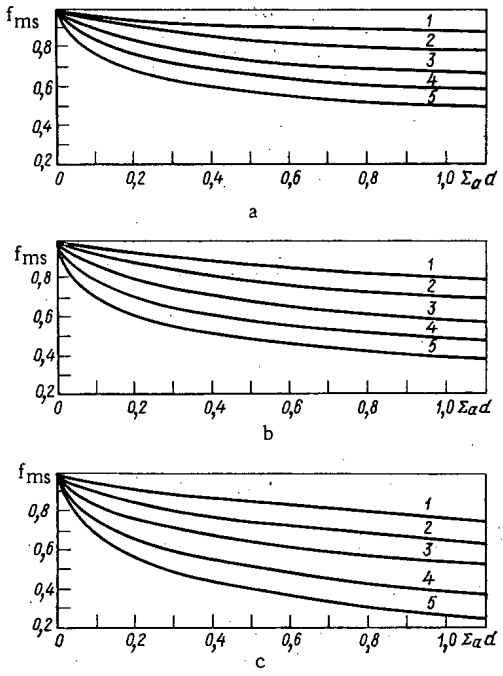

Fig. 2. Mutual-screening coefficient in two-layer (a), three-layer (b), and multilayer (c) model assmblies as a function of $\Sigma_a d$ values characterizing the assembly-element thickness: 1) $\Sigma_S d_0 = 10.35$; 2) $\Sigma_S d_0 = 6.90$; 3) $\Sigma_S d_0 = 3.45$; 4) $\Sigma_S d_0 = 1.72$; 5) $\Sigma_S d_0 = 0.69$ (Σ_S is the moderator scattering cross section; d is the moderator layer thickness).

The mutual-screening coefficient was judged from the ratio of the averaged unit γ-activity of the layers to the average unit γ-activity of a single layer irradiated under identical conditions. To supply the results to infinite layers, we determined the average unit activity of a layer by measuring 10-mm-diameter indicators cut from the center of the irradiated foils. Since one need not know the absolute activity to determine the mutual-screening coefficient, we limited the calculation to relative measurements in constant geometry.

The multilayer assembly was a five-layer composition. The central layer was considered as an element of an infinite system. All measurements were made on a PP-8 apparatus with a scintillation counter [NaI(Tl) crystal, 40 mm in diameter]. Activity caused by resonance neutrons was not taken into account. The measurement error did not exceed 10%.

Figure 2a, b, and c shows curves for the mutual-screening coefficient for two-, three-, and multilayer generators in a thermal-neutron field. The magnitude of the coefficient depends on the moderator layer and the thickness of γ-carrier layers comprising the generator. The influence of layers whose

thicknesses correspond to values $\Sigma_a d \leq 0.1$, already in a multilayer generator with distance between layers approaching $\sim\lambda_{tr}$ is small in practice, not exceeding 10-15%.

The results obtained may be used for designing two-, three-, and multilayer activity generators and for choosing optimal γ-carrier and moderator-layer thicknesses taking into account unperturbed-neutron-field distribution in the activation zone.

LITERATURE CITED

1. E. S. Sakharov et al., At. Énerg., 29, No. 1, 43 (1970).
2. G. I. Kiknadze et al., At. Énerg., 31, No. 2, 143 (1971).
3. G. I. Kiknadze et al., At. Énerg., 31, No. 2, 113 (1971).
4. V. V. Goncharov et al., The Second Geneva Conference, 1958 [in Russian], Vol. 2, Atomizdat, Moscow (1959), p. 273.

THERMODYNAMIC PROPERTIES OF LIQUID ALLOYS OF THORIUM WITH ALUMINUM

A. M. Poyarkov, V. A. Lebedev, I. F. Nichkov, and S. P. Raspopin

UDC 669.715.298

To determine the thermodynamic properties of saturated solutions of thorium in aluminum and the compound $ThAl_3$ at equilibrium with them, we measured the emf of the galvanic cell:

$$Th_{sol} \mid KCl-NaCl+ThCl_n \mid\mid KCl-NaCl+ThCl_4 \mid Th-Al_{liq}. \quad (1)$$

The alloys were prepared by fusion of shavings of metallic thorium (99.8%) with aluminum (99.97%) in crucibles of beryllium oxide, directly in the cell. The thorium content in the alloys (40-50 wt. %) exceeded its solubility in aluminum at the highest experimental temperature and corresponded to the two-phase region of the phase diagram L + $ThAl_3$ [1]. The current leads for the electrodes were prepared from titanium. The ions of the potential-determining element were introduced into a melt of preliminarily dehydrated salts in the form of anhydrous thorium tetrachloride, freed of impurities by two redistillations under vacuum at 850°C. It is known that in melts of alkali chlorides, metallic thorium reduces a substantial fraction of the Th^{4+} ions to the divalent state [2]. At the surface of the alloy, the activity of thorium in which is reduced, the ratio Th^{4+}/Th^{2+} is shifted in the direction of a substantial predominance of ions of higher valence. In order to eliminate the transfer of thorium from the metal to the alloy according to a reaction of disproportionation of Th^{2+} ions, the electrode spaces were separated by a diaphragm, and the thermodynamic properties of the alloys were calculated according to the method proposed in [3]. The equilibrium constant of the reaction $Th + Th^{4+} \rightleftharpoons 2Th^{2+}$ in a melt of KCl–NaCl varies with the temperature according to the expression [2]: $\log K = 0.0554 - 2966/T$. Considering the constant and the initial content of Th^{4+} in the electrolyte (0.493 at. %), we calculated the concentration of Th^{4+} and Th^{2+} in metallic thorium ($C_{Th^{4+}}$, $C_{Th^{2+}}$). The concentration of Th^{2+} ions in the alloy ($C'_{Th^{2+}}$) can be determined according to the value of the emf between thorium and the alloy,

$$-E = \frac{RT}{2F} \ln \frac{C_{Th^{4+}}}{C_{Th^{2+}}} \cdot \frac{C'_{Th^{2+}}}{0{,}00493 - 0{,}5C'_{Th^{2+}}}.$$

The results of the calculations are cited in Table 1.

For the alloys studied, the fraction of Th^{2+} is negligible, while the average valence of thorium ions can be assumed equal to four with a greater degree of accuracy. Therefore, for a study of the thermodynamic properties of homogeneous solutions and an establishment of the solubility of thorium in aluminum, we measured the emf of simpler galvanic cells:

$$Th-Al_{(L+ThAl_3)} \mid KCl-NaCl+ThCl_4 \mid Th-Al_{(soln)}. \quad (2)$$

TABLE 1. Fraction of Th^{2+} Ions in Thorium and Two-Phase Alloys L + $ThAl_3$

T°, K	K×10³	Concentrations and fractions of ions						
		in thorium			in alloy			
		$C_{Th^{4+}} \times 10^3$	$C_{Th^{2+}} \times 10^3$	$\frac{C_{Th^{2+}}}{C_{Th^{4+}}}$	E, V	$C'_{Th^{2+}}$	$\frac{C'_{Th^{2+}}}{C'_{Th^{2+}}}$	n_{av}
973	1,016	3,93	2,00	0,337	0,350	$5{,}7 \cdot 10^{-7}$	$1{,}1 \cdot 10^{-4}$	3,9998
1073	1,955	3,60	2,65	0,424	0,328	$2{,}9 \cdot 10^{-6}$	$5{,}9 \cdot 10^{-4}$	3,9988

Translated from Atomnaya Énergiya, Vol. 35, No. 6, pp. 434-435, December, 1973. Original letter submitted February 7, 1973.

TABLE 2. Experimental Values of the emf of Two-Phase Alloys L + $ThAl_3$ Relative to α-Thorium

T, °K	E_1, mV	E_2, mV	T, °K	E_3, mV	T, °K	E_4, mV
1086	328,5	326,1	1070	329,7	1073	338,8
1079	328,9	327,0	1036	336,0	1049	343,7
1036	340,2	339,5	1009	340,8	1013	349,9
996	349,6	349,1	980	348,9	986	355,4
946	356,8	356,6	953	352,3	958	360,7
1080	328,6	327,4	1038	335,5	1012	350,8

TABLE 3. Solubility of Thorium in Liquid Aluminum according to the Results of Measurement of the emf of the Cell [Formula (2)]

Method of isotherms				Method of polytherms	
T, °K	$x_{Th}\times10^2$	E, mV	$X_{Th}\times10^2$	T, °K	$X_{Th}\times10^2$
1056	3,52	11,2	5,7	958	3,44
1054	2,58	16,5	5,3	973	3,78
1055	1,93	27,0	6,3	986	4,15
1054	0,56	50,8	5,2	999	4,46
1054	0,52	51,7	5,1	1009	4,32
1104	4,45	11,4	7,2	1019	4,90
1115	3,32	16,7	6,7	1031	4,87
1101	2,46	24,8	7,0	1073	5,35
1101	1,72	34,5	7,4	1098	6,49
1109	1,49	35,8	6,7	1127	6,82

The thorium content in the reference electrodes corresponded to the two-phase region L + $ThAl_3$, while in the investigated alloy it varied from 0.5 at. % to values close to the solubility. Values of the emf that did not vary by more than 0.001 V in the course of 1 h were taken as the equilibrium values. After the equilibrium value of the emf was reached, the crucible with the alloy was removed from the electrolyte and cooled. The alloy was washed free of salts and analyzed for thorium content. The experiments were conducted in a hermetic quartz cells in an atmosphere of purified argon. The temperature was measured with a calibrated Chromel–Alumel thermocouple.

The established values of the emf of the galvanic cells (1), measured at various temperatures in four experiments, are cited in Table 2. The values of the emf did not depend on the thorium content in the alloy; they were reproduced within ±0.5 mV when the temperature was lowered and raised and were satisfactorily plotted on a straight line of emf vs T°K, the equation of which was found by treating the results of six experiments by the method of least squares:

$$E=(0.558\pm0.016)-(0.210\pm0.014)\cdot10^{-3}\,T\pm0.005\ \text{V}. \qquad (3)$$

Knowing this method, the partial values were calculated for α-thorium in saturated solutions and for the compound $ThAl_3$ at equilibrium with them. The following results were obtained:

$$\begin{aligned}
&\lg a_{Th}=4.235-\frac{11250}{T}\pm\frac{100}{T};\\
&\Delta\bar{H}_{Th}=-51.5\pm1.5\ \text{kcal/g-atom};\\
&\Delta\bar{S}_{Th}=-19.4\pm1.3\ \text{entropy units/g-atom};\\
&\Delta\bar{G}_{Th,\,1000^\circ\text{K}}=-32.1\pm0.5\ \text{kcal/g-atom}.
\end{aligned} \qquad (4)$$

The formation of the compound $ThAl_3$ is accompanied by the evolution of a substantial amount of heat, a decrease in the entropy and free energy of thorium. The activity of thorium in the compound is negligible, $9.6\cdot10^{-8}$ at 1000°K and $1.1\cdot10^{-6}$ at 1100°K.

The solubility of thorium in aluminum was determined, knowing the emf of the galvanic cells (2). The values were found according to the formula $\log X_{Th} = (4F/RT)E + \log x_{Th}$ by the method of isotherms. At a definite temperature the values of X_{Th} (Table 3), calculated according to the values of the emf E for solutions with different thorium contents, coincide satisfactorily, which is evidence of obedience of the activity of thorium in solutions to Henry's law. The temperature below which the emf of the cell (2) for a solution with a definite thorium content becomes equal to zero was determined by the method of polytherms. At the temperature found the thorium content in solution corresponded to its solubility in aluminum. The results obtained by different methods are in satisfactory agreement, and in a plot of $\log X_{Th}$ vs 1000/T are plotted on a straight line, the equation of which takes the form

$$\lg X_{Th}=0.632-\frac{2000}{T}\pm0.035. \qquad (5)$$

At 1000 and 1100°K, 4.29 at. % (27.0 mass %) and 6.50 at. % (37.5 mass %) thorium dissolves in aluminum, respectively. The difference of Eqs. (4) and (5) reflects the temperature dependence of the activity coefficient of α-thorium in aluminum solutions:

$$\begin{aligned}
&\lg\gamma_{Th}=\lg a_{Th}-\lg x_{Th};\\
&\lg\gamma_{Th}=3,60-\frac{9250}{T}\pm0,13.
\end{aligned} \qquad (6)$$

The excess partial values for thorium in solutions were found, knowing Eq. (6), according to the well-known function [4]. It was established that the dissolution of 1 g-atom of α-thorium in liquid aluminum, regardless of the temperature and composition of the homogeneous solution, is accompanied by an evolution of 42.3 ± 2.0 kcal of heat and a decrease of 16.5 ± 1.8 eu in the excess entropy of thorium. The activity of thorium in the solutions was characterized by large negative deviations from Raoult's law. Raising the temperature from 1000 to 1100°K leads to an increase in the activity coefficient of thorium from $2.2 \cdot 10^{-6}$ to $1.6 \cdot 10^{-5}$. Since the activity of thorium in solutions obeys Henry's law, the activity of aluminum follows Raoult's law. The thermodynamic characteristics of solutions of Th–Al are evidence of an energetic interaction of atoms of the dissolved substance with the atoms of the solvent.

LITERATURE CITED

1. V. I. Kutaitsev, Alloys of Thorium, Uranium, and Plutonium [in Russian], Gosatomizdat, Moscow (1962), p. 5.
2. M. V. Smirnov et al., At. Énerg., 5, No. 5, 419 (1970).
3. N. G. Ilyushchenko, N. I. Kornilov, and A. I. Anfinogenov, Transactions of the Institute of Electrochemistry [in Russian], No. 8, Izd. UFAN SSSR (1966), p. 65.
4. V. A. Lebedev, I. F. Nichkov, and S. P. Raspopin, Élektrokhimiya, 2, 160 (1966).

NEUTRON DISTRIBUTION NEAR THE END OF A PARTIALLY IMMERSED COMPENSATING ROD

V. P. Koroleva, Yu. G. Pashkin,
V. V. Chekunov, and L. A. Chernov

UDC 621.039.562.24

In order to determine the operating conditions of the absorbing rods used in energetic reactors, one needs to know the magnitude and distribution of the energy yield caused by neutron capture in the boron of the rods. This is especially important for the end region of a partially immersed rod, because this part usually operates under the most stressed conditions. The effect on the height distribution of the energy yield caused by the end of a partially immersed rod is large not only in the rod itself, but also in the neighboring fuel elements, there being a considerable difference between these distributions which is not observed in the case of a completely immersed rod. The purpose of the present article is to show the correctness of a proposed method for calculating the distribution of the density of neutron captures near the end of a partially immersed rod.

The distribution in height of the capture density of an absorbing rod partially immersed in a reactor will be different from the variation with height of the reactor fission field, since the fission field is determined by the distribution of neutron currents in just this place, whereas the distribution of the density of captures in the rod is determined by the distribution of neutron currents at its surface.

It can be shown that at large distances from the end of the rod (for the case in which the neutron distribution is not extremely nonlinear), the variation with height of the reactor fission field next to the rod and the distribution in height of the capture density of the rod are practically the same. It is therefore of considerable interest to calculate the increase in the capture density in the rod near its end caused by the exposure to neutrons from below (it is assumed that the rod is directed upward).

In order to obtain expressions which describe this increase, we assume the following:

1) the rod, of radius R_r, is located in an infinite nonabsorbing medium with a scattering cross section Σ_s;
2) no scattering exists in the rod;
3) below the rod there is free space;
4) the radial distribution of the neutrons in the medium is described by a smooth function of the type

$$1-[1-q(Z)]e^{-\Sigma_s r}$$

(here r is the distance along the normal to the surface of the rod; and Z is the distance along the rod measured from its end), which gives the correct value of the depression of the neutron flux at the surface of the rod q(Z) and an unperturbed unit value of the flux at large distances from the surface;

5) the transition for the asymptotic value of the depression of the neutron flux at the surface of the rod q to the unperturbed unit value of the current under the rod is described by a certain transition function which is symmetric with respect to the end, so that at the end (Z = 0)

$$q(0)=(1+q)/2;$$

6) because the effect sought decreases rapidly with height (for $Z \sim R_f$ it is effectively zero), the value of the average neutron attenuation $\overline{\exp(-\Sigma_c \bar{l})}$ can be replaced by $\exp[\Sigma_c(\bar{l})]$, in which $(\bar{l}) = 2Z$

Translated from Atomnaya Énergiya, Vol. 35, No. 6, pp. 435-436, December, 1973. Original letter submitted March 20, 1973.

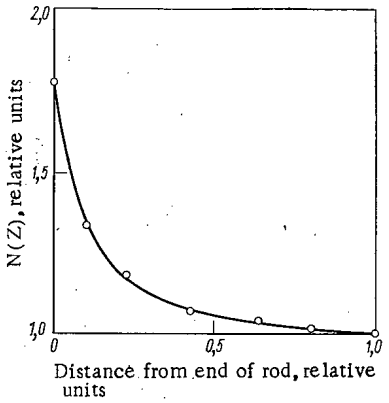

Fig. 1. Relative distribution in height N(Z) of the neutron capture density near the end of a B_4C rod partially immersed in a reactor: ○) experimental; ——) calculated.

is the neutron mean free path between the end of the rod and the plane Z; and Σ_c is the absorption cross section of the rod.

Under the assumption that the neutron flux does not vary in the axial direction under the rod, the additional number of absorbed neutrons in unit volume of the rod at a distance Z from its end caused by the exposure to neutrons from below is then given by the expression (the summation is carried out over all energy groups)

$$N(Z)=\frac{1}{8R_r}\sum_i \Phi_i(1+q_i)[\beta_i - A(\beta_i)]\,e^{-\beta_i\frac{Z}{R_r}},$$

where Φ_i is the unperturbed neutron flux at the end of the rod; $\beta_i = 2R_f\Sigma_{ci}$ is the optical thickness of the rod compared to the absorption; and $A(\beta_i)$ is the probability of the first collision in the rod and is given by the expression

$$A(\beta_i)=\frac{4}{\pi}\int_0^{\pi/2}\cos\varphi\,d\varphi\int_0^{\pi/2}\sin^2\theta\,d\theta\,(1-e^{-\beta_i\frac{\cos\varphi}{\sin\theta}}),$$

(the latter is tabulated, for example, in [1]). The calculation of N(Z) was carried out for a rod 19.2 mm in diameter made of boron carbide (natural boron) with a density of $\gamma = 2.21$ g/cm^3 in the spectrum of a uranium–berillium reactor with a nuclear density ratio of $\rho_{Be}/\rho_{5U} = 84$, normalized to the value N (Z = R).

The measurements of the relative neutron capture density distribution near the end of a boron-containing rod were carried out on a PF-4F8 assembly [2], at the center of which was placed a compensating rod made of boron carbide. The rod was loaded into the reactor from above until its end was at the central plane of the active section. The neutrons were counted by a gold–silicon semiconductor detector with an effective area equal to that of the cross section of the rod combined with a layer of ^{10}B 0.01 mg/cm^2 thick placed on a titanium backing. The final portion of the end of the rod was composed of B_4C disks, each with a thickness of 1-2 mm, with the detector placed in series between them. Figure 1 shows the experimentally obtained relative behavior of the neutron capture density, with the calculated results shown for comparison. The calculated results agree well with experiment, showing the validity of the proposed method of calculation.

LITERATURE CITED

1. G. I. Marchuk, Numerical Methods for Nuclear Reactor Calculations [in Russian], Atomizdat, Moscow (1958).
2. A. I. Mogil'ner, V. A. Osipov, and G. N. Fokin, At. Énerg., 24, 42 (1968).

γ-RAY BUILDUP FACTORS FOR CYLINDRICAL SHIELDING BLOCKS

D. L. Broder, S. A. Kozlovskii,
V. I. Kulikov, N. L. Kuchin,
K. K. Popkov, and I. N. Trofimov

UDC 539.125.52

In this paper, an attempt is made to obtain values for γ-ray dose buildup factors in the energy range 0.5-8 MeV and for long cylindrical shielding blocks. For this purpose, Monte Carlo calculations were performed. To reduce variance and accelerate convergence, splitting and Russian roulette [1, 2] were used, which made it possible to obtain satisfactory results for shield thicknesses up to $\mu r = 15$.

To check the effectiveness of the program, several calculations were made of the spatial and energy distributions of the γ-ray fluxes from sources of initial energy 0.5-8 MeV in homogeneous media. In the course of the calculations, differential energy spectra were obtained for media of infinite transverse dimensions which were compared with the results of calculations by the moments method [3]. The comparison revealed excellent agreement between the results of both calculations.

Calculations of γ-ray buildup factors in cylindrical shielding blocks were performed for the case where a point isotropic monoenergetic source of γ-rays was located in the end plane of the block on the axis of symmetry. The materials considered were water, iron, and lead, i.e., a broad range of atomic numbers was covered.

Analysis of the results led to the conclusion that the following empirical expression can be proposed to describe the dependence of γ-ray buildup factors in cylindrical shielding blocks:

$$B(\mu r, R) = B(\mu r, \infty) - [B(\mu r, \infty) - 1] e^{-\left(\frac{2.8}{r} + 1.3 \cdot 10^{-3} Z\right) R}, \quad (1)$$

where $B(\mu r, \infty)$ and $B(\mu r, R)$ are γ-ray buildup factors at a distance r from a source in an infinite medium and in a cylindrical shielding block of radius R; Z is the atomic number of the element comprising the cylindrical block.

A comparison of the dose buildup factors calculated by the Monte Carlo method, those calculated by means of Eq. (1), and those calculated by means of equations given in [4-6] shows that for small penetration depths ($\mu r \lesssim 7$), the results disagree by no more than 30%, which is of the order of the error of the Monte Carlo method. The disagreement increases at greater penetration depths.

As an illustration, Fig. 1 shows the dose buildup factors for γ-rays with an initial energy $E_0 = 2.0$ MeV in a lead cylinder with a length $r = 1.0\ \mu^{-1}$ calculated by the Monte Carlo method, in accordance with Eq. (1), and in accordance with the equations in [4-6]. Figures 2 and 3 show a comparison of the calculated results obtained from Eq. (1) and from the equations in [4-6] with experimental data [6].

An analysis of the calculations for various materials (water, aluminum, lead, tin, and iron) shows that Eq. (1) makes it possible to determine the γ-ray buildup factor in cylindrical shielding blocks of length $r \leq 15\ \mu^{-1}$ with an accuracy of 30% or better for an initial source energy of 0.5-8.0 MeV. For these conditions, the recommendations in [6] provide an accuracy of 65% or better. The empirical formula proposed in [4, 5] satisfactorily describes the $B(\mu r, R)$ dependence only for light materials (water, aluminum); in those cases, the error of the calculations does not exceed 60-70%. As the atomic number increases, the

Translated from Atomnaya Énergiya, Vol. 35, No. 6, pp. 437-438, December, 1973. Original letter submitted April 4, 1973.

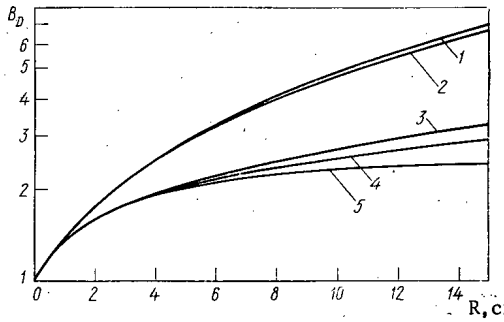

Fig. 1. γ-Ray dose buildup factor for a cylindrical lead shielding block ($R = 1\ \mu^{-1}$): 1) buildup factor for infinite lead calculated by the moments method; 2-5) respectively, calculated by the equations in [4, 5], by the Monte Carlo method, by Eq. (1), and by the equation in [6].

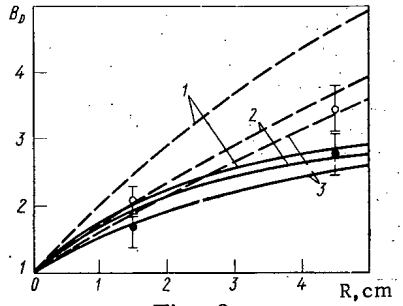

Fig. 2

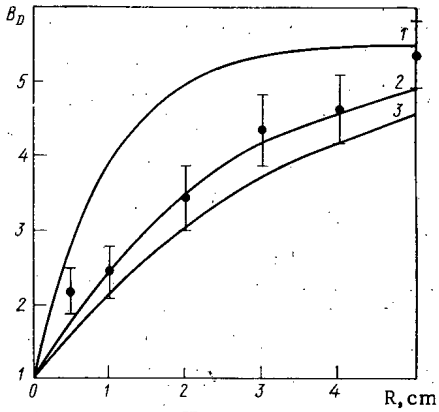

Fig. 3

Fig. 2. γ-Ray dose buildup factor for cylindrical aluminum shielding block: ———) $\mu r = 2.0$, $E_0 = 0.66$ MeV; – – –) $\mu r = 5.92$, $E_0 = 1.25$ MeV; 1-3) respectively, calculated by equations in [4, 5], in [6], and by Eq. (1); ⊤○⊥ and ⊤●⊥) experimental data [6].

Fig. 3. γ-Ray dose buildup factor for cylindrical iron shielding block ($E_0 = 1.25$ MeV, $\mu r = 4.08$): 1-3) respectively, calculated by equations in [4, 5], [6], and by Eq. (1); ⊤●⊥) experimental data [6].

error of the calculations rises reaching more than 400% for lead cylinders of small radius and a source energy $E_0 = 8.0$ MeV.

In conclusion, the authors thank Yu. M. Vishnyakov for efficient computer operation.

LITERATURE CITED

1. G. I. Marchuk (editor), Monte Carlo Method in Radiation Transport Problems [in Russian], Atomizdat, Moscow (1967).
2. H. Goldstein, Fundamentals of Reactor Shielding [in Russian], Gosatomizdat, Moscow (1961).
3. H. Goldstein and J. Wilkins, in: Shielding of Transport Equipment with Nuclear Engines [in Russian], V. V. Orlov and S. G. Tsypin (editors), IL, Moscow (1961), p. 212.
4. V. A. Klimanov and V. P. Mashkovich, in: Problems in Dosimetry and Radiation Protection [in Russian], L. R. Kimel' (editor), No. 5, Atomizdat, Moscow (1966), p. 69.
5. V. A. Klimanov et al., At. Énerg., 22, No. 3, 228 (1967).
6. D. L. Broder et al., in: Problems in the Physics of Reactor Shielding [in Russian], D. L. Broder et al. (editors), No. 4, Atomizdat, Moscow (1969), p. 161.

γ-RADIATION-INDUCED AIR GLOW

A. V. Zhemerev, Yu. A. Medvedev,
B. M. Stepanov, and G. Ya. Trukhanov

UDC 621.039.555

The characteristics of the light flash which is excited by a γ-quantum pulse in air have been investigated in [1]. Both the delay of the light signal within the irradiated region and the self-absorption of the light were taken into consideration. The time dependence of the intensity of the light flux was determined for γ-fluxes of various intensities. The conditions under which the self-absorption effect is immaterial were determined. For example, for an instantaneous γ-quantum source which emits per unit time $\dot{N}(t) = N_0\delta(t)$ γ-quanta, the condition that self-absorption is small is given by the formula

$$N_0 \ll \frac{0.1\gamma}{\alpha_i \mu^3 \nu} \approx 5 \cdot 10^{21}, \tag{1}$$

where γ, α_i, μ, and ν denote constants characterizing the ionization of the air under the influence of γ-quanta (the entire notation is similar to that of [1]).

The effect of the scattered γ-radiation in the light flux was approximated in [1] by introducing an effective absorption coefficient μ of the γ-quanta. It is worthwhile to make a precise calculation of the intensity of the emitted radiation resulting from the scattered γ-radiation, and to estimate the accuracy of the approximation used in[1]. In the present article, the effect is evaluated with the Monte Carlo method. γ-Quantum fluxes in which the self-absorption effect is immaterial are considered.

Assume that we know the energy $\dot{E}(r, t)$ absorbed per unit volume at a distance r from the source per unit time and the law according to which the deactivation of a volume element exposed to a γ-quantum pulse $K\delta(t)$ takes place. The time dependence of the intensity of the light flux at a distance R_0 from the source can be described by the expression [1]:

$$I_{\text{л}}(R_0, t) = \frac{\eta}{4\pi} \int\limits_{V_t} \frac{dv}{R^2} \int\limits_{r/c}^{t-R/c} K_\delta \left(t - \tau - \frac{R}{c}\right) \dot{E}\left(r, \tau - \frac{r}{c}\right) d\tau. \tag{2}$$

The integration is extended over the volume V_t which is bounded by the surface of the ellipsoid $r + R = ct$. The foci of the ellipsoid are the source of γ-radiation and the point at which the light flux is monitored.

Let us discuss Eq. (2) for an isotropic, monochromatic point source of γ-radiation having the energy ε_γ; the source is assumed to emit $\dot{N}(t) = N_0\delta(t)$ γ-quanta per unit time. Let us separate the light flux which is generated by the unscattered γ-radiation. In this case, the absorption of the energy $\dot{E}(r, t)$ is given by the formula

$$\dot{E}\left(r, t - \frac{r}{c}\right) = \mu\varepsilon_e \dot{N}\left(t - \frac{r}{c}\right) \frac{e^{-\mu r}}{4\pi r^2}, \tag{3}$$

where ε_e denotes the average energy of an electron knocked away by Compton scattering of γ-quanta; and μ denotes the absorption coefficient of the γ-quanta. The light flux which is generated by the unscattered γ-radiation at large ($R_0 \gg \mu^{-1}$) distances from the instantaneous source of γ-quanta is given by the following expression of [1]:

$$I_{\text{л}}(t) = \eta \frac{\mu c \varepsilon_e N_0}{8\pi R_0^2} \left\{ E_1\left(\frac{\mu c t_1}{2}\right) + e^{-\alpha t_1} \left\{ \overline{E_i}\left[\left(\frac{2\alpha}{\mu c} - 1\right)\frac{\mu c t_1}{2}\right] - \ln\left(\frac{2\alpha}{\mu c} - 1\right)\right\}\right\}, \tag{4}$$

where $\overline{E_i(x)}$ and $E_1(x)$ denote integral exponential functions [2].

Translated from Atomnaya Énergiya, Vol. 35, No. 6, pp. 438-439, December, 1973. Original letter submitted April 6, 1973.

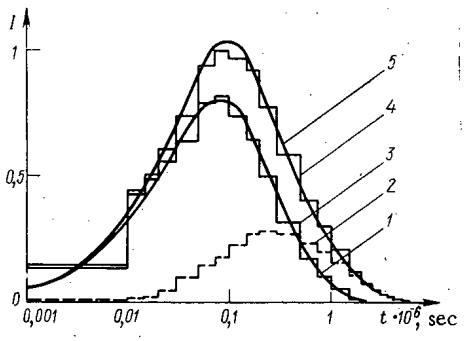

Fig. 1. Time dependence of the intensity of the light flux in units $\eta\mu\varepsilon_\gamma cN_0/8\pi R_0^2$ of the excited γ-radiation: 1) unscattered radiation; 2) unscattered radiation, calculated with the Monte Carlo Method; 3) scattered radiation, calculated with the Monte Carlo method; 4) total radiation, calculated with the Monte Carlo method; 5) results of [1].

The light flux which is generated by scattered γ-radiation can be determined with the following methods: successive calculation of the absorbed energy of the γ-radiation and subsequent calculation of the integral of Eq. (2); or direct calculation of the light flux with the Monte Carlo method. The second method was used in the present work. Direct modelling of the γ-radiation source was employed [3]. The fast electron which is generated in γ-scattering loses part of its energy η in the formation of excited states of the molecules which, after a time $-\ln p/\alpha$ (p denotes a random number and α^{-1} is the time of radiative decay of the excited states of the molecules), emit light quanta in a pattern with spherical symmetry (the direction in which the quantum is emitted is chosen at random). When a light flash produced by the γ-radiation in air is modelled, the light scattering must be taken into consideration. The characteristics of the light flash depend in this case upon the meteorological conditions. We did not bring these processes into account in the present work, because the light flux is considered at a distance of the order of several kilometers, whereas the average range of a light quantum having the wavelength ~4000 Å amounts to 10-20 km for the standard atmosphere under normal pressure [4].

The light flux which is generated by the scattered γ-radiation was calculated for a source with $\varepsilon_\gamma = 1$ MeV. The distance at which the light flux was calculated amounted to 25 μ^{-1}. Twenty thousand histories of γ-quanta were considered in the calculations. The probable error is 5-10%. The results of calculations of the light flux intensity generated by the γ-radiation at large distances from the source are illustrated in Fig. 1 in the form of histograms in units of $\eta\mu\varepsilon_\gamma cN_0/8\pi R_0^2$. For the purpose of illustrating the accuracy of the calculations, the figure includes the intensity curve of the light flux generated by unscattered γ-radiation. The curve was calculated with Eq. (4) for $\mu^{-1} = 120$ m and $\varepsilon_e = 0.44$ MeV. The total intensity of the light flux has a characteristic rise time of the order of the deactivation time α^{-1} of a volume element ($\alpha^{-1} = 6 \cdot 10^{-8}$ sec for the line of the nitrogen ion with the wavelength 3914 Å [5]). The contribution produced by the unscattered γ-radiation dominates. Beginning at times which are greater than α^{-1}, the contributions resulting from scattered and unscattered γ-radiation become comparable, and at times in excess of 1 μsec, the contribution of the scattered γ-radiation dominates. Figure 1 includes the intensity curve of the light emission; the curve was constructed from the results of [1]: $\mu_{eff}^{-1} = 300$ m and $\varepsilon_e = \varepsilon_\gamma$. The scattered γ-radiation in the light flux can be taken into account with adequate accuracy when the effective coefficient of γ-radiation absorption is assumed to be equal to 1/300 m^{-1}.

LITERATURE CITED

1. A. V. Zhemerev and Yu. A. Medvedev, At. Énerg., 29, 287 (1970).
2. G. Korn and T. Korn, Handbook of Mathematics [in Russian], Nauka, Moscow (1970), p. 625.
3. S. M. Ermakov, The Monte Carlo Method and Miscellaneous Problems [in Russian], Nauka, Moscow (1971), p. 76.
4. Handbook of Geophysics [in Russian], Nauka, Moscow (1965), p. 381.
5. A. Johnson and R. Fowler, J. Chem. Phys., 53, No. 1, 651 (1970).

ANALYSIS OF SURFACE LAYERS WITH THE AID OF ABNORMAL α-PARTICLE SCATTERING

B. I. Kuznetsov, I. P. Chernov, G. Ya. Starodub, and A. A. Yatis

UDC 539.12.04:678.01

The development of microelectronics and electronics, investigations of the stability of coating films, and research on the kinetics of several chemical processes are not feasible without in-depth investigations of both the integral and differential distribution of light elements in the surface layers of materials. Techniques of nuclear physics [1-3] are of particular importance for the solution of these problems. The most widely used method is based upon scattering [3], wherein particles whose energy is below the Coulomb barrier are used as the bombarding particles. The energy of the elastically scattered particles depends upon the mass M of the scattering nucleus, and both energy and intensity of the scattered particles can be used to determine the composition of thin layers. The method has been successfully employed in the analysis of self-supporting, 1-2 μ thick films and for the determination of admixtures consisting of heavy elements in light elements.

The present article proposes a method of determining the concentration of light elements. The method is based on anomalies in the backscattering of α-particles. The elastic scattering cross section of α-particles scattered at light nuclei has a sharp increase at angles close to 180° [4, 5] in the energy range 15-30 MeV and reaches its maximum at carbon and oxygen nuclei. At some energies, the elastic scattering cross section amounts to several barns and exceeds 10^4-10^5 times the cross section of backscattering at intermediate and heavy nuclei.

When α-particles having the initial energy E_0 are incident on a sample, there exists a certain probability that the α-particles are scattered at a certain depth into the direction defined by the angle θ, the scattering occurring at nuclei of the base material or at admixture nuclei. The particles lose the energy ΔE_1 due to ionization processes along their path. After a collision, the energy of a scattered particle of mass m decreases proportional to the coefficient k^2 which is given by the formula

$$k^2=\frac{m\cos\theta}{M+m}+\left[\left(\frac{m\cos\theta}{M+m}\right)^2+\frac{M-m}{M+m}\right]^2.$$

In the case of light nuclei, the energy of scattered α-particles at $\theta \geq 170°$ is several times smaller than $(E_0-\Delta E_1)$. The energy losses ΔE_1 of the primary particle beam on the path x are negligibly small when compared with the energy losses ΔE_2 of a moving particle which has been scattered. Thus, the entire information on the depth at which admixture elements are situated is related to the ionization losses of the scattered particles.

The minimum resolution with which the depth distribution of impurities can be analyzed depends upon the energy resolution of the spectrometer. The energy resolution of the spectrometer is composed, in essence, of the energy spread of the incident beam at the target and the intrinsic resolution of the recording system. At a resolution of 15 and 60 keV of the spectrometer, the minimum resolution amounts to 500 and 2000 Å, respectively, for germanium samples. However, when the α-particles are directed at a certain angle onto the surface of the sample, the resolution is reduced by one order of magnitude.

The greatest thickness which can be analyzed is in general dependent upon the overlap of the spectra of pulses which originate from the particles elastically scattered at neighboring light nuclei, E_0, and the atomic number of the substrate material. For example, in the case of niobium which contains admixed

Translated from Atomnaya Énergiya, Vol. 35, No. 6, pp. 439-441, December, 1973. Original letter submitted May 21, 1973.

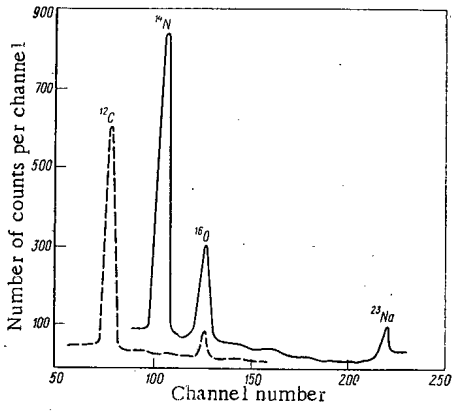

Fig. 1

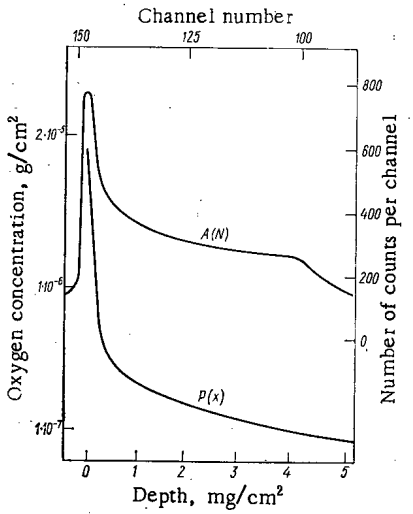

Fig. 2

Fig. 1. Amplitude spectrum of α-particles which were elastically scattered at a niobium sample (– – –) or at a germanium sample (———).

Fig. 2. Depth distribution of oxygen admixtures in a niobium sample. The depth distribution P(x) was obtained from the instrument spectrum A(N).

carbon, the differential distribution of oxygen can be measured at a depth of 8 μ at E_0 = 21.4 MeV.

The sensitivity of this method depends upon the cross sections of scattering at the impurity nuclei and the matrix nuclei, the intensity of the incident beam, the exposure time, the number of counts in the channels of the analyzer, and the depth distribution of the impurities in the sample. In the case of matrices having mass numbers $40 \leq A \leq 140$, at a current of 1 $\mu A/cm^2$ and at a solid angle of 10^{-2} of the detector, the minimum number of admixed carbon nuclei, nitrogen nuclei, and oxygen nuclei found in the surface layer amounts to $2 \cdot 10^{13}$, $1.5 \cdot 10^{14}$, and $1.0 \cdot 10^{13}$ nuclei/cm^2, respectively. The error of the measurements does not exceed 10-20%.

The applicability of the method was tested with the cyclotron of the Scientific-Research Institute of Nuclear Physics, Electronics, and Automation at the Tomsk Polytechnical Institute. The energy of the α-particles could be varied between 18 and 27 MeV. The beam of collimated particles passed through collimating slits and was incident upon the sample to be examined, which was situated in the center of the scattering chamber (residual pressure of $3 \cdot 10^{-5}$ mm Hg). A surface-barrier counter was used as the detector of the scattered particles. The resolution of the spectrometer amounted to 50-60 keV. In order to identify the α-particles which had been elastically scattered at the nuclei of light elements, the sensitive zone of the detector was chosen so that the depth of this zone was slightly greater than the range of the α-particles scattered at oxygen nuclei on the surface. The detector pulses were fed to an AI-4096 analyzer. The incident beam was monitored by measuring the current at the sample or by recording to scattered α-particles.

The concentration of the light elements was determined by comparison:

$$m_x = m_e \frac{M_e}{Y_e} \cdot \frac{Y_x}{M_x},$$

where m_x, m_e, M_x, M_e, and Y_x and Y_e denote the number of nuclei, the readings of the α-particle beam monitor, and the number of pulses in the peak for the element to be analyzed in the sample under inspection and in a standard sample, respectively. Films of Lavsan or polyacrylonitrile were used as standard samples.

Figure 1 is an amplitude spectrum of α-particles (E_0 = 18.3 MeV) scattered from a thick niobium sample on the surface of which a 100 Å thick carbon layer had been applied after chemical etching. Two peaks can be recognized in the spectrum on the weak background of pulses corresponding to α-particles scattered at the matrix: one peak corresponds to the α-particles scattered at carbon, and the other to α-particles scattered at oxygen. The latter peak is present because an oxide film was formed after the etching. When this film has the chemical composition Nb_2O_5 and the film compound is uniformly distributed,

the film thickness must be 40 Å. The number of pulses in the carbon peak corresponds to a 100 Å thick carbon film. Figure 1 includes the spectrum of pulses corresponding to the scattering of α-particles with the energy $E_0 = 21.4$ MeV in a germanium sample on the surface of which SiO_2 (80 Å) and Si_3N_4 (1160 Å) films had been deposited. The thickness of these films, which was derived from the number of pulses in the peaks, coincides with the thickness values obtained in measurements using other methods. Interestingly enough, a peak corresponding to the scattering of α-particles at sodium is observed. The sodium apparently results from the surface treatment.

The differential distribution of oxygen in the surface layer of the niobium sample was measured in a similar manner. Figure 2 illustrates the instrument-dependent spectrum A(N) of the scattered α-particles and the distribution P(x) of the oxygen in the depth of the sample. The majority of the admixed oxygen nuclei are on the sample surface; the oxygen fraction decreases with increasing depth.

The following conclusions can be drawn from our investigations.

1. Measurements of α-particle backscattering at high energies supplement the measurements of Coulomb scattering. The method makes it possible to determine with high sensitivity microconcentrations (traces) of light elements in the surface layers of almost any material.
2. The method is nondestructive and can be used to examine the distribution of oxygen, carbon, and nitrogen (or their compounds) over both the sample surface and the bulk of the sample.
3. The method can be used to investigate the dynamics of concentration changes of light admixtures in layers close to the surface of various materials which are exposed to corroding media, heat flux, and radiation fluxes.

In conclusion, the authors thank the service team of the cyclotron for the uninterrupted operation of the accelerator, and S. V. Pokrovskii for giving valuable advice and for providing the germanium samples.

LITERATURE CITED

1. I. A. Skakun and O. N. Khar'kov, At. Énerg., 27, 351 (1969).
2. G. Bowen and D. Kibbons, Activation Analysis [Russian translation], Atomizdat, Moscow (1968).
3. A. Turos and Z. Wilhelmi, Nucleonika, 13, 975 (1968).
4. J. Morgan and R. Hobbie, Phys. Rev., C. Nucl. Phys., 1, 155 (1970).
5. B. I. Kuznetsov, R. E. Ovsyannikova, and I. P. Chernov, Yadernaya Fizika, 15, 681 (1972).

DETERMINATION OF THE AMOUNT OF TRITIUM IN ORGANIC MATERIALS ACCORDING TO BREMSSTRAHLUNG

L. F. Belovodskii, V. K. Gaevoi, and V. I. Grishmanovskii

UDC 620.1.019.39:546.11.02.3

The investigation of the principles of the absorption and desorption of tritium and its oxide (HTO) by certain film materials, the study of the solubility of tritium and HTO in materials, as well as the introduction of an isotopic label, involve the necessity of determining the amount of tritium in materials.

The known methods of determining tritium and HTO are based on the chemical dissolution or thermal decomposition of samples of the materials, followed by a measurement of tritium or HTO in solution or in the liberated gases [1, 2]; the amount of tritium in materials can be determined by an autoradiographic method [3]. The basic shortcoming of these methods is the long duration of the analysis (several hours or days); moreover, the first two methods lead to a decomposition of the investigated samples.

The method under consideration does not share the indicated shortcomings; in this method the amount of tritium is determined according to the rate of count of bremsstrahlung due to the β-particles of the decay of tritium in certain organic film materials.

The bremsstrahlung of the β-particles of tritium is detected with Geiger counters with thickness of the window 3-5 mg/cm^2 or with scintillators (NaI, CsI) with thickness ~1 mm [4, 5]. The bremsstrahlung intensity is proportional to the amount of tritium in the sample of the material [4, 6]:

$$Q = kN, \tag{1}$$

where Q is the amount of tritium in the sample, Ci; N is the rate of count of the bremsstrahlung, counts/min; k is a coefficient of proportionality for the given material. In general, k depends on the atomic number of the material Z, the sensitivity of the recording apparatus to bremsstrahlung, the geometry of the measurement, the thickness of the material, and the uniformity of the distribution of tritium through the thickness. Consequently, the task of measuring tritium according to bremsstrahlung is reduced to a determination of the value of k for the investigated materials.

For the determination of k for certain film materials (see Table 1), we studied the dependence of N on Q. Samples of the investigated materials 3 cm^2 in diameter were exposed for 24-28 h in an atmosphere of HTO vapors; the tritium concentration in the vapors was 10^{-1} Ci/liter. After exposure, the bremsstrahlung of the samples was recorded on a B-2 apparatus with an SI-2B end-window counter, placed in a DS-000 lead booth. The samples were then placed in test tubes with a fixed volume of distilled water, where they were "soaked out" for 0.5 h to six days. After soaking out, the samples were dried with filter paper, their bremsstrahlung again measured, and placed in other test tubes with water. These operations were continued until the rate of count of the bremsstrahlung of the samples became $\sim 3\sqrt{N_b}$, where N_b is the background of the apparatus, counts/min. To determine the residual activity of tritium in the samples, they were subjected to combustion under vacuum, after which the liberated HTO was frozen out.

The water remaining after soaking out and combustion of the samples was analyzed on a URB-1 apparatus, which was calibrated with standard HTO with an error of ±10%. The amount of tritium liberated from the sample was determined according to its concentration in water; it corresponded to the decrease in the rate of count between two soakings of the sample. The summary amount of tritium correspond to the initial rate of count, determined after exposure. The experimental dependence N = f(Q) for certain materials is cited in Fig. 1.

Translated from Atomnaya Énergiya, Vol. 35, No. 6, pp. 441-443, December, 1973. Original letter submitted June 8, 1973.

TABLE 1. Characteristics of the Investigated Materials

Material	d, cm	ρ, g/cm^3	μ, cm^{-1}	k_e	Relative error in the determination of k_e, %	k'_e	k''_e	
							T–Ti	Sr–Y
"Kalandr" glove rubber (TU No. YaN-251-61)	$1.1\cdot10^{-1}$	1.15	21.7	$3.1\cdot10^{-6}$	9	$1.1\cdot10^{-6}$	21.2	$2.6\cdot10^5$
Nairit latex L-7 (VTU No. V-53-61)	$5.4\cdot10^{-2}$	1.28	24.2	$2.5\cdot10^{-6}$	11	$1.3\cdot10^{-6}$	25.2	$3.1\cdot10^5$
Surgical glove rubber (GOST-3-53)	$2.0\cdot10^{-2}$	0.90	17.5	$8.5\cdot10^{-7}$	12	$7.2\cdot10^{-7}$	13.9	$1.7\cdot10^5$
Polyvinyl chloride, recipe No. 80/277	$2.5\cdot10^{-2}$	1.21	22.8	$1.7\cdot10^{-6}$	16	$1.2\cdot10^{-6}$	23.2	$2.9\cdot10^5$
Polyvinyl chloride, recipe No. 80 AM	$3.0\cdot10^{-2}$	1.23	23.2	$1.7\cdot10^{-6}$	23	$1.2\cdot10^{-6}$	23.2	$2.9\cdot10^5$
Teflon-26	$2.2\cdot10^{-2}$	1.81	34.2	$7.0\cdot10^{-7}$	20	$5.0\cdot10^{-7}$	9.6	$1.2\cdot10^5$
Perfol PK-4	$6.0\cdot10^{-3}$	1.15	–	$8.7\cdot10^{-7}$	25	$8.7\cdot10^{-7}$	16.8	$2.0\cdot10^5$
Terylene (polyethylene terephthalate)	$7.5\cdot10^{-3}$	–	–	$7.1\cdot10^{-7}$	21	$7.1\cdot10^{-7}$	13.8	$1.7\cdot10^5$

Note. No correction for absorption was introduced for perfol and terylene in view of the negligible thickness of these materials.

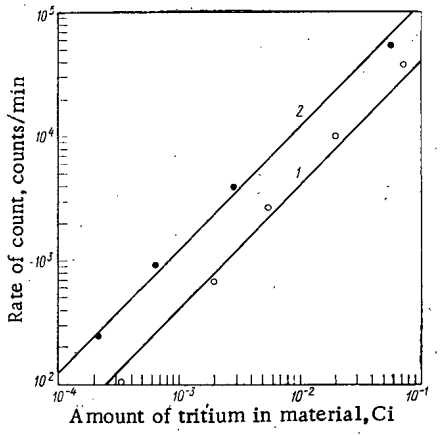

Fig. 1

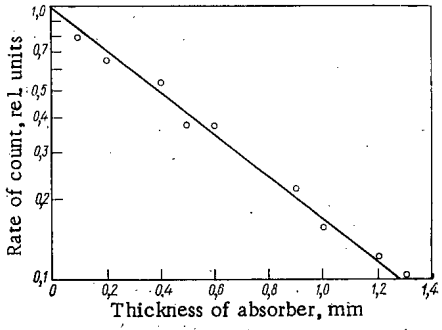

Fig. 2

Fig. 1. Dependence of the rate of count of bremsstrahlung on the amount of tritium in nairit latex L-7 (1) and perfol PK-4 (2).

Fig. 2. Dependence of the rate of count of bremsstrahlung on the thickness of the absorber.

In the experiments the values of Q were varied from 10^{-5} to 10^{-1} Ci, and those of N from 20 to $7\cdot10^4$ counts/min; in this case the value of N was measured at various distances from the window of the counter (10-100 mm), and then the values were reduced to a distance of 15 mm, considering the correction for dead time. Four to eight samples of the same material were investigated simultaneously; 8-26 values of Q_i and N_i were determined for each material.

The experimental coefficients of proportionality k_e for the investigated materials, the arithmetic mean values of which are presented in Table 1, were found from the ratios Q_i/N_i. The values of k_e lie in the range from $7.0\cdot10^{-7}$ (Teflon-26) to $3.1\cdot10^{-6}$ ("kalandr"). The standard deviation in the determination of k_e is 9-25%.

Since k in function (1) depends on several factors (see above), therefore the values obtained for k_e are correct only for constant conditions of measurement (in this case $k = k_e$). However, in k_e the dependence on Z, which determines the intensity of bremsstrahlung, is considered.

If we assume that tritium is distributed uniformly through the thickness of the material, then, depending on the thickness, N can be determined by the function [7]

$$N=\frac{N_0}{\mu d}(1-e^{-\mu d}), \qquad (2)$$

where N_0 is the rate of count without consideration of absorption in the material (for an infinitesimally thin layer); d is the thickness of the material; μ is the absorption coefficient. Since $N = Q/k_e$, then $N_0 = Q/k'_e$, where k'_e is the coefficient of proportionality without absorption. Substituting the values of N and N_0 into (2), we obtain an expression for k'_e:

$$k'_e = \frac{k_e}{\mu d}(1 - e^{-\mu d}). \quad (3)$$

Finding k'_e involves the determination of μ for the investigated materials. For this purpose we measured the absorption curve of bremsstrahlung. A polyethylene film with density $\rho = 0.92$ g/cm^3 and thickness 0.1 mm was used as the absorber. The absorption curve is presented in Fig. 2. The half-thickness $\Delta_{1/2}$ is equal to 0.04 cm, while for polyethylene $\mu = \ln 2/\Delta_{1/2} = 17.5$ cm^{-1}. For materials differing negligibly in Z, the ratio μ/ρ can be considered constant. On the basis of this ratio [it is equal to 19 cm^2/g (polyethylene)] and the known density of the materials, we calculated the values of μ, which were used for the determination of k'_e. The values obtained for μ and k'_e are presented in Table 1.

The influence of the geometry of the measurement and sensitivity of the apparatus on k'_e is considered by standardization of the values of k'_e according to a standard. For the standardization of k'_e, the measurement of samples of the investigated materials and standards was conducted in identical geometry. In this case two standards were used: tritium–titanium with an activity of $2.16 \cdot 10^{-5}$ Ci with respect to tritium and strontium–yttrium with activity $8.45 \cdot 10^{-8}$ Ci with respect to yttrium. The accuracy of the standard according to the data of the manufacturers was ±10%. The following function was used for the standardization:

$$k''_e = \frac{k'_e N_{eT}}{Q_{eT}}, \quad (4)$$

where k''_e is the standardized value of k'_e (the values of k''_e are cited in Table 1). It is evident that the activity of the tritium–titanium standard is several orders of magnitude higher than the activity of the strontium–yttrium standard; however, in the first case the values of k''_e are four orders of magnitude lower in comparison with the second standard. This is explained by the low yield and low efficiency of recording (~1%) of the bremsstrahlung of the β-particles of tritium.

The values obtained for k''_e can be used to measure the amount of tritium not only in the investigated materials, but also for other film materials with close values of Z. In this case any instruments sensitive to bremsstrahlung caused by tritium can be used. The amount of tritium in the materials is determined by function (1), in which

$$k = \frac{k''_e \mu d}{(1 - e^{-\mu d})} \cdot \frac{Q_{eT}}{N_{eT}}.$$

The sensitivity of the method with an SI-2B counter at $N_b = 60$ counts/min, $N = 3\sqrt{N_b}$, and $d \approx 0.05$ mm in the case of measurement of a surface equal to the area of the window of the counter (12 cm^2), lies in the range from $1.2 \cdot 10^{-5}$ (Teflon-26) to $3 \cdot 10^{-5}$ Ci (nairit latex-7). The sensitivity reduced to unit area is $(1.0\text{-}2.5) \cdot 10^{-6}$ Ci/cm^2. The sensitivity can be increased by reducing the background and using detectors with a greater efficiency of recording to low-energy radiations.

The authors would like to express their gratitude to V. N. Demenyuk, V. V. Migunov, and L. I. Romashova for their aid in the work.

LITERATURE CITED

1. W. Balkwell and D. Kubose, Determination of the Tritium Activity Adsorbed on the Surface of Various Metals, USNRDL-TR-890 (1965).
2. W. Hutchinson and I. Eakins, The Radiobiological Hazard from Tritium Sorbed on Metal Surfaces, AERE-5689 (1968).
3. E. Evans, Tritium and Its Compounds [Russian translation], Atomizdat, Moscow (1970).
4. T. Westmark et al., Nucl. Instrum. and Methods, 9, 141 (1960).
5. S. I. Lobov and V. A. Tsukerman, Prib. i Tekh. Eksperim., No. 4, 164 (1963).
6. V. P. Mashkovich and S. G. Tsypin, At. Énerg., 11, 251 (1961).
7. V. I. Baranov et al., Laboratory Studies and Exercises in Radiometry [in Russian], Atomizdat, Moscow (1964).

WORK EXPERIENCE OF THE COORDINATING COUNCIL OF PKIAÉ SÉV, CONCERNING THE PROBLEM OF THE RENDERING HARMLESS OF RADIOACTIVE WASTE

B. S. Kolychev

In 1971, in the role of a working body of the Permanent Commission of SÉV, concerned with peaceful use of atomic energy, a scientific–technical council was set up to deal with the problem 1-3 (KNTS 1-3): "Investigations in the field of rendering safe of radioactive waste and deactivation of surfaces."

The basic problem of KNTS 1-3 is to promote the organization of multilateral collaboration of the interested countries, the members of SÉV, on this problem with the aim of speeding up the scientific–technical progress. A program of scientific–technical collaboration on the problem 1-3 was worked out, in which the basic directions of investigation are defined. In addition, it was established in the program in which way one problem or another will be solved when work on it is carried out in two or more countries simultaneously. This enabled a clear distribution of the work between countries to be carried out, and to avoid unnecessary parallelism while carrying out the investigations.

From the instant of the organization of KNTS 1-3, in the framework of scientific–technical collaboration, investigations were carried out which allowed a number of methods to be set up that enable to unify the approach to the solution of certain practical problems, to reduce the amount of labor of the investigations being carried out, and to obtain comparable results, irrespectively of the country carrying out these investigations. The following methods have been considered and accepted on conferences of KNTS 1-3.

Unified methods for the choice and assessment of natural and artificial organic and inorganic sorbents allow examination of all sorbents which are being produced and developed. It allows their suitability to be assessed with respect to purification of nontechnological waste of a low-level activity, and as a result, to set up a catalog of all sorbents being produced in the countries of SÉV which correspond to the requirements imposed on them at the purification installations.

Preliminary methods have been produced for comparing the cost of purifying radioactive waste by sorbents of repeated and once-only use. These methods allow, without carrying out complex and highly costly experimental work, to give with a high degree of confidence, only on the basis of laboratory investigations, an unequivocal answer when choosing between sorbents of single and multiple use. They must help to solve these problems which always give rise to great arguments, since all sorbents have extensive circles of adherents. These methods have been distributed to the countries for testing. In the case of need improvements can be introduced in them.

To solve the problem without carrying out complex experimental investigations, methods have been developed for the selection of safe conditions for burying waste rendered harmless, dependent on the properties and specific activity.

Investigations into experimental storage of such waste materials carried out in the USSR enabled the necessary, limiting initial data to be obtained, which in fact were taken as the basis of these methods. They were reported on the conference of specialist of MAGATÉ (Moscow, September, 1972) devoted to the same problem. This was the first time when material developed in the framework of PKIAÉ SÉV was considered in another international organization.

The method of burying liquid radioactive waste in deep geological formations is well tested in practice by Soviet specialists. High economy was obtained in the case of high output (hundreds of thousands of

Translated from Atomnaya Énergiya, Vol. 35, No. 6, pp. 444-445, December, 1973.

cubic meters per annum), since for this method the cost of burying 1 m^3 of liquid waste of low-level activity does not exceed 1-1 ruble 50 kopecks. The experience of work of many years with a careful check of the advance of the activity front in subterranean collectors, by means of test boreholes, showed the reliability and safety of this method. With the aim of making use of the extensive experience of the Soviet Union, methods of geological, hydrogeological, and physical–chemical investigations were developed for the search, prospecting and validating the suitability of geological structures for safe burying of liquid radioactive waste.

Assigning great importance to the need to render harmless not only radioactive waste but any other harmful liquid industrial waste, and to the preservation of the environment, KNTS considered it advisable to suggest for the consideration during the meeting of the Permanent Commission the last two sets of methods, and to recommend them as the normative documents, and in the case of need to address them to all interested bodies of SÉV and MAGATÉ for subsequent use. This resolution was adopted in July, 1973.

In the framework of KNTS 1-3 work is being carried out on the theme 1-3.6: "Investigation of the migration of radioactive isotopes in the surface waters of land, seas, and oceans."

A first positive result of the combined efforts was the substantial lightening of the burden of method development. The determination of radioactive traces in a watery medium is connected with considerable difficulties. A correct approach and distribution of tasks between the participants of the investigation accelerated the preparation of the necessary radiochemical methods. On a conference of radiochemists concerned with methods, general requirements were worked out which must be satisfied by the modern methods of radiochemical analysis of objects of watery medium. Great possibilities in this field were noted in the development of direct instrumental methods for the determination of the content of radioactive matter in water and ground deposits. Introduction of nuclear physics methods, particularly γ-spectroscopy, into this field turned out to be very useful.

To unify the approach to the solution of the problem just listed, "General methodological criteria for determining radioactivity of a watery medium and ground sediments" were worked out, considered by KNTS 1-3 and confirmed by PKIAÉ.

In October, 1972, in the town of Golobczeg (Poland), KNTS 1-3 held a scientific–technical conference. Almost one hundred specialists of the member countries of SÉV took part in it; in addition, a representative of MAGATÉ was present. Altogether 81 reports were read; of these 4 were surveys, 3 were informative, and 74 were thematic. The reports presented to the conference and the discussions conducted showed that the current period is characterized by broadening of the range and by a rise in the level of investigations in accordance with the collaboration program.

During the time of existence of KNTS 1-3, in addition to the conference just mentioned, seven scientific–technical conferences of specialists were held, devoted to the consideration of the individual problems of the program noted above. These conferences, while considering the intermediate stages of the investigation, allow timely introduction of corrections into the program and the methods of conducting the investigations, into the direction of investigations, and in the case of need they allow to take resolutions about stopping the investigations. This was the case, for example, with the investigations on the inclusion of waste into molten sulfur.

During the two years of existence of KNTS 1-3 several stages of the topics listed in the program have been completed successfully and in good time. Thus, specialists of German Democratic Republic carried out their obligations concerned with the development and testing of a film-forming agent for the protection of surfaces against radioactive contamination, and means for applying it under real conditions. In Poland investigations into the development of polishing paste containing detergents and complex-forming agents for deactivation of surfaces have been completed. In the USSR work has been carried out, concerned with the investigation into the conditions of including radioactive waste, containing sodium nitrates, into bitumen. Design work has been carried out and tests have been conducted on experimental models of installations and equipment for deactivation of apparatus and contaminated localities. As was already mentioned above, the development of the methods of burying into geological formations has been completed.

Specialists of German Democratic Republic and Czechoslovakia jointly developed an instrument for analyzing dispersion content of aerosols. Scientists of the USSR and German Democratic Republic worked out methods for the calculation of the propagation of radioactive pollution in the atmosphere.

In 1972 KNTS 1-3 carried out the necessary organizational measures of the settingup, by the member countries of SÉV, of a Commission of Intercalibration for the determination of radioactive pollution of a watery medium.

Not of lesser importance than the collective development of methods is the conduction of full-scale investigations on a collaborative basis. The study of the migration of radioisotopes in the land surface waters on the territory of the countries of SÉV was formulated to that it fully guarantees measures of prevention of radioactive pollution of the watery medium at levels which are much below the limiting permissible or yearly average permissible values. The uniting of the fund of information considerably increases the value of the results thus obtained.

The advisability of collaboration is clearly demonstrated in the case of investigations into the distribution of radioactive traces in the waters and ground sediments of the river Danube. A survey of the earlier observations showed that in 1962-1963 considerable pollution of Danube with radioactive products of nuclear explosions took place. The present stage of observations is characterized, on one hand, by a reduction in the global fall-out of radioactive matter and, on the other hand, by possibility of an effect on water systems by waste and discarded matter of the developing atomic energy industry. Under these conditions a series of analyses was carried out which showed that in 1971-1972 the total β-activity of the waters of the Danube only slightly deviated from the natural level. This confirms the absence of any serious radioactive pollution. The content of ^{90}Sr in the lower layers of water of Danube does not exceed 1 pCi/liter. This indicates that from the entire catchment area of Danube during 1972 altogether only about 200 Ci of ^{90}Sr might be carried into the Black Sea. Side by side with this up to now no reduction of the amount of ^{90}Sr in the Black Sea, produced as a result of the global radioactive fallout, has been noticed. The "riddle" of the Black Sea will be solved in the subsequent joint investigations.

The study of the radioactivity of the Baltic Sea is being carried out by specialists of German Democratic Republic, Poland, and the USSR. An investigation into the accumulation of radionuclides in freshwater and sea organisms in the vicinity of atomic installations of German Democratic Republic has commenced. A detailed program of a complete combined radiological study of the rivers of Poland and hydrobionts of the Baltic Sea has been worked out. Soviet investigators have determined the content of ^{90}Sr and ^{137}Cs in the waters of the Baltic Sea, and have carried out a comparison with the data of Finnish investigators published earlier. The balance of radioactive traces in the Baltic Sea is caused by the global radioactive fallout on its water area and by the flow of the same global pollution of the waters of rivers. Admittedly, for the further study of the radioactivity of the Baltic Sea and for prevention of its radioactive pollution it is necessary to combine the efforts of all Baltic countries.

The plan of work of KNTS 1-3 is set up with such a timing that specialists of delegations would constantly be informed about the course of investigations concerned with the basic directions of the collaboration. In addition, in each session of KNTS 1-3 it is compulsory to discuss some important scientific–technical or technical–economical problem.

A network of mutual scientific information, giving the dates of distribution of the summary and informative documentation has been worked out, which enables timely acquaintance to be made with the results of investigations carried out on individual assignments by all included in the "Program of scientific–technical collaboration" on the problem 1-3.

The first two years of collaboration of the participant countries of the Permanent Commission of SÉV on the use of atomic energy for peaceful purposes can be characterized as a period of establishing connections, improving programs and developing investigations in the above field. But even during this short time the results of the investigations confirmed the fruitfulness of international collaboration. The methods already worked out and the development of collective investigations with respect to a number of tasks of the problem of rendering harmless of radioactive waste – so important for the defense against pollution of the environment where man lives and works – can serve as examples.

COLLABORATION DIARY

The regularly scheduled session of the Council of the International Economic Association for Nuclear Instrumentation, known as Interatominstrument, was held in Szeged (Hungary), from August 28 through September 1, 1973. The chairman was a member of the council, M. Bhabha, assistant general director of the Gamma-combine. The participants in this session were greeted by the chairman of the State Atomic Energy Committee of the Hungarian Peoples Republic G. Osztrowszki.

The Council discussed questions relating to scientific and technical activities, production and commercial economic activities, of the Association, as well as proposals on how to expedite specialized and cooperative modes of production of nuclear products, and organization of advertising, publicity, and information sharing. The Council heard a report by the Association's director on the activities undertaken by Interatominstrument. Resolutions were adopted on all of the topics discussed.

In line with the constitution adopted by the Association, a factory manufacturing electronic measuring instruments (in Budapest) and the Metrimpex foreign trade enterprise (also located in Budapest) became incorporated into the association. Consequently, at the present time Interatominstrument groups together 13 enterprises and foreign trade organizations. Participating in this session of the Council were representatives of the COMECON Secretariat section on peaceful uses of atomic energy. The Council drew up a tentative agenda for the following session to be held in Warsaw in December, 1973. The Council session took place in a businesslike atmosphere, in a spirit of complete mutual understanding.

* * *

The fifth session of the KNTS [Coordinating Scientific–Technical Council] on radioactive wastes and deactivation was held in Moscow, October 9-12, 1973.

Engineering requirements in the planning of nuclear power generating stations were discussed from the vantage point of wastes deactivation; basic statements on deactivation of the reactor loop in situ, on deactivation of individual loop equipment modules and contaminated surfaces of work rooms, were formulated. These requirements have to be taken into account in order to ensure radiation safety in the operation and maintenance of nuclear power stations. Cost estimates of methods and equipment for deactivating contaminated equipment and contaminated power station rooms or contaminated research centers, worked out by USSR and Czechoslovak delegations within the framework of the "Program of collaboration," were also discussed.

The specialists discussed procedures for analog computer simulation of the operating conditions of underground storage facilities for liquid radioactive wastes, holdup conditions required for reducing the toxicity of the wastes down to safe levels, and also refinements in the initial conditions and hydrodynamical pattern of the storage terrain and surrounding areas. The materials on procedures are recommended for use in the design of underground storage facilities for radioactive wastes and toxic wastes originating in other branches of industry.

The Council set down the basic trends in scientific and engineering research in the field of deactivation of radioactive wastes for the 1976-1980 period, and adopted a work plan for the Council for the 1974-1975 period; it also made refinements on the schedule of conferences to be held with specialists of COMECON member-nations on immobilization of radioactive wastes in bitumen and cleanup of air discharges to get rid of radioactive gases and aerosols. These conferences are scheduled for 1974. Topics relating to the program of research on radioactive contamination of the Danube waters and tributaries also came under discussion.

Translated from Atomnaya Énergiya, Vol. 35, No. 6, p. 446, December, 1973.

THE SIXTH EUROPEAN CONFERENCE ON CONTROLLED NUCLEAR FUSION AND PLASMA PHYSICS

V. A. Chuyanov

The Sixth European Conference on Controlled Nuclear Fusion and Plasma Physics was held in Moscow from July 30 to August 4. The Conference was attended by 553 representatives and 200 guests from 22 countries including the United States, Japan, and other non-European countries.

The first session of the Conference was dedicated to the memory of Academician L'ev Andreevich Artsimovich, the recognized leader of thermonuclear research in the USSR and entire world. To reminiscence about L. A. Artsimovich were dedicated the addresses of the Chairman of the Plasma Physics Section of the European Physical Society P. Vandenplass, Academician Ya. B. Zel'dovich (USSR), the Director of the Calem Laboratory (Great Britain), R. Pease, the Director of the Princeton Laboratory (USA) M. Gotlieb, and one of the closest associates of L. A. Artsimovich, S. V. Mirnov.

The morning plenary sessions heard 16 review papers on various problems of plasma physics; the evening sessions (three sections worked in parallel) were presented with 153 original reports.

Nearly one third of all papers dealt with tokamak studies. Review papers on this subject were presented by Academician B. B. Kadomtsev, H. Furth (USA), P. Rebioux and G. Laval (France).

After noting the successes in obtaining plasma with very high parameters in tokamaks (density $n_e = 7 \cdot 10^{13}$ cm^{-3}, electron temperature T_e up to 3 keV, ion temperature T_i up to 600 eV, retention parameter $n_e\tau$ up to 10^{12} cm$^{-3} \cdot$ sec), and in understanding certain processes taking place in tokamaks (neoclassical ion lifetime, detection of a classical effect of impurity concentration along the discharge axis), B. B. Kadomtsev discussed the principal problems of tokamak studies. The dominating mechanism of energy loss is electron thermal conductivity which is 10 to 100 times higher than predicted by the neoclassical theory. This value has been described by the pseudoclassical formula proposed by L. A. Artsimovich which only very roughly agrees with experiment. The speaker stressed the need of new ways of theoretical description of electron thermal conductivity. For the simulation of the conditions of future reactors, of great importance are experiments in which ions become collisionless (pass from the plateau region into the "banana" mode). However, attempts to obtain such modes in the T-4 machine of the I. V. Kurchatov Institute of Atomic Energy were unsuccessful as the frequency of ion–ion collisions increases with discharge current because of the great amount of impurities with high nuclear charges. Another obstacle in achieving high densities is the so-called disruptive instability. As shown in experiments with the T-6 machine, this instability is preceded by the development of helical modes. The nonlinear theory of B. B. Kadomtsev and O. P. Pogutse about the formation of cavities in tokamak plasma establishes a relationship between the helical modes and disruptive instability, and evidently gives the long-sought-for basis for understanding the occurring processes.

H. Furth discussed recent results obtained in Princeton on the ATC machine and the prospects of using adiabatic compression and neutral injection. Application of adiabatic compression made it possible to obtain in the relatively small ATC machine a plasma with parameters similar to those obtainable in much larger T-4 and ST machines ($n_e \approx 10^{14}$ cm^{-3}, $T_e \approx 2.5$ keV, $T_i \approx 600$ eV). Initial experiments with injection of relatively low-power neutral beams (30–45 kW with a particle energy 15 keV) has shown the absence of harmful effects and a small, but corresponding to calculations, effect of ion heating. The speaker pointed out the advantages of combining adiabatic compression and neutral injection: facilitated penetration of the neutral beam into plasma if injection takes place into low-density plasma before compression (otherwise, reactor systems require beams of megavolt energies which are very difficult to produce), effective multiplication of beam power by adiabatic compression, separation of plasma from the walls, and easing of the

Translated from Atomnaya Énergiya, Vol. 35, No. 6, pp. 447–449, December, 1973.

impurity and beam redischarging problems. Considering the feasibility of a "target" type of reactor (injection of beam of fast deuterons into the tokamak tritium plasma with an electron temperature of ~10 keV), the speaker noted that on this basis a zero-power reactor can be designed with dimensions foreseen for the next generation of tokamaks (T-10, PLT). This principle seems to be most promising for demonstrating the possibility of generation of useful energy by means of controlled fusion, in particular, when using a blanket of fissionable material.

First experiments with the biggest tokamak TFR (Fontenay-aux-Roses, France) have been described by P. Rebioux. The TFR tokamak has the following parameters: large radius 98 cm, chamber radius 20 cm, magnetic field up to 60 kG, maximum plasma current up to 400 kA, discharge duration up to 0.5 sec. So far experiments were made with fields up to 40 kG and currents up to 200 kA. Electron and ion temperatures of the order of 2-3 keV and 600 eV, respectively, obtained at a density of $5 \cdot 10^{13}$ cm^{-3} are in good agreement with the results obtained before in other machines. Preliminary data indicate gradual accumulation of impurities in plasma and the occurrence of turbulence at the center of the filament where the stability margin $q < 1$ which causes a drop in electron temperature and decreases the energy lifetime in discharges after the 150th millisecond.

Tentative results were also reported from other new machines of the tokamak type. Neutral injection experiments have been started in the Ormac machine (Oak Ridge, USA). The Cleo machine (Calem, England). First experimental results have been obtained from the "seal-ring" tokamak of the Institute of Atomic Energy. These results are however, only preliminary. More detailed and reliable data will be probably available the next year. Two distinct trends can be noted: first the popularity of neutral injection which is already in use or will be used in most new experiments. The available data correspond to low (as compared with ohmic heating) injection powers and can be interpreted to indicate the absence of harmful effects. The forthcoming experiments, especially with the Ormac machine, should demonstrate the effects of neutral injection at high powers. Secondly, the importance of impurities, particularly in case of prolonged discharges and high plasma parameters (T-4, TFR, Ormac), stimulated interest in experiments with diverters. This trend should be considered in planning the design of large next-generation machines.

In contrast to the high experimental and design activity in tokamaks, a relative calm has been observed in other more traditional fields of thermonuclear research. Stellarator studies indicate classical or nearly classical confinement. Obviously, really new and important results in this field can be expected only after the completion of large installations which are being planned or constructed now, such as the Wendelschtein-VII machine (Garching, FRG).

No new results have been obtained during the last year with open traps. Experiments at the Kurchatov Institute of Atomic Energy and also at the Livermoore Laboratory (USA) indicated, in spite of the predictions of the simplified theory, the principal possibility of the existence of a stable collision plasma in a mirror trap. Recent works of M. S. Ioffe and collaborators (Institute of Atomic Energy) confirmed the role of cold plasma in suppressing conical instabilities in open traps noted before by R. Post (Livermoore, USA). However, experiments on prolonged sustaining of collision plasma stability by means of neutral injection, conducted at the Livermoore Laboratory with the 2X-II machine, gave no conclusive results. The Conference has been informed about the injection of a 20-keV, 10-A beam of neutrals into a plasma produced in the 2X-II machine by adiabatic compression of a plasmoid. These experiments are now at the same level as tokamak injection: no harmful effects have been observed but for positive results the injection power is too low. To maintain in a mirror trap a plasma with a density of the order 10^{13} cm^{-3} and an ion temperature of 20 keV throughout the injection cycle, the injection power must be increased by one order of magnitude. An injection of about 200 eq. A is now being readied.

Experiments with toroidal pinches of different shapes for the production of plasmas with high β (the ratio of plasma pressure to magnetic field pressure) are conducted at the Los Alamos Laboratory and at several European laboratories. As a rule, these experiments show that sufficiently hot plasmas can be produced relatively easily, but that the observed lifetimes are very short and lie in the microsecond range. Experiments conducted at Los Alamos and Garching (FRG) proved the feasibility of producing toroidal zero-current equilibrium plasma configurations with high β. The main problem is the instability of these configurations with respect to the $m = 1$ mode. It has been shown that this mode can be stabilized by dynamic methods and feedbacks but the application of these methods on an engineering scale meets with enormous difficulties. Thus, experiments are now being prepared with very little compression of heated plasma which should reveal conductive-wall stabilization effects of the $m = 1$ mode. The most promising of current configurations is the belt pinch configuration which is in fact similar to the seal-ring tokamak.

Belt pinch experiments (Garching) have shown a β of the order 0.5 with a temperature of 10 eV and plasma formation lifetimes up to 100 μsec. No strong instabilities were observed, the plasma lifetime being apparently limited by classical diffusion. Two new experiments of this kind, TENQ at Ulich (FRG) and Belt Pinch II at Garching, are now being prepared and will start operating in 1974. They are expected to provide temperatures of about 1 keV and a containment time up to 1 msec.

Two new developments in thermonuclear research: electron beams and superpower lasers, have been extensively discussed at the Conference. The use of lasers in thermonuclear fusion has been considered in two papers presented by USA workers. L. Wood of the Livermoore Laboratory described the results of calculations on supercompression of matter as a consequence of spherical implosion. K. Brueckner talked about laser fusion experiments conducted at the KMS Company and on a laser system providing a 840-J, 3 nsec pulse and capable with some pump lamp overloading to give 1400 J/pulse. The target is irradiated on both sides. A system is now being designed for shaping the leading edge of the pulse. Experiments with this laser were also reported in which neutrons and hard γ-quanta have been observed. The observed neutron yield (several hundred per 3 nsec at 100-200 J) is in good agreement with numerical calculations. According to these calculations the electron temperature should be of the order 2 keV and the ion temperature about 500 eV. No compression experiments were made so far.

Relativistic electron beams were reviewed by R. Sudan (Cornell University). The parameters of electron beams now obtainable are quite impressive: energies up to 15 MeV, currents in excess of 10^6 A, pulse energies up to 3 MJ, powers 10^{13} W, current densities up to $5 \cdot 10^6$ A/cm^2, and pulse lengths of 100 nsec.

In combination with high accelerator efficiency, these parameters make electron beams worthy rivals of superpower lasers in supercompression applications, and indicate many other applications of electron beams in controlled fusion: plasma generation and heating, generation of minimum-B fields in toroidal configurations. The main problems in supercompression application of electron beams are associated with the need of shortening the beam time to less than 10 nsec while retaining its energy and with focussing the beam to current densities of 10^8-10^9 A/cm^2. The use of electron beams in magnetic confinement schemes are associated with problems of their injection and capture in toroidal magnetic fields. Solutions to these problems are sought now by many specialists. In particular, beam focussing is much helped by effects of high-current beam pinching, by plasma injection into a diode, and by the possible use of external converging fields. The very strong magnetic field of the beam allows the development of original methods of injection into toroidal fields utilizing the short time interval when the beam field changes the overall field topology and allows capture of the beam into the toroid. R. Sudan pointed out in conclusion that the time is now ripe to consider the generation of high-current ion beams by modifying the technology already available: suppression of electron emission by a transverse magnetic field, production of ion-emitting plasma surfaces with the aid of lasers, etc.

The Conference brought no great surprises. Decisive experiments are still in the future.

The next Seventh European Conference on Plasma Physics and Controlled Fusion will take place in Lausanne (Switzerland) in September, 1975.

SEMINAR ON WELDING IN THE ASSEMBLY OF ATOMIC POWER PLANT EQUIPMENT

S. S. Yakobson

From May 31 to June 2, 1973 the Head Office of Thermal Electrical Plant Construction (HOTEPC) and the Power Information Bureau (PIB) of the Ministry of Power and Electrification of the USSR held at the I. V. Kurchatov Beloyarsk Atomic Power Station a seminar on welding in atomic plant building. The seminar was attended by representatives of institutes and organizations of the Power Ministry and the State Atomic Energy Commission (SAEC) of the USSR.

V. A. Kazarov (HOTEPC) spoke about the share of atomic plants in the Ninth Five-Year Plan and the tasks of building organizations.

S. A. Belkin and V. V. Shefel' (Power Plant Construction Office, PPCO), V. P. Tavrovskii (Central Power Plant Construction Bureau, CPPCB), and V. I. Grinenko (SAEC) discussed problems of automatic welding in the assembly of atomic power plant equipment. Representatives of the PPCO reported on advances in technology and automation of pipeline welding operations in atomic plants, and presented data based on practical experience and laboratory studies on the desired level of mechanization of welding operations and on the type of automatic machines most needed in atomic plant construction. Representatives of the CPPCB reported the design and application of automatic butt-welding machines for nonrotating 0Kh18N12T steel pipes 560 × 32 mm in diameter used in the construction of the Novo-Voronezh Atomic Power Station.

G. M. Ginzburg (CPPCB) told about the application of manual methods (electrical argon arcs) for welding austenitic steel pipes and stressed the measures for improving the seam metal continuity.

Interesting papers were presented by S. A. Gel'pern (North-West Power Plant Construction Bureau), V. V. Tsygankov (East Power Plant Construction Bureau), and V. A. Pavlakov (SEAC) on welding the structure and pipe system of the Kol'sk, Bilibinsk, and Leningrad Atomic Power Stations. The speakers described in detail the setting up, welding, and quality control operations, explained the organization of the welding and quality inspection services, and pointed out the specific techniques employed in individual units of the power stations.

V. B. Bogoda (Power Building Design Bureau) described on-site quality control methods for inspecting welded joints in atomic power plant assemblies, and discussed various nondestructive testing techniques.

S. Sh. Roitenberg, representative of the South Power Plant Construction Bureau, described experiments on improving welding techniques as applied to the assembly of the equipment of the Armenian and Chernobyl'sk Atomic Power Stations.

The results of testing the performance of welded joints in several Soviet atomic power plants have been described by F. A. Khromchenko (All-Union Heat Engineering Institute). He conducted a detailed analysis of the defects in the metal and welded joints in the equipment of the Novo-Voronezh Atomic Power Station.

After an exchange of views, the participants outlined specific measures intended to improve the quality of assembly of atomic power plants and to facilitate welding and quality control operations. Basic improvements are afforded by maximum mechanization of welding, especially in difficult cases. For this purpose, one of the factories of the Power Ministry of the USSR should organize the design and manufacture of special-purpose welding machines and power sources; design and research work on this subject should

Translated from Atomnaya Énergiya, Vol. 35, No. 6, p. 449, December, 1973.

also be expanded. Together with improving quality control techniques for inspecting welded joints, the development and introduction of new flaw detection techniques and instruments, which improve the reliability, performance, and efficiency of quality control, it is necessary to formulate technically sound norms on testing and evaluation of the quality of welded joints in atomic power plant assembly.

ALL-UNION CONFERENCE ON NEUTRON PHYSICS

S. I. Sukhoruchkin

The Second All-Union Conference on Neutron Physics took place in Kiev from May 28 to June 1 with the participation of more than 150 Soviet Specialists and scientists from several socialist and capitalistic countries (France, Federal Republic of Germany, etc.). Twenty-six review papers and many original reports were presented to the Conference at plenary meetings and six sections held in succession. The Conference began with a discussion of the need of nuclear data for the design of fast (L. N. Usachev, Physics and Power Institute) and controlled thermonuclear reactors (G. B. Yan'kov, Institute of Atomic Energy). A comprehensive analysis of the effect of inaccurate nuclear data on the accuracy of such basic nuclear power reactor parameters as critical mass and conversion ratio has been made possible by a series of works by L. N. Usachev, S. M. Zaritskii, M. F. Troyanov, M. N. Nikolaev, and their collaborators. Of particular importance in this field is the method of determining the optimum contribution of differential and integral experiments into the derivation of estimated nuclear data and averaged reactor group constants described by L. N. Usachev. An economical justification has been given for the need of a broad program of measurements of the cross sections and constants of fissionable and structural materials, of estimating the accuracy of these data, and, most important, of a careful analysis of all possible systematic error sources which has not been always given due attention before. It is now generally accepted that to obtain reliable values of nuclear constants it is desirable to compare the results of several independent measurements. The estimation of data, including a full analysis of all experimental errors, is an important step in creating a Soviet nuclear data library. V. A. Konshin, M. N. Nikolaev et al. presented examples of such data estimation for ^{239}Pu and ^{238}U. A similar problem of nuclear data estimation in France has been discussed by P. Ribeau (Saclay). As international exchange of estimated data is rather limited, most countries with important reactor design programs create their own libraries of estimated nuclear data. In a report devoted mostly to a collection of lists of necessary nuclear data (WRENDA publication), J. Schmidt (Director of the Nuclear Data Section of IAEA) discussed also the role of this international organization in the exchange of numerical information. Unlike estimated data, which take into account the results of integral experiments and the experience gained in the operation of prototype models, preliminary experimental data can be freely circulated among nuclear data centers, and the IAEA serves as a mediator in passing these data to the Soviet Union and back. In his concluding remarks J. Schmidt called on Soviet scientists to make greater use of numerical information available at foreign neutron laboratories and suggested the arrangement of a comparison of estimated data on plutonium and uranium.

Of considerable interest were reports dealing with theoretical questions. A review paper by V. M. Strutinskii discussed a systematic approach to the calculation of parameters of the double-humped fission potential of many nuclei. This made it possible to explain the parabolic functions in spontaneous fission periods and fission asymmetry. A review by V. G. Solov'ev cited several examples of the microscopic approach to neutron spectroscopy developed at the Joint Institute of Nuclear Research. The paper discussed splitting of simple single- and three-quasiparticle states into many highly excited levels and predicted intensification of certain transitions such as transitions to two-phonon levels with emission of α-particles and transitions to three-quasiparticle states with emission of γ-quanta. This microscopic approach is supplementary (and a logical step forward) in relation to the statistical model. The approach allows a more detailed analysis of the different properties of individual nuclear resonances, of partial-widths correlation, etc. The microscopic resonance structure has been also discussed in papers by P. Z. Nemirovskii on input state statistics and by D. F. Zaretskii on the role of shell structure in neutron scattering. The latter paper described how to use nuclear spectroscopic factors obtained from deuteron stripping and pick-up reactions for improving the agreement between the predictions of the optical model and experimental data on the strength function in nuclei close to tin. Former attempts to solve this problem by various other

Translated from Atomnaya Énergiya, Vol. 35, No. 6, pp. 450-451, December, 1973.

modifications of the optical model were largely unsuccessful. Application of the statistical model of the nucleus (including nucleon pairing) to the calculation of nuclear-level density and of simple and compound processes in capture reactions (and charged-particle escape) were discussed in the review by A. V. Ignatyuk. Satisfactory agreement with experiment is observed within 50% accuracy limits, although neither the statistical model nor the microscopic approach can claim better accuracy. Such theoretical estimates are particularly important in cases when certain nuclear constants are difficult to measure experimentally as, for example, in the case of fission fragments cross sections.

The review of the results obtained at Saclay (D. Paya, France) and Karlsruhe (S. Ziriacks, FRG), as well as the papers by Yu. P. Popov and F. Birchwarge (JINR) on the experimental study of decay properties of neutron resonances, were received with great interest at the section devoted to experimental studies of the interaction of thermal and resonance neutrons with nuclei. D. Paya discussed data on reactions involving the escape of α-particles, i.e., type (nα) and (n$\gamma\alpha$) reactions. From an analysis of the (n$\gamma\alpha$) reaction on ^{143}Nd nuclei it has been possible to find the radiative transitions hindrance factor (with respect to the Weisskopf single-particle estimate) between compound, highly excited states. This factor has been found to be two-three orders of magnitude stronger than the hindrance for lower (i.e., relatively simple) states, which agrees with contemporary theoretical considerations. F. Birchwarge discussed the interpretation of γ-spectra of resonance neutron capture obtained with the aid of large germanium detectors. A group of JINR physicists devised a method of multidimensional measurements and processing of experimental spectra, and carried out a series of studies of nuclei in the rare-earth range. The data of F. Birchwarge made it possible to refine the data obtained earlier at the Institute of Atomic Energy, and the measurements of resonance neutron capture provide now valuable material for testing the statistical model and for finding systematic deviations from this model (i.e., partial-widths correlation, etc.). The review paper by G. V. Muradyan on the statistical properties of neutron resonances discussed the distribution of neutron-level spacing and described a new method of estimating the probability of equidistance in neutron resonance positions which is more substantiated than the one suggested by K. Ideno and M. Okubo. New data on technetium obtained at the Institute of Atomic Energy indicate good agreement with deductions of the statistical model. G. S. Samosvat (JINR) discovered an interesting effect of anomalous anisotropy in the scattering of slow neutrons with nearly completely filled shells.

Much consideration has been given to the study of interaction between fast neutrons and nuclei and of the process of fission, and the rich experimental material accumulated during the two years elapsed since the last conference has been presented in reviews by K. A. Petrzhaka, M. V. Blinov, Yu. A. Khokhlov, M. B. Fedorov, M. V. Savin, and V. Ya. Golovin. Significant refining of results has been achieved in several directions. For example, the effective temperature in the expression for the spontaneous-fission neutron spectrum of californium has been studied in the Radium Institute and in the Physics and Power Institute, and the observed results are in good agreement: T = 1.42 ± 0.05 and 1.39 ± 0.03, respectively. The fine structure in the neutron fission spectrum has been confirmed at the Scientific-Research Institute of Atomic Reactors. For the first time, results were obtained on the number of secondary neutrons for a wide range of curium isotopes (allowing a comparison with data for plutonium isotopes and the detection of different dependence of the number of secondary neutrons on the atomic number Z). Considerable experimental material has been presented also in the papers by A. Michadon (Bruyeres-les-Chatel, France), I. Sabot (Cadarache, France), A. Deruytter (Gale, Belgium), and J. Boldeman (Austria). J. Boldeman obtained the exact number of secondary neutrons of spontaneous fission of californium (ν = 3.744 ± 0.014). Preliminary measurements in the Radium Institute gave the value ν = 3.770 ± 0.045. Two reports (Institute of Atomic Energy and Institute of Theoretical and Experimental Physics) discussed new data on the measurement of the α-ratio constant of the capture and fission cross section of ^{239}Pu. The present state of α-constant measurements will be reviewed in one of the forthcoming issues of this journal.

A new time-of-flight spectrometer, based on the Y-240 isochronous cyclotron now being built at the Institute of Nuclear Research of the Academy of Sciences of the Ukrainian SSR, has been described at the section "Experimental methods of neutron physics"; the same section also heard a report about the operation of the spectrometer based on the ÉG-5 accelerator of the same Institute. Yu. Ya. Stavisskii proposed to use the planned "meson factory" as a source of resonance and fast neutrons. V. I. Lushchikov reviewed the methods and results of producing sources of ultracold neutrons. Studies in this direction, which are vigorously pursued in the USSR, produced several modifications of the methods of ultracold neutron sources and can now be expected to be applied in experimental investigation of fundamental properties of neutrons such as, for example, the dipole moment and lifetime.

The results of the Conference were summarized in the concluding statements by V. I. Mostovoi and J. Schmidt; the Chairman of the Organizing Committee, M. V. Pasechnik, communicated that Neutron Conferences will be held in Kiev approximately every second year. The proceedings of the Conference will be published in 1974.

THE THIRTEENTH CONFERENCE ON NUCLEAR SPECTROSCOPY AND THEORY OF THE NUCLEUS

K. Ya. Gromov and N. A. Golovkov

In accordance with the schedule of scientific meetings organized by the Joint Institute of Nuclear Research (JINR), the Thirteenth Conference on Nuclear Spectroscopy and Theory of the Nucleus was held in Dubna on June 19-23. The Conference was attended by 90 scientists from Soviet scientific institutions, 28 scientists from JINR member-countries, and approximately 150 members of the JINR staff.

As the preceding conferences, the Thirteenth Conference was devoted to experimental and theoretical studies of the structure of atomic nuclei and to the enhancement of international cooperation in the JINR. A secondary topic of discussion was computer processing of spectrometric data.

A collection containing detailed summaries of 97 of the presented papers has been published at the time the proceedings of the Conference began.

The program of the Conference consisted of review papers on subjects common to the presented papers. Several of the reports were presented by speakers especially invited by the Organization Committee.

Theoretical papers dealt primarily with the description of the structure of so-called transitional nuclei, i.e., nuclei occupying an intermediate place between spherical nuclei and nuclei with a stable deformation, and to different approaches to the theory of orbital motion of atomic nuclei.

The principal difficulties arising in the description of transitional nuclei are associated with conspicuous deviations of the observed properties of their states from those predicted by the shell and collective models of the nucleus. Experimental data indicate the instability of the average field of transitional nuclei and a strong anharmonicity of their states. This has been emphasized in the reports of R. Jolos and V. V. Pashkevich (JINR). An important role in transitional nuclei play also interactions of quasiparticles with collective excitations as demonstrated in papers of Ch. Stoyanov and V. Paar (JINR).

The development of a microscopic theory of orbital motion is one of the most important problems of the atomic nucleus. This problem has been considered at the Conference by V. G. Zelevinskii who together with S. T. Belyaev (Siberian State University) developed a sequential method of isolation of rotational states which strictly obeys all conservation rules. Orbital motion in atomic nuclei is now of considerable interest in connection with studies with beams of α-particles and heavy ions which make it possible to excite nuclear states with spins up to I = 20. These studies revealed a number of anomalies in rotational bands of even–even and odd nuclei. Theoretical questions associated with these anomalies have been discussed by I. M. Pavlichenko (Institute of Atomic Energy), L. Munchow (GDR), N. I. Pyatov and I. Piperowa (JINR).

Even though studies of α-decay of atomic nuclei are decades old, we still do not have a satisfactory quantitative theory of this effect. Some qualitative progress in α-decay theory has been reported by V. I. Furman (JINR) and S. G. Kadmenskii (Voronezh State University).

Certain advances have been recently made in experimental studies of the structure of transitional nuclei and nuclei remote from the stability band. The studies are carried out on the JINR synchrocyclotron (YaSNAPP program) and the heavy-ion accelerator. The extensive experimental information presented by V. G. Kalinnikov and K. H. Kauna (JINR), I. Mahunki (Hungary), U. Hagemann (GDR), H. G. Ortlepp (JINR), and others stresses the need for the development of advanced models describing the structure of low-lying excitations in transitional nuclei.

Translated from Atomnaya Énergiya, Vol. 35, No. 6, pp. 451-452, December, 1973.

New information about properties of rotational states of deformed nuclei has been presented by H. Sodan (GDR). It is interesting to note that a considerable portion of the new data has been obtained with the new Soviet-made ÉG-10 electrostatic tandem accelerator which has been put into operation last fall at the Central Institute of Nuclear Research of the GDR (Dresden).

It has been recently possible to use a new approach to the study of the properties of high-lying (3-8 MeV) nuclear states where the state density is high. Experimental means have been made available for studying the microstructure of these states. Yu. P. Popov (JINR) analyzed specific possibilities of obtaining nuclear spectroscopic data from reactions with resonance neutrons. V. A. Karnaukhov and Yu. P. Gangrskii (JINR) discussed problems associated with spectroscopic information provided by new phenomena discovered at the JINR: delayed-proton emission and spontaneously fissionable isomers.

Several papers were heard on organizing the acquisition and processing of spectrometric information. Of special interest were the papers of V. M. Tsupko-Sitnikov (JINR) and I. A. Kondurov (Leningrad Institute of Nuclear Physics, Academy of Sciences of the USSR), and others. Programs for computer processing of spectrometric information have been described in several papers.

There is no doubt that the Thirteenth Conference on Nuclear Spectroscopy and Theory of the Nucleus has been very fruitful for the exchange of the latests results of experimental and theoretical studies of the structure of atomic nuclei and for strengthening the cooperation of atomic physicists of Socialist Countries.

SYMPOSIUM ON NUCLEAR PHYSICS EMPLOYING THERMAL AND RESONANCE NEUTRONS

A. D. Gul'ko

The trilateral Soviet–Belgian–Dutch Symposium on Nuclear Physics Employing Thermal and Resonance Neutrons, organized jointly by the State Commission of Atomic Energy Institutes of the USSR, the Center of Nuclear Energy (CEN, Belgium), and the Netherlands Reactor Center (RCN, the Netherlands), took place in Petten (Netherlands) on May 22-25, 1973. The Symposium heard nearly 25 reports which, according to their topics, can be grouped as follows: γ-quanta spectroscopy after capture of thermal neutrons (nonpolarized and polarized), reactions with resonance neutrons (nonpolarized and polarized neutrons and nuclei), neutron-induced fission, experiments with polarized nuclei produced by capture of polarized neutrons, methodical developments (neutron and nuclei polarization).

Most papers dealing with γ-quanta spectroscopy were presented by the Dutch group (K. Abrahams, J. Kopecky, F. Stecher-Rasmussion, A. Spits, and A. Opp den Kamp) who conducted experiments in Petten using the high-flux HRF reactor (flux at the center $3 \cdot 10^{14}$ neutrons/$cm^2 \cdot$ sec, polarized neutron beam intensity $3 \cdot 10^7$ neutrons/$cm^2 \cdot$ sec, polarization 90 ± 5%). γ-Quanta were recorded with 40-60 cm^3 Ge(Li) detectors and 12 × 12 cm NaI crystals.

Nearly half of the presented papers, especially those by Soviet and Belgian workers, dealt with investigation of neutron resonance parameters.

A. B. Popov (USSR, JINR) described measurements of neutron resonance spins of ^{111,113}Cd, ^{147,149}Sm, ^{157}Gd, and ^{161,163}Dy isotopes based on the multiplicity of γ-quanta emitted in neutron capture. The neutron energy range covered 150-400 eV. A trial was made to evaluate the spin effect by model calculations and the results were compared with experiment. The obtained data made it possible to analyze spin effects in terms of level densities D and strength functions S^0. The following results were obtained: for ^{147}Sm, $D_{J=3} = 15.0 \pm 1.5$ eV, $D_{J=4} = 12.8 \pm 1.2$ eV, $S^0_{J=3} = (4.4 \pm 1.6) \cdot 10^{-4}$, $S^0_{J=4} = (4.2 \pm 1.5) \cdot 10^{-4}$: for ^{149}Sm: $D_{J=3} = 5.2 \pm 0.5$ eV, $D_{J=4} = 4.1 \pm 0.3$ eV, $S^0_{J=3} = (6.3 \pm 2.1) \cdot 10^{-4}$, $S^0_{J=4} = (7.7 \pm 2.2) \cdot 10^{-4}$; for ^{157}Gd: $D_{J=1} = 13.1 \pm 1.5$ eV, $D_{J=2} = 9.5 \pm 0.9$ eV, $S^0_{J=1} = (2.1 \pm 0.7) \cdot 10^{-4}$, $S^0_{J=2} = (2.3 \pm 0.6) \cdot 10^{-4}$. The results indicate that there is no marked dependence of the strength function of the resonance spin.

É. I. Sharapov (USSR, JINR) reported on the calculation of neutron resonance parameters (E_0, $g\Gamma_n$, D) of ^{191,193}Ir isotopes on the basis of radiative neutron capture measurements (upper energy limit 200-400 eV).

H. Keilemann (Belgium) analyzed neutron resonances of ^{143}Nd in the 55-2000 eV range and gave the figures for $2g\Gamma_n$ and Γ_t, and $S^0 = (3.42 \pm 0.7) \cdot 10^{-4}$. A comparison of these results with the data obtained at the JINR and in Saclay shows good agreement. The results of an analysis of γ-spectra of two ^{177}Hf resonances with different spins were described by K. Koczewa (Belgium).

E. Reddinguis (the Netherlands) and É. I. Sharapov used polarized neutrons and nuclei to determine the resonance level parameters. A joint American–Dutch group experimentally determined the neutron resonance spins of ^{235}U in the Brookhaven reactor by passing polarized neutrons (reflected from a Co–Fe crystal) through a target containing polarized ^{235}U nuclei (adiabatic demagnetization method, $T \approx 0.05°K$, $H \approx 28$ kOe, 5.5% polarization of ^{235}U). The spins of 15 ^{235}U resonances have been for the first time determined with some reliability:

Translated from Atomnaya Énergiya, Vol. 35, No. 6, pp. 452-454, December, 1973.

Energy, eV	Spin	Energy, eV	Spin
0.275	3	7.08	4
1.14	4	8.79	4 (+30% 3)
2.04	3	9.28	4
3.15	3	10.16	4
3.61	4	11.67	4
4.85	4	12.39	3
6.15	3	14.0	3
6.39	4		

Magnetic moments of neutron resonances have been measured by the method proposed by F. L. Shapiro (USSR, JINR) which is based on the observation of resonance shifts caused by hyperfine interactions. Unlike in the Brookhaven experiment on 0.460 and 0.584 eV resonances of ^{167}Er, where polarized neutrons were passed through a nonpolarized target, the Dubna group passed nonpolarized neutrons through a polarized ^{167}Er target (for the same resonances). A temperature of 0.02°K and an internal field of $7.1 \cdot 10^6$ Oe ensured a 97%-polarization of ^{167}Er nuclei. The following resonance energy shifts have been obtained: $\Delta E(0.460) = (27 \pm 7) \cdot 10^{-6}$ eV and $\Delta E(0.584) = (44 \pm 16) \cdot 10^{-6}$ eV, whence the magnetic moments of these resonances were calculated as: $\mu(0.460) = (0.9 \pm 0.4)\mu_N$ and $\mu(0.584) = (1.8 \pm 0.9)\mu_N$. These figures are markedly different from the results of the Brookhaven experiment.

Measurements of capture and scattering cross sections and total cross sections of ^{236}U (up to 2 keV) and ^{242}Pu (up to 1 keV) nuclei were described in two papers of the Belgian group (J. Theobald, L. Mewissen, et al.). The experiments were carried out with the linear electron accelerator of the Belgian Center (Euratom). Of special methodical interest is the high-pressure (nearly 250 atm) ^{3}He neutron scintillation detector having high efficiency and excellent time properties. Neutron widths Γ_n and radiative widths $\overline{\Gamma}_\gamma$ have been found for 99 and 56 resonances, respectively, of ^{236}U. Average $\overline{\Gamma}_\gamma = 22.3 \pm 0.5$ (stat.) $\pm$ 1.0 (syst.) meV, average level spacing below 1 keV $\overline{D} = (17.28 \pm {}^{0.4}_{0.31})$ eV, average reduced width $\overline{\Gamma}^0_n = (2.06 \pm {}^{0.48}_{0.36})$ meV, strength function $S^0 = (1.05 \pm {}^{0.16}_{0.14}) \cdot 10^{-4}$. For 25 resonances of ^{242}Pu, the figures are $\overline{\Gamma}_\gamma = 21.9 \pm 0.4$ (stat.) $\pm$ 1 (syst.) meV; for 71 resonances: $\overline{\Gamma}^0_n = 1.52$ meV, $S^0 = (0.89 \pm 0.1) \cdot 10^{-4}$.

Using the values of Γ_n and Γ_γ, and the resonance fission integrals of ^{242}Pu adopted from other works, the authors obtained the fission widths as functions of energy from which the height of the second fission barrier $E_B = 5.18$ MeV has been calculated (the height of the first fission barrier $E_A = 5.8$ MeV, barrier widths $\hbar\omega_B = 0.5$ MeV and $\hbar\omega_A = 0.6$ MeV).

In a paper on theoretical description of neutron resonance, H. Weigmann (the Netherlands) tried to describe the available experimental data on total radiative widths by means of a semiempirical expression with four parameters. In addition to the usual term associated with the statistical model, the expression contains a term taking into account the effect of external nucleons. In the mass range $40 \leq A \leq 247$ the obtained values of radiative widths do not differ on the average by more than 25% from the known experimental values.

Four Belgian and one Soviet papers dealt with fission physics. P. van Ass reported on the study of differences in mass distribution of fission fragments resulting from fission by thermal and resonance (0.297 eV) ^{239}Pu neutrons. The fission fragments (mass numbers 87, 88, 97, 105, 107, 111, 115, 127, 128, 129, 140, and 149) were identified by γ-emission and half-lives. The authors observed a reduction of resonance fission yield not only in the mass range of nearly symmetrical fission but also for strongly asymmetrical fission.

H. Wegener-Penning described an experimental comparison of the distribution of total kinetic energy and fragment masses, as well as of the mass distributions for different total kinetic energies (in steps of 5 MeV in 152-207 MeV range) for the same ^{240}Pu nucleus in ground state (spontaneous fission) and in an excited state (^{239}Pu + thermal neutron). The total kinetic energy for ^{239}Pu + n_t and ^{240}Pu is 177.95 $\pm$ 0.04 and 176.85 $\pm$ 0.14 MeV, respectively. The difference is 1.1 MeV and disagrees with the former value (~3.7 MeV) both in value and sign. The result indicates that the excitation energy of a nucleus undergoing fission is strongly scattered over degrees of freedom not related to fission. J. Theobald and C. Wagemans described attempts to find a spin dependence of fission characteristics. J. Theobald reported preliminary results of measurements of the number of neutrons for various ^{235}U and ^{239}Pu resonances (up to 40 eV). No clear difference has been observed in resonances with two different spins. Of special interest was the method of comparing binary and ternary coincidences in a neutron detector in measuring the number of fission neutrons. The ratio of ternary to binary fission events for ^{239}Pu was measured in the neutron energy interval from 0.02 to 50 eV (C. Wagemans). Only one resonance (15.5 eV) has been observed to have a markedly higher (by 10%) value of this ratio. The authors attribute $J^\pi = 0^+$ to this resonance and $J^\pi = 1^+$

to all other resonances. G. A. Otroshchenko (USSR, Institute of Atomic Energy) described measurements of the yield of a fissionable isomer in the reaction ^{235}U + 1-MeV neutron.

Experiments with polarized nuclei produced by polarized-neutron capture have been reported in two Soviet papers (Institute of Theoretical and Experimental Physics). P. A. Krupchinskii described experiments carried out at the Institute for detecting nonconservation of spatial parity and violation of time-reflection symmetry in nuclear interactions using polarized neutrons. The search for P-noninvariant effects in $^{113}Cd(n, \gamma)^{114}Cd$ reactions led to a discovery of weak nucleon–nucleon interaction predicted by theory. The 0-π-escape asymmetry of 9.04-MeV γ-quanta was measured. Three experiments gave the following values for the asymmetry parameter: $-(3.7 \pm 0.9) \cdot 10^{-4}$, $-(3.5 \pm 1.2) \cdot 10^{-4}$, and $-(2.5 \pm 0.9) \cdot 10^{-4}$. The weighted mean is $-(3.3 \pm 0.6) \cdot 10^{-4}$ giving for the ratio of the parity-noncorserving potential to the parity-conserving potential the figure $2 \cdot 10^{-7}$ (theoretical estimates are 10^{-7}). Time-reflection symmetry in nuclear electromagnetic transitions has been studied in $^{35}Cl(n, \gamma)^{36}Cl$ reactions by analyzing correlations of the form $\sigma_n[\gamma_1\gamma_2]$, where σ_n is the neutron spin and γ_1 and γ_2 are the momentums of two consecutive γ transitions with energies 7.79 and 0.79 MeV, the first one being a mixed transition. The asymmetry parameter has been found to be $-(0.9 \pm 1.1) \cdot 10^{-4}$ giving for the phase difference of reduced matrix elements in the mixed electromagnetic transition at 7.79 MeV of ^{36}Cl the figure $\Delta\eta = (-1.8 \pm 2.2) \cdot 10^{-3}$ (in case of T invariance $\Delta\eta = 0$) which determines the upper bound for the T-noninvariant fraction of the potential ($\leq 2 \cdot 10^{-3}$).

A. D. Gul'ko described the use of polarized thermal neutrons in generating polarized β-active nuclei and the study of their nuclear magnetic resonance (NMR). He proposed a method for measuring the shape function of NMR lines of short-lived, polarized β-active nuclei from which the g factor and the internal-field distribution can be found. The line shape was measured from the disruption of angular anisotropy of β-emission from the nucleus by means of a radiofrequency field. A specific feature of the method is the possibility of measuring the NMR line shape at a great distance from the resonance center. Experimental data and theoretical calculations have been presented for β-active ^{8}Li ($T_{1/2} = 0.85$ sec) nuclei in LiF samples (single crystals of three orientations and a polycrystalline aggregate). The second moments have been obtained, showing that internal local fields in ^{8}Li nuclei have a Gaussian distribution with a deviation towards Lorentzian shape at the wings.

Methodical questions were discussed by F. Stecher-Rasmussion (the Netherlands) who reported on the design of a new thermal-neutron polarizer for the HRF reactor in Petten. The system is to consist of four sections: a focussing precollimator of 85 graphite mirrors, a focussing collimator of 85 nickel mirrors (100 cm long), a polarizing system of 85 magnetized mirrors 100 cm long (50% each of Co and Fe), and a focussing collimator for absorption of nonpolarized neutrons that passed through the system. The mirrors are approximately 1 mm thick. The system is located in a thermal column allowing large solid-angle neutron collection. The new polarizer will be capable of producing a polarized neutron flux of up to $5 \cdot 10^{8}$ neutron/cm^2 · sec or 18 times as much as existing polarizers ($3 \cdot 10^{7}$ neutron/cm^2 · sec). The height of the beam will allow two experiments to be carried out simultaneously.

In conclusion one should mention the excellent organization of the Symposium by the Dutch group. Copies of the forthcoming reports were available every single day of the Symposium. The timing of the meetings was such that there was ample time for general discussions and personal contacts. The Reactor Center of the Netherlands plans to publish a collection of all materials presented at the Symposium.

MEETING OF THE SCIENTIFIC COMMISSION OF CERN AND INSTITUTE OF HIGH-ENERGY PHYSICS

A. V. Zhakovskii

The Ninth Meeting of the Scientific Commission, acting in accordance with the agreement on scientific cooperation between CERN and the State Atomic Energy Commission (SAEC) of the USSR, took place at the Institute of High Energy Physics (IHEP) (Serpukhov) on May 15-17. Y. Goldschmidt-Clermont, B. Kuiper, B. Langeset, W. Lock, and others represented the CERN while the IHEP was represented by R. M. Sulyaev, Yu. D. Prokoshkin, A. A. Naumov, V. I. Kotov, K. P. Myznikov, and others.

The Commission discussed problem of cooperation associated with the operation of the accelerator, fast beam extraction and transportation systems, high-frequency separation, and also the progress of preparations for joint experiments.

Seven runs of accelerator operation have been carried out in 1972 totalling 4570 operating hours. Maximum intensity was $2.5 \cdot 10^{12}$ proton/pulse, the average intensity for the year being $1.2 \cdot 10^{12}$ protons /pulse. The intensity has been increased by increasing the duration of the linear accelerator pulse and by using two- and three-revolution injection in the ring accelerator.

Putting into operation of the fast extraction system, parallel operation with two targets, and simultaneous improvement of accelerator operation made it possible to increase the average yearly coefficient of simultaneous operation to 3.85. After the summer shutdown, the fast extraction system has been used in six accelerator runs. Nearly 940,000 inclusions have been carried out during this period. The system operated stably and reliably, the time lost as a result of failure was less than one half of planned time. The Commission noted the high quality of equipment delivered by CERN and the fast mastering of this equipment by the staff of the IHEP.

The beam transportation system was put into operation, after the summer shutdown, in five accelerator runs. The total number of inclusions during this time was 900,000. Standstill due to failure did not exceed 0.5% of planned time.

The first operating run of the Mirabel chamber in separated particle beams proved that the background situation of the chamber needs significant improvement, particularly in operation with positive particle beams. The addition of a shield made it possible to use the Mirabel chamber in experiments with various particles including K- and π-mesons; foreign impurities did not exceed 2%. Standstill of the Mirabel chamber as a result of the separator system failure during four runs did not exceed 2%.

The Commission noted with satisfaction that the second joint experiment provided important scientific information. The Commission congratulated all participants of the experiments on the excellent work and on satisfactory conclusion of the experiment.

The third joint CERN—Institute of Theoretical Experimental Physics experiment on neutron–proton charge exchange (tentatively called "Neutron") has been completed in June, 1973. Preliminary data have been obtained in runs carried out in December, 1972 and February, 1973. Nearly $3 \cdot 10^6$ events, including 40,000 elastic scattering events, have been recorded on magnetic tape. Final processing of the experimental results will be made at CERN.

The Commission expressed its satisfaction with the state of the fourth joint experiment whose purpose is the study of interaction of π^--mesons with protons with the generation of neutral particles only (NICE experiment). The results obtained in the first and second runs in 1973 indicate that the principal units of the setup (γ-detector, electronics, the safety system, and proportional chambers) operate satisfactorily.

Translated from Atomnaya Énergiya, Vol. 35, No. 6, pp. 454–455, December, 1973.

The assembly of a total-volume γ-detector is now being completed for operation in 1973.

The Commission heard a report of L. Mosk on the state of works with the Mirabel chamber and on the latest results obtained in the course of preliminary experiments with separated particle beams. So far 100,000 photographs have been obtained in $\pi^{\pm}$, $K^{\pm}$, and proton beams.

In conclusion the Commission discussed certain organizational problems.

NEW EQUIPMENT

KGÉ-2.5 ELECTRON ACCELERATOR

I. V. Kuritsina, V. A. Lagutin,
A. V. Lysov, O. F. Nikonov,
and O. B. Ovchinnikov

Expanding research in radiochemistry and radiobiology, and widespread application of ionizing radiations in many branches of the economy, have created a need for appropriate radiation sources. As compared with other radiation sources, direct-acting accelerators have in many cases the following advantages: large dose rates, accurate control over a wide range of radiation intensity and energy, and negligible radiation hazard once the unit is switched off.

The Soviet industry manufactures accelerators of the Élektron type operating at an energy of 700 keV with a beam power of 7 kW, and type RTD accelerators operating at 1 MeV and 3 kW, respectively. However, industrial radiation processes require electron irradiators of still higher power.

The KGE-2.5 direct-acting accelerator designed and built at the D. V. Efremov Scientific-Research Institute of Experimental Atom Physics has a beam power of 25 kW and has been in operation for many years (Fig. 1). The principal design parameters of the accelerator are: maximum electron energy 2.5 MeV, energy control limits 0.5-2.5 MeV, energy stability better than 1%, maximum electron beam current 10 mA.

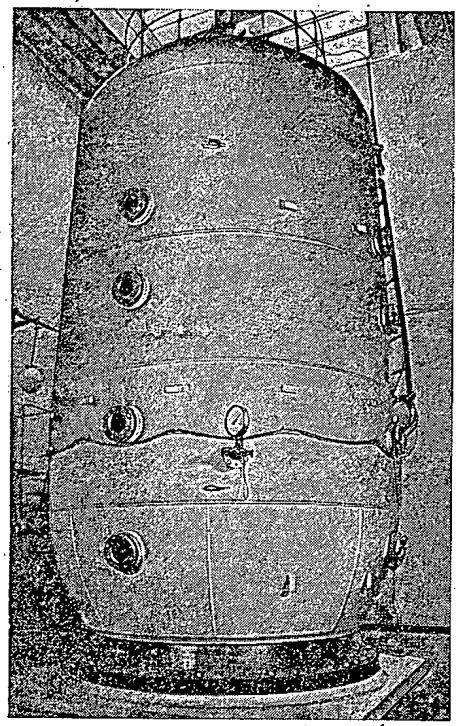

Fig. 1. External view of KGÉ-2.5 accelerator.

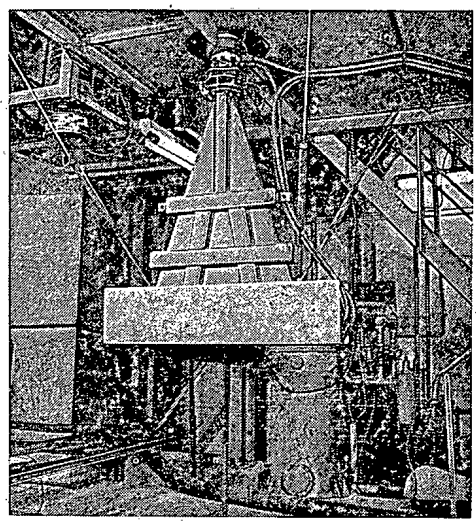

Fig. 2. Scanner.

Translated from Atomnaya Énergiya, Vol. 35, No. 6, pp. 455-456, December, 1973.

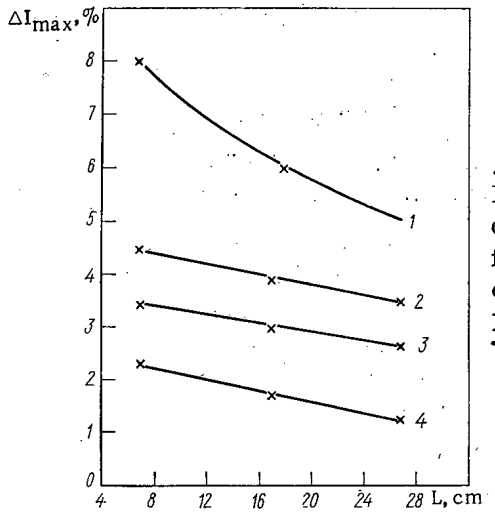

Fig. 3. Variation of extracted beam density as a function of distance from the exit window for different energies: 1) 0.5; 2) 1; 3) 1.5; 4) 2 MeV.

The high-voltage source is a 12-stage rectifier using a symmetrical multiplier circuits [1]. The rectifier consists of three capacitor columns (two discharge and one filter column) composed of type IM-250-0.008 capacitors (250 kV, 0.008 μF) and VS-250-IV selenium rectifiers (250 kV, 12 mA).

The power supply has compensating inductance coils which reduce currents due to parasitic capacitances [2].

The high-voltage source, the accelator tube, and electron gun with its power supply are mounted in a steel tank filled with a 25% CO_2 + 75% N_2 gas mixture at a pressure of 13 atm diff. Heat release in the vessel during operation is removed by a special cooling system.

The electron beam shaping, acceleration, and extraction system consists of an electron source (electron gun with a BaNi cathode), an accelerating tube, electron guide, a beam scanning and extraction setup, and a vacuum system with a VA-2-IR mercury pump. The electron beam is scanned at 50 Hz and is extracted to the atmosphere through a window in the scanner (Fig. 2). The window (40 × 950 mm) is covered with either 100 μ aluminum foil or 50-80 μ titanium foil.

The accelerator operation is remotely controlled and monitored (at a central control desk). The stabilization and control system allows the high voltage to be smoothly varied from 0.5 to 2.5 MV with a stability better than 0.25%.

Electron beam defocusing caused by the electromagnetic fields of the compensating inductances is reduced by proper selection of the coil winding directions. Selection of the entrance lens parameters (governing the conditions under which the beam enters the accelerating tube) ensure reliable accelerator operation in the 0.5-2.5 MeV range with an extracted electron beam of about 10 mA. The scanning and extraction system keeps current density variations to less than 8% over the entire length of the exit window.

Current density variations are calculated from the expression

$$\Delta I_k = \frac{I_k - I_{av}}{I_{av}} \cdot 100\%,$$

where I_k is the current density at point k.

The maximum current density variation of the electron beam is given by

$$\Delta I_{max} = \frac{I - I_{av}}{I_{av}} \cdot 100\%,$$

where

$$I_{av} = \frac{I_{max} + I_{min}}{2}.$$

Figure 3 shows the dependence of ΔI_{max} on the distance to the exit window for different energies. The accelerator is in operation since 1969. Most of the time the accelerator operates in the 1.0 to 2.2 MeV interval with an extracted beam of 8 mA.

Operating experience indicates that the accelerator is reliable and can be used in various branches of the economy.

LITERATURE CITED

1. B. I. Al'bertinskii et al., Prib. i Tekh. Éksper., No. 3, 43-46 (1971).
2. B. I. Al'bertinskii, in: Electrophysical Instruments [in Russian], No. 2, Atomizdat, Moscow (1964), pp. 71-79.

INDEX

SOVIET ATOMIC ENERGY

Volumes 34-35, 1973

SOVIET ATOMIC ENERGY
Volumes 34-35, 1973

(A translation of Atomnaya Énergiya)

L

M

SOVIET ATOMIC ENERGY

Volumes 34-35, 1973

(A translation of Atomnaya Énergiya)

Volume 34, Number 1 January, 1973

Volume 34, Number 2 February, 1973

Volume 34, Number 3 March, 1973

Engl./Russ.

Volume 34, Number 4 April, 1973

Volume 34, Number 5 May, 1973

Volume 34, Number 6 June, 1973

Engl./Russ.

Volume 35, Number 2 August, 1973

Volume 35, Number 3 September, 1973

Engl./Russ.

Volume 35, Number 4 October, 1973

Volume 35, Number 5 November, 1973

Volume 35, Number 6 December, 1973

The Plenum/China Program.

An event of singular importance for international science and technology.

Following closely upon the appearance of the first scientific periodicals in China since the Cultural Revolution, Plenum proudly announces the publication of authoritative, cover-to-cover translations of the major, primary journals from China, under the Plenum/China Program imprint.

These authoritative journals contain papers prepared by China's leading scholars and present original research from prestigious Chinese institutes and universities.

In addition to the biomedical and geoscience journals listed for 1974, the Plenum/China Program will publish cover-to-cover translations of periodicals in physics, chemistry, computer science, automation, mathematics and the engineering disciplines. The translations will be prepared by a large team of experts selected especially for the program, and each journal will be under the direct supervision of an outstanding authority in the field.

The first issue of each of the translation journals will be published in early 1974, and, as with our Russian periodicals under the Consultants Bureau imprint, the translations of the Chinese journals will be available within six months following the appearance of the original Chinese edition.

Subscriptions are now being accepted. Examination copies will be available in early 1974.

available in 1974

	Subscription Rates*
Acta Botanica Sinica (2 issues)	$ 75
Acta Entomologica Sinica (2 issues)	$ 55
Acta Geologica Sinica (2 issues)	$ 75
Acta Geophysica Sinica (1 issue)	$ 27.50
Acta Microbiologica Sinica (2 issues)	$ 55
Acta Phytotaxonomica Sinica (4 issues)	$125
Acta Zoologica Sinica (4 issues)	$125
Chinese Medical Journal (12 issues)	$195
Geochimica (4 issues)	$110
Kexue Tongbao—Scientia (6 issues)	$ 90
Scientia Geologica Sinica (4 issues)	$125
Vertebrata PalAsiatica (2 issues)	$ 60

forthcoming

Acta Astronomica Sinica (2 issues)

Acta Biochimica et Biophysica Sinica (2 issues)

Acta Mathematica Sinica (4 issues)

Genetics Bulletin (4 issues)

Huaxue Tongbao—Chemical Bulletin (6 issues)

*These prices are for the 1973 Chinese volumes which will be published in translation during 1974. Prices somewhat higher outside the U.S.

plenum
PLENUM PUBLISHING CORPORATION
227 West 17 Street, New York, N.Y. 10011
In United Kingdom: 8 Scrubs Lane, Harlesden, London, NW10 6SE, England

Declassified and Approved For Release 2013/01/22 : CIA-RDP10-02196R000400020006-3

breaking the language barrier

WITH COVER-TO-COVER ENGLISH TRANSLATIONS OF SOVIET JOURNALS

in mathematics and information science

Title	# of Issues	Subscription Price
Algebra and Logic *Algebra i logika*	6	$120.00
Automation and Remote Control *Avtomatika i telemekhanika*	24	$215.00
Cybernetics *Kibernetika*	6	$140.00
Differential Equations *Differentsial'nye uravneniya*	12	$175.00
Functional Analysis and Its Applications *Funktsional'nyi analiz i ego prilozheniya*	4	$110.00
Journal of Soviet Mathematics	6	$135.00
Mathematical Notes *Matematicheskie zametki*	12 (2 vols./yr. 6 issues ea.)	$185.00
Mathematical Transactions of the Academy of Sciences of the Lithuanian SSR *Litovskii Matematicheskii Sbornik*	4	$150.00
Problems of Information Transmission *Problemy peredachi informatsii*	4	$125.00
Siberian Mathematical Journal of the Academy of Sciences of the USSR Novosibirski *Sibirskii matematicheskii zhurnal*	6	$215.00
Theoretical and Mathematical Physics *Teoreticheskaya i matematicheskaya fizika*	12 (4 vols./yr. 3 issues ea.)	$160.00
Ukrainian Mathematical Journal *Ukrainskii matematicheskii zhurnal*	6	$155.00

Back volumes are available.
For further information, please contact the Publishers.

SEND FOR YOUR FREE EXAMINATION COPIES

PLENUM PUBLISHING CORPORATION
Plenum Press • Consultants Bureau
• IFI/Plenum Data Corporation
227 WEST 17th STREET
NEW YORK, N. Y. 10011

In United Kingdom: 4a Lower John Street,
London W1R 3PD, England